

# Understanding the impact of ageing and late-life dietary restriction on murine white adipose tissue with single-nucleus RNA sequencing



Inaugural-Dissertation

zur

Erlangung des Doktorgrades

der Mathematisch-Naturwissenschaftlichen Fakultät

der Universität zu Köln

vorgelegt von

**Nathalie Jauré**

**aus Carshalton, United Kingdom**

Köln, 2022



***This is a dissertation accepted by the Faculty of Mathematics and Natural Sciences of the University of Cologne***

Date of the thesis defense: 10.01.2023

Gutachter: **Prof. Dr. Linda Partridge**

**Prof. Dr. Peter Kloppenburg**



# Table of Contents

<b>Acknowledgments</b> .....	VIII
<b>Abbreviations</b> .....	X
<b>Summary</b> .....	XII
<b>1 Introduction</b> .....	<b>1</b>
<b>1.1 Extending healthy lifespan by dietary restriction (DR)</b> .....	<b>2</b>
1.1.1 Ageing and age-related diseases .....	2
1.1.2 Genetic and pharmacological interventions can extend healthy lifespan by targeting nutrient sensing pathways .....	3
1.1.3 The effects of DR and late-life DR .....	5
<b>1.2 The White adipose tissue (WAT)</b> .....	<b>7</b>
1.2.1 Metabolic role and morphology of WAT .....	7
1.2.2 Effects of ageing on adipose tissue .....	10
1.2.3 Effects of DR on AT .....	11
<b>1.3 Single-cell RNA sequencing</b> .....	<b>13</b>
1.3.1 New insights provided by single-cell data .....	13
1.3.2 Methods for single-cell experiments .....	14
1.3.3 Distinction between single-cell and single-nuclei RNA sequencing .....	16
1.3.4 Bioinformatic challenges of single-cell data analysis .....	17
<b>1.4 Aims of the work presented in this thesis</b> .....	<b>20</b>
<b>2 Methods</b> .....	<b>22</b>
<b>2.1 Animal husbandry and DR protocol</b> .....	<b>23</b>
<b>2.2 RNA-sequencing (RNA-seq) measurement</b> .....	<b>23</b>
<b>2.3 Nuclei isolation</b> .....	<b>25</b>
<b>2.4 Fluorescence-activated cell sorting (FACS)</b> .....	<b>25</b>
<b>2.5 Droplet-based methods for single-cell sequencing</b> .....	<b>26</b>
2.5.1 Nadia Instrument .....	26
2.5.2 10X Chromium .....	27
<b>2.6 Published sequencing datasets used in the study</b> .....	<b>28</b>
2.6.1 Published RNA-seq data .....	28
2.6.2 Published single-cell data .....	29

<b>2.7</b>	<b>Data analysis and statistical methods .....</b>	<b>29</b>
2.7.1	RNA-seq data pre-processing and analysis.....	29
2.7.2	Processing of raw single-nuclei dataset.....	30
2.7.3	Single-nuclei data analysis .....	32
2.7.4	Deconvolution analysis .....	34
<b>3</b>	<b><i>Optimization of methods to analyze single-nuclei sequencing data from murine white adipose tissue.....</i></b>	<b>37</b>
<b>3.1</b>	<b>Introduction .....</b>	<b>38</b>
3.1.1	Characterization of the murine WAT at the single cell level.....	38
3.1.2	Cell-type deconvolution of biological data.....	39
<b>3.2</b>	<b>Results .....</b>	<b>42</b>
3.2.1	Optimization of single nuclei sequencing protocol for WAT .....	42
3.2.2	Understanding changes in cell type composition with deconvolution analysis .....	58
<b>3.3</b>	<b>Discussion .....</b>	<b>69</b>
3.3.1	10X Chromium with FACS provided better data quality for WAT .....	69
3.3.2	Evaluation of deconvolution methods for WAT .....	70
<b>4</b>	<b><i>Single nuclei RNA profiling of white adipose tissue under dietary restriction reveals decreasing responsiveness with age .....</i></b>	<b>73</b>
<b>4.1</b>	<b>Introduction .....</b>	<b>74</b>
<b>4.2</b>	<b>Results .....</b>	<b>75</b>
4.2.1	Generating a cell-type landscape from young and aged murine white adipose tissue under dietary restriction .....	75
4.2.2	Cell-type landscape changes with age and DR .....	78
4.2.3	Adipocytes exhibit greater variety in relation to nutrition and age.....	80
4.2.4	A specific type of mature adipocyte emerges from the switch of DR at 16M.....	84
4.2.5	With aging, the metabolic flexibility of WAT is impaired.....	87
4.2.6	The transcriptional memory of the WAT is caused by gene expression changes in mature adipocytes and cell type composition of immune cells .....	91
<b>4.3</b>	<b>Discussion .....</b>	<b>96</b>
4.3.1	The effects of age and diet on the cell-type landscape of the WAT.....	96
4.3.2	Late-onset DR at 16 months leads to a unique subtype of adipocyte.....	98
4.3.3	WAT transcriptional flexibility is impaired with age .....	99
4.3.4	Conclusion, limitations and future perspectives.....	101
<b>5</b>	<b><i>Extended data .....</i></b>	<b>105</b>
<b>6</b>	<b><i>List of figures .....</i></b>	<b>121</b>

<b>7</b>	<b>List of supplementary figures .....</b>	<b>123</b>
<b>8</b>	<b>List of tables.....</b>	<b>124</b>
<b>9</b>	<b>Contributions .....</b>	<b>125</b>
<b>10</b>	<b>References.....</b>	<b>126</b>
<b>11</b>	<b>Eidesstattliche Erklärung.....</b>	<b>143</b>
<b>12</b>	<b>Curriculum vitae.....</b>	<b>144</b>
	<b>.....</b>	<b>145</b>

# Acknowledgments

First and foremost, I would like to express my deepest appreciation to Prof. Dr. Linda Partridge and Prof. Dr. Andreas Beyer, for the opportunity to conduct my PhD in their lab, and who generously provided knowledge and expertise. I am grateful for your support throughout the years in helping me grow as a better scientist, as well as your guidance and encouragements.

Many thanks to Dr. Sebastian Grönke for the supervision, critical discussion and support through the project. I would like to thank Dr. Peter Tessarz for being a member of my TAC, thesis committee and being so helpful and supportive while working single-cell experiments. I am incredibly grateful to Prof. Dr. Peter Kloppenburg for being part of my PhD thesis committee.

I am also thankful to all members of the Partridge laboratory and members of the Beyer laboratory, past and present, for contributing to an enjoyable and helpful atmosphere. Thank you for all the exchanges and feedback that helped me to grow in my scientific path. I would like to thank Christine Lesch for always being helpful and supportive with the administrative work, Oliver Hendrich and Virginia Kroef for their help in organizing the lab. I also have to thank Dr. Daniela Morricks for being available, listening, and helping me navigating during my PhD.

Special thanks to the PhD of the Partridge lab, thank you all for being really encouraging, caring and fun. I am happy to have shared retreats, parties and crazy murder mystery dinners with all of you. I feel really lucky to have met so many interesting, brilliant minds with kind and rich personalities. Thank you to my office neighbors Pingze and Helena, I was always happy to have a chat and catch up on what was happening in the lab! Thank you to Jonathan and Dennis for being part of our supportive LP bioinfo group, many thanks to my fellow F1 friends, Maarouf, Larissa, even if we were not cheering for the same team, it has been really fun (and unexpected) to share this weird passion with so many of you, to Sophie and Bruna for the fun travels, art activities and board games that made us escape the cold of the German winter! I could not have gone through this journey without my mice girls, Carol and Lisonia, thank you for your constant moral support, your altruism, and being such amazing friends (we will keep on rising!).

I would also like to thank my all my friends back in France, especially my longtime friends Justine and Xuan-thi, always there for me, sharing the struggles and the fun of life despite the distance. Thank you, to my precious friends Leila and Alphonse, for helping me day after day, since my first university days and showing me new horizons. Enfin, merci infiniment à ma famille et surtout à vous, Maman et Papa, vous m'avez toujours encouragé à donner le meilleur de moi-même, toujours là pour m'écouter et me remonter le moral, sans vous je n'aurais pu avancer aussi loin. Je finis par toi Mehdi, merci d'être à mes côtés tous les jours, merci de m'avoir fait grandir et de m'aider à m'épanouir, je ne pouvais espérer une plus belle personne que toi pour m'accompagner dans ma vie.

# Abbreviations

Acaca	Acetyl-CoA carboxylase 1
Acly	ATP-citrate lyase
AL	Ad libitum
AL_5	Ad libitum at 5 months
AL_24	Ad libitum at 24 months
ALDR16	AL to DR at 16 months
ALDR20	AL to DR at 20 months
ARDs	Age-related diseases
BAT	Brown adipose tissue
Bp	Base pair
DEG	Differentially expressed gene
DR	Dietary restriction
DR_5	Dietary restriction at 5 months
DR_24	Dietary restriction at 24 months
Elovl5	Elongation of very long chain fatty acids protein 5
Elovl6	Elongation of very long chain fatty acids protein 6
FACS	Fluorescence-activated cell sorting
Fasn	Fatty acid synthase
FOXO	Forkhead box
FOXO3	Forkhead box protein O3
GEO	Gene Expression Omnibus
GH	Growth hormone
Ghr	Growth hormone receptor
Gpam	Glycerol-3-phosphate acyltransferase
HSCs	Hematopoietic stem cells
IIS	Insulin/Insulin-like growth factor-1 signaling
Igf	Insulin-like growth factor
Igf-1	Insulin-like growth factor 1
Irs1	Insulin receptor substrate 1
Irs2	Insulin receptor substrate 2

Kbp	Kilobase pair
LC-MS/MS	Lipid chromatography-tandem mass spectrometry
Mbp	Megabase pair
MCT	Medium-chain triglyceride
Me1	Malic enzyme 1
mTOR	Mammalian target of rapamycin
mTORC1	Mammalian target of rapamycin complex1
mTORC2	Mammalian target of rapamycin complex2
p62	sequestosome 1
Pkb	Pyruvate kinase b
RNA-seq	RNA sequencing
Scd1	Stearyl-CoA desaturase 1
scRNA-seq	Single-cell RNA sequencing
SNP	Single nucleotide polymorphism
sNuc-seq	Single-nuclei sequencing
Srebf1	Sterol regulatory element binding factor 1
Tdg	Thymine-DNA glycosylase
UMI	Unique Molecular Identifier
SAT	Subcutaneous adipose tissue
WAT	White adipose tissue

## Summary

Dietary restriction (DR), defined as reduced food intake without malnutrition, increases lifespan and improves health in most organisms including mammals. In mice, onset of DR late in life does not provide the same benefits as lifelong DR. While lifelong DR increases lifespan, late-onset DR initiated at 24 months of age does not extend survival. Mice lose their responsiveness in lifespan to DR between 16 and 20 months of age. The liver and white adipose tissue (WAT) are key organs for maintaining energy homeostasis. Interestingly, gene expression in the liver is fully responsive to the late-life DR switch, while most genes in the WAT do not change their expression in response to late-onset DR, indicating a memory of gene expression in the WAT. However, the cause of this memory effect and which cell types in the WAT contribute to memory formation is currently unknown.

In order to address these questions, in my PhD project I employed single-nuclei sequencing of WAT from control and DR animals at young and old age. Furthermore, I analyzed the WAT from animals that were switched from AL to DR at 16 and 20 months of age, to correlate the responsiveness in gene expression with the longevity of these animals. When I started my PhD thesis, there were not methods available to perform single-cell sequencing of the whole WAT including mature adipocytes, which due to their large size and fragile nature, cannot be analyzed by traditional single cell sequencing approaches. Thus, I first optimized a protocol to isolate WAT nuclei, and then tested which droplet-based single-cell RNA-seq platform would provide the best data quality. Based on the results from the pre-test, I generated a comprehensive single-nuclei landscape of the WAT under DR using 10X Chromium. The results showed that cell types were distributed in three super clusters including mature adipocytes, immune cells, and the stromal-vascular fraction containing stem cells and precursor cells. Only mature adipocytes clustered in different sub-groups depending on diet and age. Interestingly, I identified a cluster of mature adipocytes that was unique to the AL to DR switch at 16 months of age, but not present in the DR switch at 20 months. Gene expression analysis showed that this cluster was enriched for pathways linked to insulin sensitivity and fat tissue homeostasis. This finding suggests that the earlier DR switch generates a partial reprogramming of the WAT in response

to DR, which is not the case when animals are switched to DR later in life. To confirm my findings, I validated the cell-type proportion changes observed in the SNuc-seq data, by deconvolution of a corresponding bulk RNA-seq data. In addition, by including additional time points in the bulk analysis, I provide evidence that the transcriptional flexibility of the WAT decreases with age. Finally, using the single-nuclei data, I show that the dietary memory originates mainly from differences in gene expression of mature adipocyte but also from changes in the proportion of immune cells.

# 1 Introduction

## 1.1 Extending healthy lifespan by dietary restriction (DR)

### 1.1.1 Ageing and age-related diseases

Ageing is characterized by functional degradation, a lowering chance of reproduction with increasing adult age as well as an increase in disease susceptibility that ultimately leads to death of the organism. The ageing process is widespread among organisms, but to some known exception like the hydra, a multicellular organism that escapes senescence thanks to three stem-cell populations with regenerative capacity (Tomczyk et al., 2015). The maximum lifetime of each species affects how quickly an animal ages, larger animals like elephants and whales typically live longer than smaller species like mice (Speakman, 2005). Ageing has various effects on sexes of the same species due to sex-specific reproductive costs and interactions with the local environment. It was shown that females had on average an adult median lifespan 18.6% longer than males in wild mammals. This trend is conserved in humans from different geographic groups, where women median lifespan is 7.8% longer than males (Lemaitre et al., 2020). Rather than a difference in ageing rate between sexes, the interaction between sex specific biological traits such as differences in mating strategies, immune system, sex hormones, and different environmental conditions, results in higher mortality chances for male organisms (Lemaitre et al., 2020).

An important research effort has been done over the years to describe the fundamental mechanisms of aging, and these processes have been divided into age-related hallmarks (Lopez-Otin et al., 2013). Telomere attrition, genetic instability, altered nutrient signalling, stem cell exhaustion, epigenetic alterations, cellular senescence, loss of proteostasis, mitochondrial dysfunction and altered intracellular communication are the main directions in ageing research. These hallmarks are interconnected, and understanding their core mechanisms and also their interactions is crucial for developing healthy ageing interventions. Numerous diseases that affect various organs or metabolic processes all share age as a risk factor for their progression (Niccoli & Partridge, 2012). By targeting one hallmark it is possible to limit the simultaneous progression of multiple age-related diseases (ARDs). ARDs associated with five aging mechanisms, namely altered intercellular communication, mitochondrial dysfunction, cellular senescence, stem cell exhaustion, and deregulated

nutrient sensing, could account for increased co-occurrence of these diseases in patients (Fraser et al., 2022). For example ARDs linked to metabolism and thus deregulated nutrient sensing, including obesity, type 2 diabetes, and fatty liver are usually found in the same patients. The global rise of multimorbidity cases and the number of elderly patients, is a challenge for healthcare systems and a motivation for biomedical research to find solutions. To tackle numerous ARDs simultaneously and promote healthy aging, it is necessary to understand the biological pathways that are impacted by aging.

### 1.1.2 Genetic and pharmacological interventions can extend healthy lifespan by targeting nutrient sensing pathways

The evolution of most cellular functions has been influenced by the selection pressure of nutrient scarcity. Metabolic pathways are modulated by the levels of sugars, amino acids, lipids, and metabolites, generating specific responses of the organism. Nutrient sensing pathways trigger different signals in response to food availability. Abundance of food favors storage and anabolic pathways, while absence of food mobilizes stored energy. Deregulation of nutrient sensing pathways are usually observed in metabolic diseases which are a major part of ARDs (Efeyan et al., 2015). As the prevalence of obesity increased drastically in children and adults worldwide, with all co-occurring morbidities, understanding why and how nutrient sensing pathways are dysregulated is important to design treatments for metabolic diseases while supporting healthy ageing. The insulin and insulin-like growth factor pathway (IIS) is an evolutionally conserved cellular network that plays a key role in regulating the ageing process. Interventions that decrease IIS activity increase lifespan in the roundworm *Caenorhabditis elegans*, the fruit fly *Drosophila melanogaster*, and also in mammals including mice (van Heemst, 2010).

The transcription factor FOXO and the mammalian target of rapamycin (mTOR) complex are among the most studied targets of the IIS network. In contrast to lower organisms like worms and flies, the mammalian genome encodes several *foxo* genes. FOXO3 was found to be positively associated with longevity in Japanese

centenarians, and in long-lived individuals from Italy and the Netherlands (Willcox et al., 2008). mTOR is a conserved serine/threonine kinase involved in a multitude of cellular functions including cell growth, survival, metabolism, autophagy and stress response. mTOR is present in two protein complexes, mTORC1 and mTORC2, both reacting to growth factors, but only the activity of mTORC1 is regulated by nutrient sensing via glucose or amino acids. mTOR modulates cell growth based on nutrient availability activating anabolic pathways under nutrient rich conditions. mTOR activity is dependent on the insulin signaling pathway. When there is high glucose concentration, insulin is released into the blood to promote glucose uptake in fat and skeletal muscle, in order to lower glycemia and activate anabolic pathways. Insulin-stimulated protein kinase B (PKB, also known as Akt) indirectly activates mTORC1, yet mTORC1 negatively regulates insulin signaling by phosphorylating insulin receptor substrate (IRS1), creating a negative feedback regulation. Excessive flux of nutrients could over-stimulate the activation of mTORC1 and result in an increase of phosphorylation of IRS1, leading to insulin resistance (Ong et al., 2016).

Genetic modification of the IIS pathway by deletion of IRS1 in mice induced lifespan extension in both males and females (Selman et al., 2011). Deletion of ribosomal protein S6 kinase 1, a component of mTOR pathway, also led to increased lifespan in females and protection against age-related defects such as immune and motor dysfunction and insulin resistance (Selman et al., 2011). Furthermore, in addition to extending lifespan, downregulation of the IIS pathway also has beneficial effects on healthspan. A recent study showed that mice with genetically reduced circulating insulin through IRS2 mutation, showed improve insulin sensitivity at old age compared to control, and overall healthier ageing (Templeman et al., 2017).

Additionally to genetic interventions, the use of drugs that could mimic the same action on key actors of the nutrient sensing pathways have been studied. Rapamycin is an antifungal, antitumor, anti-inflammatory drug, produced by a bacteria *Streptomyces hygroscopicus*, found in the Easter Island (Arriola Apelo & Lamming, 2016). Through characterization of its action it was discovered that Rapamycin inhibits mTORC1 activity, inducing autophagy and leading to lifespan extension in worms, flies and mice (Niccoli & Partridge, 2012). Since 2009, thirty studies in mice of different strains have been conducted to assess the effect of rapamycin on lifespan (Selvarani et al., 2021). 90% of these studies showed increased lifespan upon rapamycin treatment, demonstrating that the effect of rapamycin on survival is robust and

reproducible. Furthermore, lifelong or late-onset administration of rapamycin increased lifespan (Harrison et al., 2009), and its effects can persist even after administration has ceased (Quarles et al., 2020). E.g. treating 20-month-old mice with rapamycin for only 3 months was sufficient to extend lifespan (Juricic et al., 2022; Quarles et al., 2020). Taken together these recent findings provide solid ground for the development of rapamycin interventions in humans knowing that beneficial effects can be obtained from temporary treatments and can last even after administration has ceased. Indeed, first pilot studies in humans showed enhanced immune response to influenza vaccination after a low dose of rapamycin during 6 weeks and a 2-week drug free interval in old individuals (Mannick et al., 2014), while another study showed that rapamycin could be a potential topical treatment reducing skin senescence (Chung et al., 2019). Rapamycin can also present some negative side-effects including impaired wound healing (Weinreich et al., 2011), ulcers in mouth and lips, diabetes, hyperlipidemia and hypercholesterolemia (Soefje et al., 2011). Additional studies are needed to define a working dosage in humans and the effect of temporary dosage. There are multiple ongoing clinical trials that use rapamycin, one is in phase two, the Participatory Evaluation (of) Aging (With) Rapamycin (for) Longevity Study (PEARL), which should provide a great source of data for better understanding of effects of rapamycin on humans.

Studies looking at interventions into the nutrient sensing pathway either with genetic modifications or drug administration showed robust results of lifespan extension and health benefits, but their application in humans needs further work to define working dosage and the potential long-term effects. In contrast, dietary habits directly impact the same pathways and have the advantage that they can be easily adjusted in animal models and also in humans. Due to this, several studies became interested in dietetic therapy, particularly dietary restriction (DR).

### 1.1.3 The effects of DR and late-life DR

Dietary restriction (DR) is one of the most promising interventions to increase lifespan and protect against ARDs across multiple animal models, from worms to primates (Green et al., 2022). DR refers to the reduction in food intake without malnutrition and its beneficial effect was first reported in 1935, by showing that that DR increased

lifespan in rats (McCay et al., 1935). Since then, many studies have confirmed the link between nutrition and ageing, where DR protects against metabolic diseases like diabetes, cardiovascular diseases but also neurodegeneration (Wilson et al., 2021). Despite its benefit, there are some limitations to its application in humans. DR is challenging to implement on a full-length controlled trial, because of the duration of the study and the complications of human lifestyle, with additional factors to take into account such as diet quality or meal frequency (Most et al., 2017). Short duration clinical trials in humans with moderate caloric restriction such as CALERIE or CRON studies showed beneficial effects on health by reducing the prevalence of metabolic pathologies such as diabetes, heart disease and cancer (Most et al., 2017). In contrast, severe caloric restriction in human, similar to the amount of food restriction applied in mice studies, demonstrated serious side effects such as immune system impairment or reproduction issues (Most et al., 2017). In addition to physiological side-effects, due to the variety of factors that need to be taken into account for an intervention in humans, notably complexity of the diet and behavior, a dietary therapy presents a lot of challenges (Redman & Ravussin, 2011). Temporary instead of chronic DR is a more feasible option and can reduce potential adverse effects. Identifying the latest age of onset at which DR still demonstrates positive effects on health and survival would be the most favorable solution, limiting the duration of DR and targeting an age period where development or reproduction would not be affected (Sun et al., 2021).

Understanding the underlying mechanisms of DR is necessary to translate its benefits to human metabolism, and knowing when DR would still be effective would help the development of simpler and appropriate intervention in older patients. To define this DR effective period in humans, research in model organism, particularly mice, is needed. In order to benefit from DR, its effector mechanisms must maintain responsiveness to the nutritional environment. The ability to respond to DR appears to fade with age. For instance, the timing of the onset of DR in mouse or rat models had an impact on the survival effect (Das et al., 2017). Similar results were observed in rhesus monkeys, where DR at old age didn't extend lifespan but improved metabolic profiles (Mattison et al., 2012). A previous study in mice showed that late onset DR at 24 months of age did not extend mouse survival (Hahn et al., 2019). In contrast, an older study subjecting mice to caloric restriction at 19 months of age, observed significantly increased lifespan and reduced tumour load (Dhahbi et al., 2004). A

recent study in which mice were switched from ad libitum (AL) to DR at 12, 16, 20, 24 months of age (Lisa F. Drews, 2021), showed that the period in which DR can positively affect survival ended between 16 and 20 months of age. Understanding how metabolism changes between 16 and 20 months of age and what the underlying causes are, would aid in the development of late-onset DR interventions that might be more applicable to humans.

## 1.2 The White adipose tissue (WAT)

### 1.2.1 Metabolic role and morphology of WAT

The main function of the white adipose tissue (WAT) is to store lipids in the form of triacylglycerols as a potential source of energy. For decades the WAT remained understudied, considered as an inert organ and its contribution to systemic metabolic responses was underestimated. With the rise of obesity, an excessive proportion of body fat, now considered a pandemic, WAT is an organ of growing interest (O'Neill & O'Driscoll, 2015). More studies are trying to understand the function of adipose tissue, within the tissue but also its effect at the whole-body level. It is the largest endocrine organ and the central link to metabolic syndrome, a cluster of conditions that increase the risk of diabetes, cardiovascular diseases, and other widely spread and related health issues (Martinez-Sanchez, 2020). The WAT is found in two main depots: subcutaneous adipose tissue (SAT), which is under the skin and visceral adipose tissue (VAT), which is lining internal organs. Each depot has a different role in metabolic function and biochemical processes. VAT is more metabolically active with lipolysis, storage, and insulin regulation, making it a better indicator of metabolic dysregulation and prediction of mortality (Ibrahim, 2010). The body fat distribution is affected by ethnic background and gender in humans, and adipose tissue repartition is an important factor for metabolic diseases (Yaghootkar et al., 2020). Excessive visceral and ectopic fat is more detrimental than excessive subcutaneous fat. Some studies even showed that after body mass index adjustment, SAT had a protective effect against insulin resistance IR (McLaughlin et al., 2011).

Adipose tissue was initially classified into two types based on its color, the white and the brown adipose tissue, displaying different type of adipocytes with different metabolic functions. WAT is the largest tissue and is found in mammals including

humans. Its main role is to store lipids for energy, but it also secretes hormones and adjusts insulin sensitivity to maintain energy balance. The brown adipose tissue (BAT) is found in mammals, especially after birth or during hibernation to ensure non-shivering heat production, which is critical for body temperature maintenance. Previously, BAT was only associated with infants in humans, but recent studies showed that this tissue is also present in adults, with a higher prevalence in women and younger people (Cypess et al., 2009). BAT in adults can be metabolically active and involved in diet-induced thermogenesis and fat oxidation, but its small percentage and complex activation makes it a potential target to improve whole-body metabolism. Adipocytes of WAT contain a large unique lipid droplet with the nucleus and organelles in the periphery of the cell. In contrast, brown adipocytes have multiple lipid droplets and a large number of iron-rich mitochondria, giving the brown color to the tissue (Richard et al., 2000). BAT mitochondria contain uncoupling protein 1 (UCP-1), which causes heat production by short circuiting the proton gradient of the inner mitochondria membrane enabling the thermogenic function of the BAT. White adipocytes can store large amounts of lipids and expand their sizes up to 100µm, while brown adipocytes are smaller and only reach half of their size. Interestingly, an intermediate profile of adipocyte, called beige adipocyte, seems to appear in subcutaneous WAT from potential brown preadipocytes or through transdifferentiation of white adipocytes. Beige adipocytes also have thermogenic potential, and therefore the capacity to dissipate energy more actively than white adipocytes. The process of beiging of the fat is mainly observed in rodents but is also possible in humans, and seems to be activated through cold exposure and also interventions such as diet or exercise, making it a potential novel therapeutic treatment (Lizcano, 2019).

Adipocytes are the main cell type of adipose tissue. They stock lipids and also have a crucial role in communication in local and systemic responses by secreting paracrine and endocrine hormones, adipokines, cytokines. Signals emitted by the adipose tissue are fundamental to maintain energy balance, which is mainly controlled by the central nervous system. Leptin is a key hormone produced by adipocytes, which interacts with the nervous and immune system to regulate energy homeostasis (Martinez-Sanchez, 2020). Leptin resistance is a consequence of obesity, where excessive adiposity diminishes the leptin signal, preventing its anorexigenic functions (Izquierdo et al., 2019).

The WAT is a heterogeneous tissue, mainly composed of mature adipocytes but it also displays a large variability of cells, with a stromal vascular fraction that includes immune cells, endothelial cells, adipocyte precursors, and stem cells. (Duerre & Galmozzi, 2022). The metabolic function of the tissue depends on its composition, which is affected by multiple factors such as obesity or age. Mature adipocytes take up to 90% of the tissue space-wise, but account for less than 50% of the cell types (Lee et al., 2013). Maintaining a pool of pre-adipocyte to store lipids is crucial for the flexibility of the tissue and the adipogenesis capacity can be impaired in metabolic disorders. Adipocyte progenitors go through multiple stages of differentiation, monitored closely by expression levels of specific genes, to complete maturation. Among important factors for differentiation, PPAR $\gamma$  is a transcription factor highly expressed during maturation and crucial for regulating lipid metabolism. Subtypes of adipocyte progenitors were recently characterized depending on their functions. Most progenitors go through adipogenic differentiation in order to stock lipids, yet some subtypes are refractory to differentiation. Those progenitors are pro-inflammatory, and they could have a role in preventing fat deposition in skeletal muscle by attenuating adipogenic processes in surrounding adipocytes (Hepler et al., 2018).

Presence of immune cells can also be a sign of malfunction of the tissue and inflammation. Macrophages are the main immune cell found in WAT and they can promote pro or anti-inflammatory signals. Their role in a healthy tissue is to maintain the plasticity by clearing debris, modifying the extra cellular matrix or buffering lipid accumulation. In disease states, such as obesity, where the tissue needs increasing storage and expansion, vascularization is impaired which leads to fibrosis and macrophage infiltration (Reyes-Farias et al., 2021). Other immune cell-types, such as lymphocytes, T-cell and B-cell, can also be present, recruited in early stages of obesity and promoting inflammation through the release of cytokines and immunoglobulins such as IgG, IgM (Reyes-Farias et al., 2021).

A growing number of studies are investigating the heterogeneity of WAT through single-cell and single-nucleus data, trying to capture the best representation of the cell-type landscape of the tissue. Recently, spatial transcriptomics added a layer of information showing that different subtypes of mature adipocytes cluster together in the tissue, but also that progenitors tend to be in proximity of M2 macrophages, acting to maintain remodeling potential of the tissue (Backdahl et al., 2021). More research

characterizing the spatial distribution under different metabolic conditions would provide important information on the communication among different cell types inside the tissue and could possibly identify additional sub-cell types.

### 1.2.2 Effects of ageing on adipose tissue

Similar to obesity, ageing is an important contributor to adipose tissue dysfunction and metabolic disorder progression. Body fat distribution is important for metabolic health. With age, VAT proportion increases while SAT decreases, when SAT is considered beneficial for health. While fat depots are affected by age, the proportion of different fat tissues also changes, with a decrease of brown and beige adipose tissue. This affects thermoregulation in old people but also is detrimental for metabolism, since the declining tissues are highly metabolically active. Increase of BAT by surgical simulation or molecular knock-out protected against obesity, improved metabolism and enhanced lifespan (Vatner et al., 2018).

With fat redistribution during ageing, more lipids are stocked in adipocytes of VAT, leading to adipocyte hypertrophy and ectopic fat deposition. This is observed notably in the liver, causing nonalcoholic fatty liver disease (Frith et al., 2009). Furthermore, ageing reduces angiogenic capacity, leading to defective vascularity of the tissue, tissue fibrosis and hypoxia (Donato et al., 2014).

All those factors trigger immune infiltration, where macrophages surround dysfunctional adipocytes and form crown-structures. Macrophages secrete pro-inflammatory cytokines such as IL-1b, Il-6, or TNF-a which reduce expression of PPAR $\gamma$ , a transcription factor essential for adipocyte maturation. This has direct consequences for the plasticity of the tissue and its potential to adapt to changes in metabolic activity and storage.

Adipose stem cells (APSC) are the least differentiated cell-types that can mature into adipocytes. They are an important pool of cells that can respond to changes in metabolic activity of WAT. These cells have a mesenchymal origin, and can also differentiate into osteocytes, chondrocytes, and myocytes, which make them attractive targets for stem cell therapy. The adipogenic differential potential of APSCs declines with age (Liu et al., 2017), with the differential capacity in other cell-types being impaired along with their proliferative capacity. Additionally, ageing affects their

paracrine activity and doubles the time needed to differentiate (Frankish et al., 2021). The stemness capacity of APSCs could also be affected by senescent cells accumulating in the tissue with age. These cells show a senescence-associated secretory phenotype, including cytokines, chemokines and growth-factor. This leads to more immune cell infiltration to clear the accumulation of senescent cells but at the same time increases inflammation signaling and compromises the integrity of the extracellular matrix, promoting fibrosis of the tissue.

Multiple factors induce inflammation in ageing WAT. Another is the dysregulation of autophagy, with the elevation of reticular endoplasmic stress and increased secretion of pro-inflammatory cytokines IL-6 and MCP-1 (Ghosh et al., 2016). Taken together, these results show that ageing hinders adipose tissue remodeling capacity by affecting adipogenesis and triggering inflammation reactions that could participate in insulin resistance in old individuals (S. M. Kim et al., 2014).

As an endocrine organ, if the WAT function is altered, it has repercussions at the systemic level through the dysregulation of adipokines and secretion of pro-inflammatory cytokines. For example, leptin regulation is affected with age, leading to leptin resistance, which increases the risk of obesity, but also to liver cirrhosis or fibrosis (Tsochatzis et al., 2006). Furthermore, 30% of IL-6, a major inflammatory factor contributing to systemic inflammation, is produced by WAT (Starr et al., 2009).

To prevent metabolic illnesses and encourage healthy aging, normal AT metabolic activity is essential.

### 1.2.3 Effects of DR on AT

To prevent age-related dysfunction, one robust intervention is DR, which acts directly on the AT by reducing adiposity and leading to better metabolic health. Reducing WAT by caloric restriction, energy expenditure or selective removal, leads to lifespan extension by improving glucose sensitivity and insulin action, suggesting a direct link between organismal ageing and WAT function (Weiss & Holloszy, 2007) (Muzumdar et al., 2008). Multiple studies looked in detail at the effect of DR on WAT and the mechanisms affected through it. An early study looked at the effect of short- and long-term energy restriction in male mice, and found that long term energy restriction had

a stronger effect on the WAT transcriptome, with downregulation of inflammation genes, and promotion of structural remodeling genes (Higami et al., 2006). A study of caloric restriction (CR) during ageing in mice showed that it attenuated adipocyte hypertrophy while maintaining the beiging potential of the WAT (Sheng et al., 2021). By limiting food intake, the storage of lipids was also decreased, and adipocytes remained small in size compared to those in AL mice. Small adipocytes prevented the secretion of pro-inflammatory cytokines and general inflammation of the tissue, and preserved insulin sensitivity. Beige adipocyte are more metabolically active than those in WAT, and could generate a resting metabolic activity, helping to burn more stored fat. CR enhanced beiging of WAT from young to old age, but weakened function of BAT. Another study showed that CR promoted beiging of the WAT in both VAT and SCAT through recruitment of M2 Macrophages, which are anti-inflammatory, but also accumulation of adipose-resident eosinophils important for tissue remodeling and metabolic homeostasis (Fabbiano, Suarez-Zamorano, et al., 2016). Among other beneficial aspects of CR, CR mice showed less accumulation of autophagy substrates like p62 compared to AL mice (Ghosh et al., 2016), limiting autophagy dysregulation which is one of the hallmarks of ageing (Lopez-Otin et al., 2013).

Age of onset of DR and its duration affect its health benefits. A previous study in mice showed that late onset dietary restriction has no beneficial effect on survival. In addition, gene expression in the WAT, but not the liver, were refractory to the diet switch (Hahn et al., 2017). The WAT transcriptome of young animals responded rapidly to DR, suggesting that, rather than being an intrinsic feature of WAT, the low transcriptional responsiveness to DR in this tissue was specific to aged individuals. This result showed that, in contrast to the liver, WAT metabolic flexibility declined with age. Interestingly, the WAT transcriptome of DR mice showed upregulation of PPAR $\gamma$  and its downstream target the de-novo-lipogenesis (DNL) pathway. It has already been demonstrated that this pathway is upregulated during DR (Solinas et al., 2015). DNL produces long fatty acids, either for mitochondrial biogenesis or to function as adipokines activating transcription factors, preserving a healthier metabolic equilibrium (Song et al., 2018). Nevertheless, further work is needed to understand how the DNL signal is triggered by DR and to better characterize its repercussions at the systemic level. A minimum level of adiposity is needed to observe the benefits from caloric

restriction in mice (Mitchell et al., 2016), indicating the importance of adipocytes in DR response, but more information is needed on the role of other the cell-types.

## 1.3 Single-cell RNA sequencing

### 1.3.1 New insights provided by single-cell data

Massive advances in high-throughput technologies have made it possible to analyze differences at the genome, transcriptome, and epigenome level in recent decades. This has enabled generation of numerous biological databases, getting more informative and comprehensive with time. Transcriptomic approaches evolved from microarray-based platforms, where only expression levels of known transcripts could be measured, to RNA-seq technology, which additionally provides information on isoforms, splice junctions and novel transcripts (Byron et al., 2016). RNA-seq allows to capture a comprehensive transcriptomic profile of a sample, to gather valuable information on different tissues, in different models, highlighting the effects of a disease, a drug or any intervention on metabolism. Nevertheless, organs are complex, comprising different cell-types, at different levels of differentiation, in different proportions, and none of these details can be captured using bulk RNA-seq transcriptomics. However, since 2009, it is possible to measure gene expression with single-cell resolution using Single-cell RNA sequencing (Tang et al., 2009). In the last decade, the single-cell approach developed into a new field, offering ever-more-effective techniques and creating new cell-type atlases of organs, allowing the scientific community to examine their biological heterogeneity and diversity. For example, multiple brain atlases have been generated in different model organisms, in mice (La Manno et al., 2021), fly (Davie et al., 2018), even looking at the effect of age or diet on the cell-types, providing great resources for research (Ximerakis et al., 2019). Comprehensive databases have been built, including data from several organs, like the Fly cell atlas (Li et al., 2022), the Human cell landscape (Han et al., 2020), or the Tabula Muris (Tabula Muris et al., 2018). With time, more specific datasets are generated, characterizing novel cell-types (Travaglini et al., 2020), comparing cell-types profiles and proportions between conditions (Melms et al., 2021), or looking at

differentiation processes (Alsinet et al., 2022). Single-cell approaches brought new layers of information, changes in gene expression in a cell but also changes in cell-type proportions, both having an impact on metabolic changes in a tissue. This combination of information showed great advantages to understand physiological and pathologic processes in particular tumor heterogeneity (Tang et al., 2019). The amount of single-cell data generated is quickly increasing, nevertheless the methods used to produce those datasets are challenging, with strict protocols, expensive instruments to generate the libraries, and constantly developing bioinformatics analytical pipelines (Adil et al., 2021). In order to properly create specialized datasets to address more complicated biological questions, choosing the right experimental design and method is essential.

### 1.3.2 Methods for single-cell experiments

By isolating individual cells, collecting their RNA, and converting it to cDNA to create a sequencing library, single-cell RNA sequencing techniques allow the analysis of the mRNA transcriptome of a single cell. The number of methods to perform single cell sequencing analysis is still increasing, offering higher yield, quality and specification, such as looking at the methylation or the spatial localization of cells. Most methods target transcriptomic information and they differ in the techniques used to isolate cells and produce cDNA. The use of different instruments or protocols result in differences in sensitivity and accuracy (Oulhen et al., 2019). Some methods like Smart-seq or CEL-seq2 separate cells into individual wells to generate single-cell data. Other methods use fluorescence-activated sorting to separate cells, like MARS-seq, SCRB-seq, and Smart-seq2. Methods based on microdroplets to capture single cells or nuclei, are the most widely used thanks to their high performance, i.e. the number of cells captured and data quality. In contrast to other methods that isolate cells using selection, they have an unbiased approach that enables a comprehensive representation of the tissue of interest. Additionally, the isolation step is based on microfluidics, which is easier and cheaper than manually selecting single cells. InDrop, Drop-seq, and 10X Chromium are the three most commonly used droplet-based platforms. InDrop and Drop-seq are published methods while 10X Chromium is a

commercial platform, but overall, these three methods use a similar approach. They individually encapsulate several thousands of cells per second in oil drops, producing millions of micro compartments for capturing single transcriptome profiles. In order to generate transcriptome profiles for each cell, beads covered with a PCR primer, cell barcode, an UMI and a poly-T tag, are introduced in the oil droplets. The PCR primer is used for amplifying the mRNA captured by the poly-T tag, the cell barcode is used to identify from which cell the mRNA came, and the UMI to correct for duplication bias in quantitative analysis. This amplification bias comes from the fact that a single cell does not yield a lot of mRNA after lysis and some will not be captured or reverse transcribed, large amplification is needed afterwards to build a library, and with the use of UMI a more precise quantification of each transcript is possible (Chen et al., 2018).

In each method, beads and cells are introduced at a low rate to avoid having doublets of beads or cells in the same droplet (Zhang et al., 2019). This leads to errors in the analysis, especially cell doublets, which can be wrongly interpreted as novel cell-types. InDrop and 10X use soft gel beads, they have a better encapsulation rate, following a Super-poissonian distribution, whereas Drop-seq uses hard beads which follow a Poisson distribution and results in a lower bead occupancy and cell capture efficiency (Zhang et al., 2019). Following encapsulation, cells are lysed, either directly from the buffer of the beads for InDrop and Drop-seq, or in the case of 10X the beads are dissolved, releasing the lysis buffer for the cells. In addition, dissolving beads allows more primer to be released and a better capture efficiency. Another advantage of InDrop and 10X, is that the reverse transcription from mRNA to cDNA is done in the emulsion, the use of small compartments for this reaction gives more accurate results. Then, for all methods, a step of demulsification is done to pool all cDNA collected, to then amplify it to make libraries. These last steps are different depending on the method, notably Drop-seq and InDrop have a more challenging and long protocol, while 10X is a commercially simplified pipeline. Previous studies compared the different methods and overall 10X provides better results and has a faster protocol (Zhang et al., 2019). But a lot of tissues require to adapt the protocol to their specificity, and 10X doesn't provide a lot of room for change, while InDrop and Drop-seq allow to modify the rate of beads/cells encapsulation or the size of the droplets, or even the buffer used during encapsulation. They are also cheaper approaches which can be a

strong argument when trying to generate an atlas with numerous tissues and replicates. Most of single-cell transcriptomics studies use 10X approach nowadays but it is interesting to consider different single cell approaches and the choice of the method should depend on the scientific question.

### 1.3.3 Distinction between single-cell and single-nuclei RNA sequencing

Droplet-based methods of single-sequencing aim to target cells to capture all transcriptomic information available. In some cases, using cells is not possible because of the cell shape or their organization in the tissue. For example, the brain displays a great variety of cells with complex layering leading to loss of some specific cell-types during the cell dissociation process (Bakken et al., 2018). Mature adipocyte, the main cell-type of white adipose tissue, can expand to stock lipids, and this leads to its cells being too large to be encapsulated in droplets (Rondini & Granneman, 2020). Additionally, while it can be difficult to obtain fresh tissues for single-cell methods, frozen post-mortem tissues can directly be used with single-nuclei sequencing (Lake et al., 2016). Single-nuclei sequencing (sNuc-seq), is a great alternative for complex specific tissues or to process a large number of samples that don't need to be freshly isolated. Cell identities or specific gene expression profiles can be retrieved with solely nuclei transcriptomes. A number of studies looked at potential differences or bias from using nuclei instead of cells in single transcriptomic studies. The majority of studies comparing sNuc-seq to single-cell showed similar sensitivity and high concordance in results, while some differences might occur depending on the tissue. For example, comparison of single-nucleus and single-cell data in neurons showed differences in transcript abundance, more nascent transcript in the nuclei data, and more mitochondrial respiratory relative transcript in the cellular data since they accumulate in the cytosol (Lake et al., 2017). Despite those differences, similar results in cell-type profiles, cell-type proportions and metabolic gene markers were observed, in both datasets. Another study compared single-cell and single-nuclei methods on cell lines, peripheral blood mononuclear cells and brain tissue, and found similar sensitivity and cell type classification between the methods, also showing that single-nuclei data prevented gene expression artefacts from dissociation stress (Tabula Muris, 2020). Some studies also showed, by comparing

the two approaches on kidney tissue, that using single-nuclei could prevent the bias induced by dissociation and recovery of some cell-types absent in single-cell data, even if immune cells were underrepresented in nuclei data compared to cell (Gaedcke et al., 2022). Despite some differences depending on the tissue, using nuclei instead of cells can provide similar results, especially for cell-type identification and finding metabolic gene markers. The choice of method should depend on the scientific question, single-nuclei being a more interesting option if nuclear transcripts can provide enough information or if the tissue of interest would be subjected to bias because of the dissociation process.

#### 1.3.4 Bioinformatic challenges of single-cell data analysis

High throughput methods changed the way of analyzing biological data, dataset size is increasing rapidly, demanding more technological resources in terms of memory and computing power. Gene expression datasets are usually in the form of a matrix, with genes detected and their respective level of expression for a sample. With RNA-seq bulk dataset only a few samples would be measured, while in the case of single-cell approaches, the size of the matrix is significantly larger since thousands of cells are measured. To properly analyze this new type of data, a lot of development has been done in the bioinformatic community to create adequate pipelines and address these new problems. A few commercial pipelines are available, notably Cell Ranger from 10X and Fluidigm, but there is not yet a reference pipeline in single-cell analysis (Hwang et al., 2018). A lot benchmarking reviews on methods are available to researchers to design their own pipelines, also available methods are constantly and quickly improving by using novel data analysis methods, like deep learning (Ma & Xu, 2022).

From the raw sequencing files, a few steps are needed to obtain a gene expression matrix. Reads need to be aligned on a reference genome, de-duplicated to have accurate quantification and collecting information on which transcript came from which cell. This can be done via the Cell Ranger software, or the zUMIs pipeline (Parekh et al., 2018), or STAR (Dobin et al., 2013), which has adapted its mapping method to single-cell data. The end results are dependent on the first steps of the pipeline, meaning data quality assessment and normalization. From cell to cell the quality varies

a lot, from really low expression, to high content due to doublets, or high mitochondrial gene expression observed when cells are going through apoptosis. Not all transcripts are caught during cell lysis, leading to what is called a dropout, an absence of expression of a gene in some cells. This is another factor contributing to the high variability across cells and different samples. It can be explained by the low amounts of mRNA released from lysis of individual cells and inefficient mRNA capture, as well as the stochasticity of mRNA expression. The dropouts are the reason why scRNA-seq data is usually sparse and the high amount of zero counts cause the data to be zero-inflated (Zhang et al., 2019). To address this issue, some imputation methods are designed to infer missing level expression data based on gene to gene or cell to cell similarities, like scImpute (Li & Li, 2018) or MAGIC (van Dijk et al., 2018). But the real challenge is to differentiate real dropouts from the ones that are from low technical sensitivity, and the risk with imputation is to infer expression when there is none. A lot of filtering steps are necessary to limit the high heterogeneity in the data and to have information reflecting the cell-type landscape of the tissue. From the normalized dataset, the main analysis can be divided between one part focusing at the cell level and one at the gene level. One of the main purposes of single-cell analysis is to define similar group of cells in the mix of cells from the tissue, identify their cell-type, and possibly their level of differentiation thanks to trajectory analysis (Trapnell et al., 2014). To define when cell composition changes, clustering techniques are used to determine whether cells are comparable and may be from the same cell type, which is crucial information for not only the dropout imputation methods but also for all the downstream analysis and biological interpretation. Since single-cell data is sparse and carries a lot of technical noise, highly variable genes are selected to do dimension reduction analysis with either principal component analysis (PCA) (Jolliffe & Cadima, 2016) or t-Distributed Stochastic Neighbor Embedding (tSNE (Kobak & Berens, 2019)) or UMAP (Becht et al., 2018). Highly variable genes carry differences in their expression levels that can differentiate cell clusters in a mixed cell population, and are less affected by dropouts (Yip et al., 2019). After identifying clusters of similar cells and their cell-type identity, the analysis can be done at the gene-level, for example, functional enrichment analysis to determine the biological function of a cluster, or inferring gene-regulatory network to get better understanding of which genes are co-expressed in a specific cell-type and, or condition. While differential gene expression analysis is the golden standard analysis in bulk RNA-seq, it is still a field in development in single-cell data,

where improvement is needed to detect differences in gene level expression between cells because of biological and not technical variability. Some methods address this problem such as DEsingle (Miao et al., 2018). The high variability can be an issue when looking at replicates and comparing different conditions. Batch correction methods for technical variability are available, but by correcting technical variability, some biological variability is lost, and possibly also more subtle changes, such as novel information on sub-cell-types or metabolic activity in specific group of cells.

Lately single-cell approaches have been extended to the epigenome, proteome or the spatial position of cells in the tissue. The main motivation is to combined several layers of information from the same cell to depict a hyper precise profile of it and its interaction with other cells. As complete as it sounds, it is also bringing new challenges, and a higher level of complexity, exacerbating all the issues mentioned for transcriptomic analysis (Subramanian et al., 2020). These multimodal assays are forcing scientists studying single-cell bioinformatic analysis to foresee new problems. As a result of this emerging discipline, several cutting-edge tools are being published at a rapid rate so that further work is needed for the bioinformatic field to converge towards common best practices for analysis.

## 1.4 Aims of the work presented in this thesis

Dietary restriction (DR) ameliorates ageing in multiple animal models, ranging from worms to mammals including primates (Balasubramanian et al., 2017). In order to benefit from the DR treatment, an organism has to be able to adapt to the nutritional change. In mice, the ability to adapt to DR is lost with age in the WAT, where gene expression is mostly refractory towards a late onset AL to DR switch (Hahn et al., 2019). This transcriptional memory of prior AL feeding in the WAT might explain why DR cannot extend lifespan in old animals. Indeed, mice lost the ability to increase their lifespan in response to DR between 16- and 20-month of age (Drews 2021). Thus, comparing the response in WAT gene expression towards a DR switch at 16 and 20 months might provide novel insights into processes that contributes to the better health and increased lifespan of the DR animals. The white adipose tissue is highly heterogeneous with multiple cell types in different proportions (Ràfols, 2014). Thus, in order to elucidate the molecular basis for the transcriptional memory in the WAT, I used single-cell RNA sequencing to address which cell types contribute to the memory, and whether it is caused by changes in gene expression and/or cell composition.

At the time I started my PhD project, there were no methods available to do single cell RNA sequencing on mature adipocytes due to their large size, which is incompatible with traditional microfluidic approaches. Thus, my first aim was to develop and optimize a single-nuclei protocol for the WAT using droplet-based sequencing methods. In particular, I addressed the following questions:

- 1) How to optimize the nuclei isolation protocol using WAT?
- 2) Which single-cell platform provides the best data quality given the low cDNA concentration usually obtained from WAT?

After establishing the protocol, I designed the experimental layout, generated and bioinformatically analyzed the single-nuclei data to answer the following questions:

- 3) What is the cell type composition of the murine white adipose tissue?
- 4) How do age and DR affect the cell-type landscape of the murine WAT?

- 5) Does the late-onset DR treatment rejuvenate the white adipose tissue?
- 6) What are the differences in single cell gene expression and cell type composition between the DR switch a 16 and 20 months of age?
- 7) Does the WAT need longer to adapt to DR if the switch is done at old age?
- 8) Is the transcriptional memory a result of gene expression or cell composition changes?
- 9) Can cell-type composition information be extracted from bulk RNA-seq using a deconvolution approach? Is it validating the observations made from sNuc-seq data?

## 2 Methods

## 2.1 Animal husbandry and DR protocol

Females of the F1 hybrid strain C3B6F1 were used throughout, and were part of a cohort study that examined the effects of switching diets at 12 (ALDR12), 16 (ALDR16), 20 (ALDR20), and 24 (ALDR24) months of age, together with mice fed chronic AL and DR diets (Drews et al., 2021). Ad libitum fed (AL) mice had ad libitum access to chow food while dietarily restricted (DR) animals received 60% of the amount consumed by AL-fed animals (i.e. food intake was reduced by 40%). Food consumption of AL mice was monitored weekly. Four distinct cohorts were created, for lifespan analysis (n=320 mice), tissue collection (n=320 mice), metabolic (n=90 mice) and fitness phenotyping (n=72 mice). For each mouse of the tissue collection cohort, the WAT was snap frozen in liquid nitrogen and then stored at -80°C. Those samples were used for bulk RNA sequencing (RNA-seq) or sequencing of single nuclei (SNuc-seq).

## 2.2 RNA-sequencing (RNA-seq) measurement

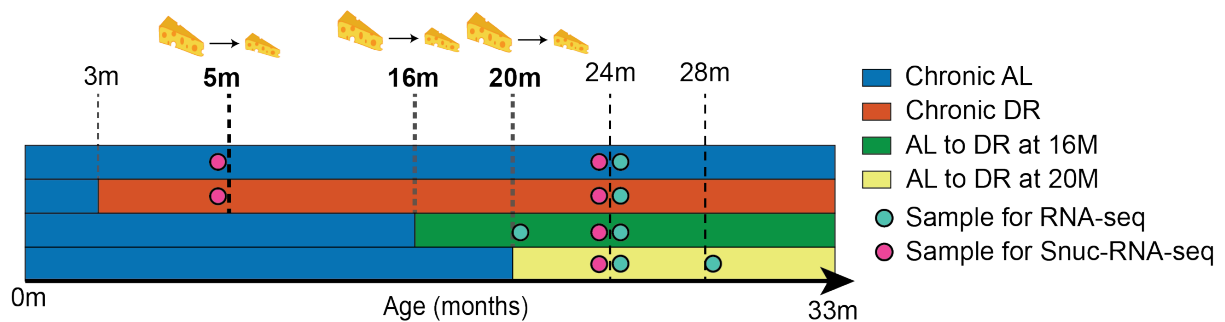


**Figure 2-1 Experimental design for SNuc-seq and Bulk RNA-seq**

RNA from perigonadal WAT of conditions of interest were isolated in three biological replicates by Dr Lisa Drews. Conditions were the following: AL and DR mice of 5 and 24 months old, ALDR16 of 20 and 24 months old, and ALDR20 of 24 and 28 months old (**Figure 2-1**). Between 70-120mg of snap-frozen WAT from each sample were homogenized in 1000µl Trizol (15596018 ThermoFisher Scientific) and incubated for 5min at RT followed by centrifugation at full-speed for 10min at 4°C to collect free-

floating fat (Drews et al. 2021). Samples were treated to remove genomic DNA contamination using the DNA-free™ DNA Removal Kit (AM1906, Invitrogen) according to manufacturer’s protocol, and RNA concentration was measured using a Qubit™ RNA BR Assay Kit (Q10210, ThermoFisher Scientific) according to manufacturer’s protocol.

RNA-seq library preparation and sequencing was performed by the Max Planck Institute for Molecular Genetics, Berlin, Germany (<https://www.molgen.mpg.de/>). According to the facility’s procedure, stranded TruSeq RNA-seq libraries were prepared using TruSeq RNA Library Prep Kit (RS-122-2001, Illumina) according to manufacturer’s protocol. Libraries were sequenced with 2x40 mio, 100 bp paired-end reads on an Illumina Novaseq 6000 (Illumina, San Diego, California, USA).

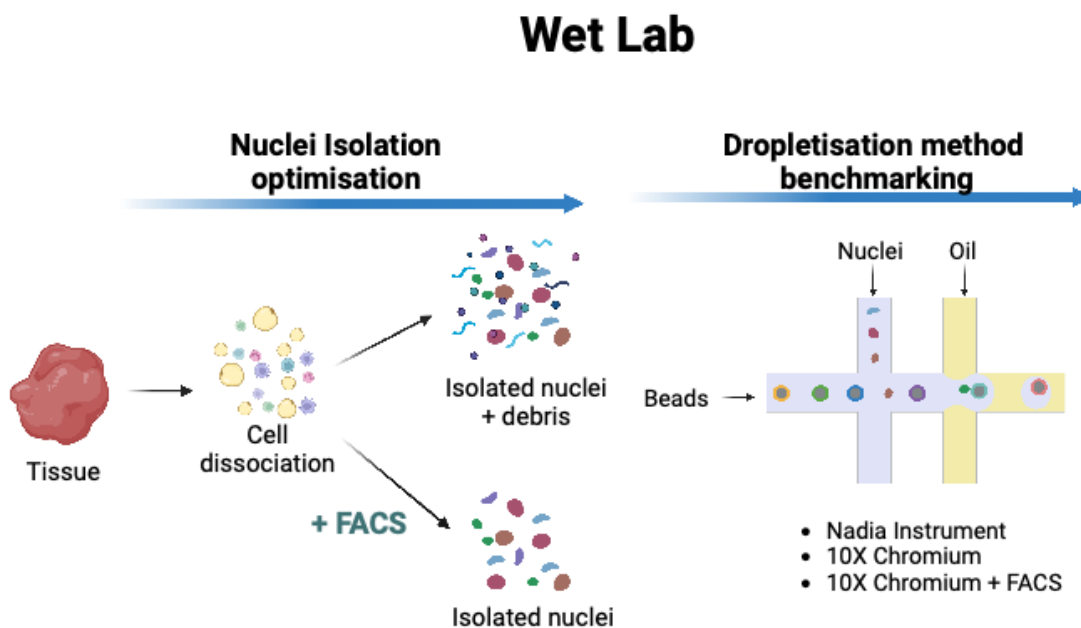


**Figure 2-2- Single-nuclei wet lab workflow.**

*Wet Lab optimization was divided into two steps, first getting an optimal isolated nuclei solution, without cellular debris and floating RNA. Multiple changes in different steps of the protocol were tested, notably sorting nuclei with FACS after isolation to get a cleaner solution. The second part of protocol optimization for the experiment was to assess which droplet-based platform was the best suited for WAT, and would give the best data quality. Test data were acquired from a Nadia Instrument, a 10x Chromium, and a 10X chromium with FACS before dropletisation.*

## 2.3 Nuclei isolation

sNuc-seq was done on WAT from AL and DR mice of young (5 months) and old (24 months) age, and on ALDR16 and ALDR20, both at 24 months (**Figure 2-1**). Nuclei were extracted from snap-frozen tissues, using a custom protocol adapted to work with adipose tissue. The main steps of the protocol were designed based on “Massively parallel single-nucleus RNA-seq with DroNc-seq » (Habib et al., 2017), to retrieve isolated nuclei from all the cell types present in the tissue. To lower inter-sample, 100mg of fat from 3 different mice were pooled together. On ice, fat pads were cut and minced using surgical scissors and were then transferred to a 1mL douncer with 0.8mL of EZ lysis buffer (NUC-101, Sigma-Aldrich). Tissue was homogenized first using a loose then a tight pestel 20 times. The homogeneous solution was transferred to 5 ml conical tubes and kept on ice with additional 2mL of EZ lysis buffer for 20min, vortexing every 5 min. After centrifugation for 5min at 500xg (4 °C), the supernatant was discarded and the pellet, containing the nuclei, was resuspended in 3mL of EZ lysis buffer, and kept on ice for 5min. The solution was centrifugated again for 5min at 500xg (4 °C), the supernatant was discarded and the pellet was resuspended in 3mL of PBSA buffer (PBS + 1% BSA) to wash the nuclei and prevent them clumping. After centrifugation for 5min at 500xg (4 °C), the supernatant was discarded and the pellet was resuspended in 0.5mL of nuclei resuspension buffer (PBSA + RNase inhibitor). The solution was filtered through a 35 µm cell strainer (352235, Falcon) to discard clumped nuclei, and kept on ice.

## 2.4 Fluorescence-activated cell sorting (FACS)

To get a clean solution of isolated nuclei, Fluorescence-activated cell sorting was done directly after nuclei isolation. The nuclei were processed as quickly as possible to avoid deterioration and apoptosis of the nuclei, which would be reflected in the transcriptome data. The FACS & Imaging Core Facility of the MPI for Biology of Ageing did the FACS sorting based on DAPI+ staining, to select nuclei regardless of the cell-type. Nuclei were stained with DAPI (1µg/µ L) and sorted on a BD FACSAria Fusion

(BD Biosciences) and a 70 $\mu$ m nozzle and 70psi shear pressure, with chillers to preserve nuclei. Singlet DAPI+ signal was selected to discard doublets, clumped nuclei, debris and floating ambient RNA.

## 2.5 Droplet-based methods for single-cell sequencing

### 2.5.1 Nadia Instrument

#### 2.5.1.1 *Nuclei encapsulation optimization*

The Nadia instrument from Dolomite Bio requires a certain ratio of beads and nuclei per droplet to avoid doublets and false transcriptome profiles. To assess the right amount of tissue needed to reach the ratio of nuclei to introduce into the Nadia Instrument, test-runs were done without adding the lysis buffer that would normally lyse the cells into the droplets. In that way, the nuclei concentration, the ratio of only encapsulated beads, only encapsulated nuclei, and both, were assessed. Multiple amounts of AL and DR WAT tissue from young mice (5 months) were used for nuclei isolation, ranging from 0.7g to 0.2g. After the isolation step, nuclei concentration was assessed with TC20 Cell Counter (TC20, Biorad), and the nuclei solution was diluted to reach 300k nuclei/mL. As indicated in the manufacturer protocol, Emulsion oil (QX200<sup>TM</sup> Droplet Generation Oil for EvaGreen), the nuclei suspension and the barcoded beads (Macosko-2011-10, ChemGenes) resuspended in *nuclease-free H<sub>2</sub>O* instead of the lysis buffer were loaded in the cartridge designed for encapsulation on the Nadia Instrument. After the run, the creamy emulsion was collected using a P1000 pipette and loaded into a Neubauer Haemocytometer counting chamber. Finally monodispersity of droplets and counts of nuclei, beads encapsulation was assessed using a Nikon microscope.

### 2.5.1.2 *Protocol for benchmarking dataset*

To assess which platform would yield better results, similar WAT samples were tested on the Nadia and 10X Chromium platform. 0.3g of sample from AL or of DR young mice (5 months) were used for nuclei isolation. Nuclei were processed on the Nadia following the manufacturer's protocol, from run on the Nadia Instrument for encapsulation and lysis to the creation of libraries. To summarize, after breakage of the emulsion, the cDNA libraries are made in several steps. Firstly, reverse transcription is done to get cDNA from mRNA captured on the beads, and exonuclease 1 treatment enables removal of the excess of primers that didn't capture mRNA. Then the cDNA that is still attached to the beads is amplified by PCR, 21 cycles were needed to get a working cDNA concentration for each sample. The number of cycles depends on the quality of the starting material and the capture efficiency. Beads were then washed with AMPure beads to get cDNA, which was measured on a TapeStation HSD5000. Finally, in order to sequence the captured transcripts, Nextera XT DNA libraries (FC-131-1024, Illumina) were used to add illumina indexes. The final Nextera products were measured on a TapeStation to confirm that the read length was between 500 and 680 bp. Libraries were sequenced in paired-end mode for 100 million reads of 100bp for each sample by the Molecular Genetics Sequencing Facility in Berlin.

## 2.5.2 10X Chromium

### 2.5.2.1 *Protocol for benchmarking the dataset*

In order to compare the data quality between the Nadia Instrument and the 10x Chromium, 0.3g of young (5 months) AL or DR WAT tissues were used on the chromium platform. Two experiments were done, one where the nuclei were loaded directly for the Chromium protocol, and another where the nuclei were sorted by FACS based on DAPI+ staining. When loaded directly, the concentration of nuclei per mL was assessed with aTC20 Cell Counter (TC20, Biorad), while with FACS a fixed we aimed for a fixed number of nuclei, in our case 8000. Library preparation and sequencing was done at the Cologne Center for Genomics. Sequencing was performed on an Illumina HiSeq 4000 (Illumina, San Diego, CA, USA) instrument with

PE100bp reads and an 8 bp index read for multiplexing, for 10 million reads per sample.

#### 2.5.2.2 *Protocol for the main dataset*

The main dataset had more conditions, chronic AL and DR at young (5 months) and old (24 months), and two time points of diet switch, ALDR16 and ALDR20 at 24 months. Three samples from 3 mice were pooled for each condition, with two replicates per condition. For each sample, 0.1g was taken from frozen WAT pads. The 12 samples were organized into 4 batches, with randomized samples, to avoid confounding effects. The pooling of the 3 samples per replicate was done from the beginning of the nuclei isolation protocol, where the tissue is cut and were homogenized using a douncer. After FACS sorting, approximately 8000 nuclei per sample were loaded onto Single Cell 3' Chip (10xGenomics, CA) per channel with an expected recovery rate of 2000–3000 nuclei. Library preparation and sequencing were done at the Cologne Center for Genomics. The Chip was placed on the 10X Chromium Instrument for Single Nuclei partitioning and to generate single nuclei gel beads in emulsion (GEMs). Single nuclei RNA-Seq libraries were prepared using Chromium Single Cell 3' Library and Cell Bead Kit according to manufacturer's instructions.

The molar concentration of the library was quantified and library fragment length was estimated using a TapeStation (Agilent, Santa Clara, CA, USA). Sequencing was performed on an Illumina HiSeq 4000 (Illumina, San Diego, CA, USA) instrument with PE100bp reads and an 8 bp index read for multiplexing.

## 2.6 Published sequencing datasets used in the study

### 2.6.1 Published RNA-seq data

To test deconvolution methods on white adipose tissue and assess differences in cell-types between WAT of mice from chronic and switch diets, we downloaded the corresponding RNA-seq data from a previous study on diet-switch from our laboratory

(Hahn et al., 2019). Datasets were downloaded from the GEO repository under accession ID GSE92486 and GSE124772 .

## 2.6.2 Published single-cell data

In order to infer cell-type proportions of RNA-seq bulk data, and analyze changes of proportions as a function of age and diet, we downloaded several single-cell or single-nuclei datasets of white adipose tissue to use as references.

The Tabula Muris consortium generated a compendium of single cell transcriptome data from 20 different mice tissues (Tabula Muris et al., 2018). The files of gene expression matrices, metadata, and annotation were downloaded through figshare (DOI: 10.6084/m9.figshare.5715040.v1). White adipose tissue data was captured with FACS-based full length transcript analysis, so no mature adipocytes were captured, only progenitors, but this dataset was used as a reference for the single-cell landscape of white adipose tissue. To match the datasets generated in our study, cells from female mice and from subcutaneous adipose tissue (inguinal pad) were selected.

Another single-cell dataset was used for deconvolution analysis, single-cell of WAT of mice published as a single-cell atlas of human and mouse white adipose tissue (Emont et al., 2022). Datasets, in the format of Seurat object, were downloaded from the Single Cell Portal (study no. SCP1376). Only cells from female mice and inguinal fat pads were selected.

## 2.7 Data analysis and statistical methods

### 2.7.1 RNA-seq data pre-processing and analysis

The Molecular genetics sequencing facility sent the raw reads in the fastq format. After assessing the reads quality with FastQC (Andrews, 2010), the reads were mapped to genome 105 of *Mus musculus* with Hisat2 (Kim et al., 2019) using the paired-end option. The resulting sam files were converted to a compressed bam format with Samtools (Tang et al., 2009), and the gene expression matrix generated by

featurecount (Liao et al., 2014). In addition, data visualization was performed using SeqMonk (<http://www.bioinformatics.babraham.ac.uk/projects/seqmonk>).

Analysis from the gene count matrix was done using custom R script, based on the Deseq2 (Love et al., 2014) package for differential expression analysis, prcomp (Buhmann, 2008) for PCA analysis and GGplot (Wickham, 2016) for plotting results. Gene expression levels were plotted based on normalized counts using Deseq2 normalization method, using the median of ratios. It takes into account the sequencing depth and the RNA composition. It first creates a pseudo reference sample that is equal to the geometric mean across all samples and then compute the ratio of each sample to this reference for every gene. Then the median of all ratios per sample is used as the normalization factor for the sample and is used to normalize the expression of all genes.

### 2.7.2 Processing of raw single-nuclei dataset

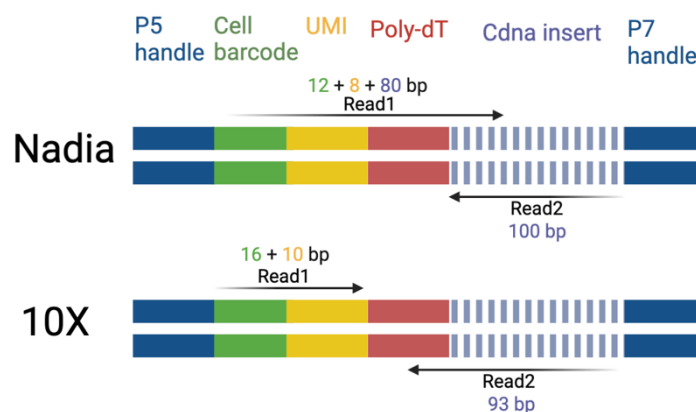


**Figure 2-3 - Read format structure from the Nadia Instrument and 10X Chromium protocols.**

*The Nadia Instrument protocol generates paired end reads of 100bp, read 1 having the cell barcode the UMI and the end of the cDNA insert. Read 2 has the beginning of the cDNA insert. 10X Chromium protocol generates paired end reads as well, but Read 1 only has the cell barcode and the UMI, while Read 2 has the cDNA insert.*

### 2.7.2.1 *Dataset generated from Nadia instrument*

Raw reads were again provided as fastq files from the Molecular genetics sequencing facility, and were first tested for quality with FastQC (Andrews, 2010).

To obtain matrix of gene count per cell, the protocol entitled Drop-seq Core Computational Protocol (Nemesh, 2015) was followed, since it deals with the different customs tags used in the Nadia's protocol. After quality check using FastQC, the first step was to trim the reads to remove the Nextera adapter and cDNA primer used for amplification with Trimgalore (Krueger, 2012) (v.0.6.5, parameters: -- paired --length 60, --a2 G TACTCTGCGTTGATACCACTGCTT ). Trimmed reads were then converted from fastq to unaligned and unpaired bam format files with the Picard toolkit (Institute, 2018), with FastqtoSam function. Then the Drop-seq-tool (Nemesh, 2015) was used to extract bases from the cell barcode and the UMI barcode and tag each bam entry with correct identification barcodes. The function TagBamWithReadSequenceExtended was used with the parameters "BASE\_RANGE=1-12 TAG\_NAME=XC" for cell barcode and "BASE\_RANGE=13-20 TAG\_NAME=XM" for UMI barcode (**Figure 2-3**). Afterwards, reads where the cell or molecular barcode were of low quality were removed with Drop-seq\_tools function FilterBam. With trimmed reads and cell and molecular barcodes extracted, reads could be aligned on the genome but first they needed to be converted back to fastq format, using SamToFastq function from Picard program. The alignment step was done with STAR program version 2.7.3a with the following parameters "-- genomeDir Star\_index\_273a\_92 --outFileNamePrefix star --outFilterScoreMinOverLread 0.4 --outFilterMatchNminOverLread 0.4". The custom index was made with STAR's function genomeGenerate, supplying GENCODE annotation (Frankish et al., 2021) (release M20, primary assembly) and the following parameter "--sjdbOverhang 92". Then the aligned sam files were sorted and compressed into a bam format with Picard's function SortSam. Having the sorted aligned bam file and the unaligned bam having the cell and UMI barcodes, those two bam files were then merged to a single bam file with MergeBamAlignment from the Picard program. Reads were then single-end, trimmed, aligned, tagged with cell and molecular barcodes. In addition, Drop-Seq\_tools' function TagReadWithExonFunction and TagReadWithGeneFunction were used with the same annotation file used for alignment, to get information on which reads match which gene. To finish a function was used to get an expression

matrix, DigitalExpression from Drop-seq\_tools, with “NUM\_CORE\_BARCODES=1 LOCUS\_FUNCTION\_LIST=INTRONIC” so that cells that have at list 1 read would be reported in the matrix and that intron information would be counted.

### 2.7.2.2 *Dataset generated from 10X Chromium*

According to the 10Xgenomics three chemistry, the first 26 bp of Read 1 consist of the cell barcode and the UMI, and the last 74 bp on the read are not used. Read two contains the single cell transcripts (**Figure 2-3**). Digital gene expression matrices (DGEs) were obtained using 10x Genomics’ Cell Ranger v4.0.0 software suite. The bcl files obtained from the Cologne Center for Genomics were demultiplexed and converted to fastq files using the mkfastq function in Cell Ranger. The counts function in Cell Ranger was used to generate DGEs from the fastq files. The resulting fastq files are aligned to a reference genome (refdata-gex-mm10-2020-A\_premrna). Reads which align to exonic and intronic regions were used, since nuclei experiment is resulting in lower mRNA quantities, intronic information can be useful for cell type identification. Then, additional filtering was carried out using R (team, 2013) and the Seurat package (Hao, Hao et al. 2021). Single cells were identified from background ambient mRNA using (Gao et al., 2015) thresholds of at least 100 genes expressed, genes kept if they were detected in at least 10 cells and a maximum mitochondrial fraction of 2%.

### 2.7.3 Single-nuclei data analysis

#### 2.7.3.1 *Cell-type identification*

The Seurat R package version 4.0.0 (<https://github.com/satijalab/seurat>) was used to preprocess raw matrix files, perform quality control, filtering and normalization, and integrate the replicates for each condition. The method identifies across the datasets, pairs of cells that are in a matched biological state (‘anchors’). These anchors are used to correct batch effects or other technical differences, and integrate multiple datasets by matching shared cell populations across datasets. In our case, we matched similar cell population across replicates, and followed with the usual steps of scRNA-seq

analysis. For each condition all sequenced cells were processed by a Principal Components Analysis, to lower the dimensionality of the dataset. The first 30 principal components were used in another dimensional reduction technique, the Uniform Manifold Approximation and Projection (UMAP). The specified parameters for the function are 'min.dist=0.5' and 'spread=0.8'. The same package was then used to construct a nearest-neighbor graph to identify clusters of cells by optimization of modularity function. Only the resolution parameter in the FindClusters() function was changed depending to the dataset (0.6-0.8).

We defined specific genes markers for each cluster in each condition by using the FindAllMarkers function in Seurat. It identifies differentially expressed genes in each cluster by comparing it to all of the others using a Wilcoxon Rank Sum test. Gene markers can be shared between clusters. To be used in the analysis, the gene had to be expressed in at least 20% of the single cells of one of the clusters and there had to be at least a 0.30 log fold change in gene expression between the groups.

To identify cell type identities, multiple approaches were used. First, we used the top gene markers of each cluster and looked at already published and annotated dataset via tools like ScFind (Lee et al., 2021), a search engine for cell atlases. Another approach was to use the R package SingleR (Aran et al., 2019), an automated cell type assignment based on gene marker correlation with reference datasets.

### 2.7.3.2 *Functional enrichment*

All clusters were tested for significant enrichment of annotated gene sets obtained from MsigDB (Subramanian et al., 2005) (Liberzon et al., 2015): GO Biological Processes, Curated gene sets and Hallmark. The enrichment analysis was done by two R packages, VISION version 2.1.0 (Rosen, 2022) and clusterprofiler (Wu et al., 2021). VISION has a workflow that provide gene set enrichment analysis on genes differentially-expressed between groups. Clusterprofiler was used to detect enrichment of the different hallmarks in each cluster using over representation analysis, p-values being calculated by a hypergeometric distribution and adjusted with multiple testing analysis with the Benjamini-Hochberg method. Results from different approaches were compared to validate cell type assignment to each cluster, and to get insight on their biological function.

### 2.7.3.3 *Differential gene expression analysis*

The Seurat package was used for differential expression testing within clusters of the same condition. It identifies differentially expressed genes between two groups of cells using a Wilcoxon Rank Sum test. To compare clusters between conditions the R package Desingle (Miao et al., 2018) was also used. It takes into account the sparsity of single-cell data where, in addition to difference in expression abundance, there is difference in proportion of zeros.

### 2.7.3.4 *Statistical analysis*

Overlap of gene list were tested for significance using Fisher's exact test in comparison with a genomic background. The null hypothesis is that the odds ratio is no larger than 1.

To assess the accuracy of the prediction from deconvolution methods, Pearson correlation was used, which measures the relation strength of a linear association between two continuous variables. A value greater than 0 indicates a positive association, the closer to 1 being the strongest association. Another measure was used, the Root Mean Square Error (RMSE) which is the standard deviation of the residuals (prediction errors). High values of residuals signify, larger differences between models' predictions and actual values. Additionally, performance between methods were compared using the mean of their Pearson correlation per sample with Kruskal-Wallis or Anova, depending if the data were normally distributed or not.

### 2.7.4 Deconvolution analysis

To assess cell-type proportions in bulk RNA-seq datasets, deconvolution methods can be used. In our case, to extract changes in cell-type proportions depending on age or diet, multiple datasets and pipelines were tested. Deconvolution methods that are reference-based need two inputs, the bulk RNA-seq from which proportions need to be inferred, and corresponding single-cell or single nuclei datasets. In this project, bulk RNA-seq datasets of white adipose tissue were tested, firstly the previous diet-switch dataset from our lab (Hahn et al., 2019) and, second, the current multiple time point

diet switch bulk RNA-seq dataset. As references, single-cell datasets from Tabula Muris (Tabula Muris et al., 2018), single-cell WAT atlas (Emont et al., 2022), and the single-nuclei dataset generated from our study.

Three deconvolution methods were tested, Cibersortx (Steen et al., 2020), a method accessible through a web tool, and two R packages, SCDC (Dong et al., 2021) and MuSiC (Wang et al., 2019). The methods were selected using results from benchmarking studies on deconvolution methods for transcriptomics data (Jin & Liu, 2021) (Avila Cobos et al., 2020), and if they were fitting our data and question.

All three methods were first tested with Single-cell data from Tabula Muris (Tabula Muris et al., 2018) and WAT atlas (Emont et al., 2022), converted to a pseudo-bulk dataset so that the estimation of each deconvolution method could be compared to the real known proportions. Then we used our dataset of Single-nuclei data to assess if performance of the deconvolution methods were modified by using single-nuclei instead of single-cell data as reference. Finally, MuSiC and SCDC were used to predict cell type proportions in the first diet switch RNA-seq dataset and the one generated from this study with multiple time switches.

To access Cibersortx tool, an account needs to be created to use the online tool, and all steps are done online. The first step is to create a Signature Matrix from the single-cell dataset, this will serve as reference with selected gene markers of each cell-type. Then the bulk data is deconvoluted using the signature matrix to get cell-type fraction estimation. The output is available as a data frame to be downloaded.

The MuSiC package needs two type of input, raw read counts for bulk sample to deconvolute and multi-subject single cell expression with associated cell-types. The MuSiC model is based on derivation of the relationship between RNA-seq bulk expression and cell type gene expression in single-cell. It uses a weighted non-negative least squares regression (W-NNLS) and attributes weights to informative genes, if they have consistent expression profile across similar subjects and if they can differentiate cell-type clusters. The input data, bulk and single-cell need to be under the format of an expression set. To get proportions, the function 'music\_prop' is used with input datasets, and parameters indicating the name of the cell-types to deconvolute, and a vector with the ID of different samples.

SCDC uses single-cell dataset of multiple samples as input. Its method is based on weighted non-negative least squares regression and it measures the quality of the reference datasets to remove potentially misclassified cells and adjust how they can contribute to the estimation of cell type proportions accordingly. Estimations are conducted for each reference datasets separately, then the results are combined and weights are attributed to each dataset, with higher weights to the ones that recapitulate better the cell-type profile mixture. For the SCDC package, Seurat objects with raw expression counts were transformed into the format 'expression set' via the function `getESET()` to be used in the pipeline. Then quality control was done on the reference sample removing all cells that had poor quality or seemed to be wrongly associated to a cluster, via the function `SCDC_qc()` with parameters `qcthreshold=0.7`. Proportions were estimated with the function `SCDC_prop()` and, to make easier interpretation, some cell-types were gathered in categories as follows : Macrophage and Myeloid cell as Immune cells and Precursor and Progenitor as Progenitors.

### 3 Optimization of methods to analyze single-nuclei sequencing data from murine white adipose tissue

## 3.1 Introduction

### 3.1.1 Characterization of the murine WAT at the single cell level

The white adipose tissue is a highly active metabolic tissue, understanding its role and its composition is crucial to better understand metabolic diseases. The majority of early research relied on bulk sequencing, which is effective for tissues with a limited number of cell types but inadequate for the WAT. A lot of diverse cell-types are present in the tissue, adipocytes are the main cell-type, but mesenchymal stem cells, progenitors of adipocytes, support cells like endothelial cells or immune cells have also important roles and impact the tissue function. The impact of each cell-type, by its gene expression or its proportion in the tissue is lost with bulk sequencing approach. Thanks to recent advances in transcriptomics approach, developing multiple methods to look at the single-cell level, a better characterization of this tissue was made possible. Single-cell RNA sequencing methods enable the transcriptome of multiple cells to be captured in an unbiased and high throughput approach. Previous studies generated single-cell WAT dataset, with sorted and targeted cells, losing the benefit of an unbiased approach and missing potential new cell-types (Hildreth et al., 2021). Other studies used a high-throughput approach with droplet sequencing but then focused on the stromal fraction or pre-adipocyte and missing information on mature adipocyte (Vijay et al., 2020). Mature adipocytes are the main functional cell type of WAT, but their large size, high lipid content and fragile nature presents a challenge for single-cell, droplet-based methods (Hagberg et al., 2018). Targeting nuclei, instead of cells, is an alternate method (sNuc-seq) to capture single transcriptomes regardless of cell shape or size and has been widely used for brain datasets (Lake et al., 2016). At the start of this study there was no protocol available for sNuc-seq of the WAT. Therefore, I first established a single-nuclei protocol, from nuclei isolation to sequencing, for the WAT.

### 3.1.2 Cell-type deconvolution of biological data

Even if the number of single-cell datasets is rapidly increasing, yet it is not always possible to generate single-cell data because of the laborious and expensive protocols. Doing a bulk RNA-seq analysis remains the easiest way to get relevant and extensive transcriptomic information on a sample, but it does not capture the cell-type heterogeneity. Still, it is possible to estimate cell-type proportions from a bulk RNA-seq sample, by using a deconvolution method (Avila Cobos et al., 2018). To deconvolute is to resolve something into its constituents, by removing the complexity of it. In genomics, deconvolution methods can be used to extract and estimate information from gene expression levels. The main goal of deconvolution methods is to estimate cell-type proportions from a mixture from cells of a bulk RNA-seq sample, but also in the case of tumors analysis, estimating tumor clonality (Lei et al., 2020) or purity (L. Wang et al., 2020). The initial hypothesis for deconvolution is that the mixture of gene expression signals follows a linear mixed model. The level of expression for a gene  $M$  observed in bulk sample equals the sums of the proportions of each cell type  $P$ , multiplied by the gene expression level for each cell-type  $C$  (Avila Cobos et al., 2018). The aim of a deconvolution method is to obtain  $P$ , by using known  $M$  and  $C$  (**Figure 3-1**). To estimate cell-type proportions  $P$ , if  $M$  is a bulk sample,  $C$  should be a specific cell-type gene expression measurement, usually a single-cell dataset with individuals cells associated to known cell-types.

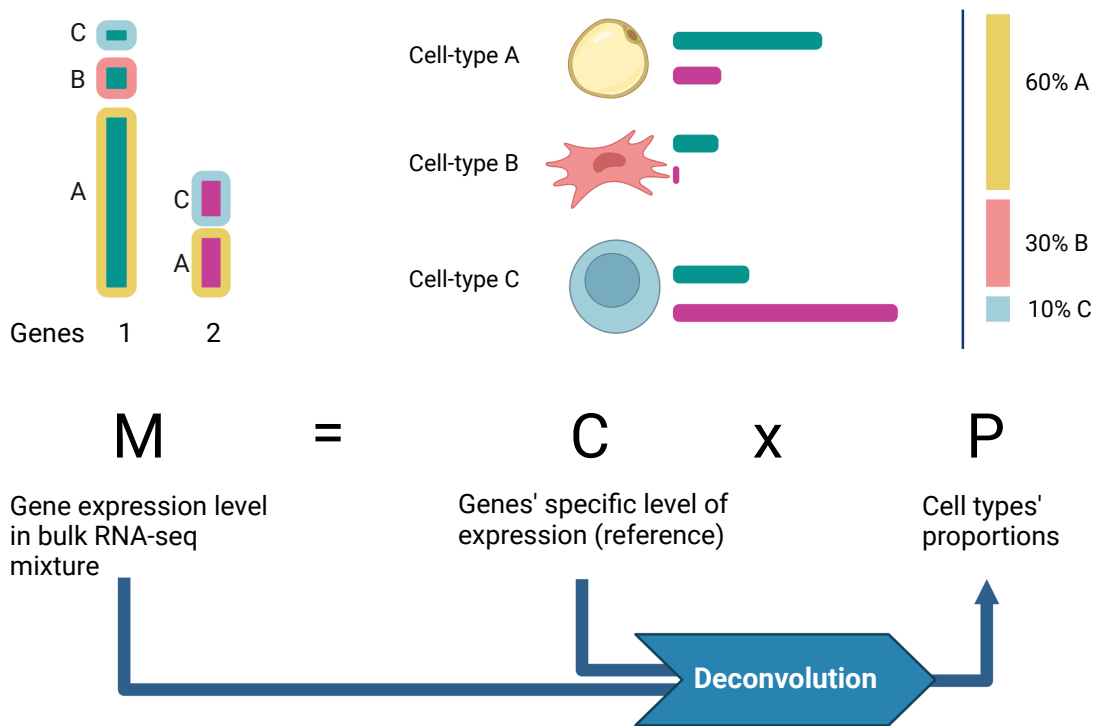


**Figure 3-1 Deconvolution application to cell composition analysis**

*Schematic illustration of the deconvolution of bulk RNA sample to extract cell type composition.  $M$  is a matrix of gene level expression; each gene expression level is a sum of the mixture from all cell types.  $C$  is the specific level of expression for each gene per cell type.  $C$  is the reference dataset used to extract the cell type proportions  $P$ , from  $M$ , using a deconvolution method.*

Depending on the deconvolution method used, the input can either be profiles of a few cells per cell-types, or single-cell datasets of multiple samples, or just a few known gene markers per cell-type and their respective levels of expression. Methods are also distinguished between supervised, where the cell-types are known, and unsupervised where the cell-types to estimate and specific expression profiles are unknown. Supervised methods demonstrated better results in benchmarking studies compared to unsupervised (Avila Cobos et al., 2020).

In addition to the input data varying between methods, the type of deconvolution model is also evolving, with more complex models and precise prediction in the most recent approaches. Most are based on regression models, such as support vector machine for Cibersort (Steen et al., 2020) or weighted non-negative least squares regression

for MuSiC (Wang et al., 2019) but also some methods use enrichment like xCell (Aran et al., 2017).

Studies were done to compare the accuracy of results between different type of deconvolution packages, using a pseudo-bulk dataset as input. By merging all cell transcriptomic profiles from a single-cell dataset, it is possible to create a pseudo-bulk dataset with known cell-type proportions, which enables to validate the results of a deconvolution method. Benchmarking studies showed that supervised methods using multiple single-cell samples were the most accurate since they can better estimate the variability between samples (Avila Cobos et al., 2020). Nevertheless, few studies look at the impact of single-cell or single-nuclei as input dataset, like we had in our study. Bulk RNA-seq datasets are made from a mixture of complete cells, taking RNA transcripts from all compartments, while single-nuclei only account for genes present in the nucleus. One study compared deconvolution results of bulk RNA-seq data with single-cell and single-nuclei data coming from the same brain samples (Sutton et al., 2022). Accordingly, the single-cell cell-type estimation outperformed the ones based on single-nuclei data. Only when they filtered and kept genes located in the nuclei in the bulk samples, prediction of single-nuclei data matched the ones based on single-cell data.

Based on the benchmarking reviews assessing the pros and cons of each method, we selected the best deconvolution methods that were fitting our input dataset. Since we had two replicates of single-nuclei data for multiple conditions, we selected only supervised methods that can take into account variability from multiple samples, MuSiC and SCDC. We also used Cibersort, which is one of the most cited and versatile method. We first evaluated their performances using single-cell and single-nuclei data of WAT, from our dataset or published ones. By finding the optimal deconvolution pipeline for WAT sNuc-seq, we would then be able to estimate the cell-type proportion in our bulk dataset. This would be used to verify if we could observe the same change in population size as the ones observed in single-nuclei data between conditions.

## 3.2 Results

### 3.2.1 Optimization of single nuclei sequencing protocol for WAT

#### 3.2.1.1 Determination of parameters for optimal nuclei isolation

Nuclei isolation was the first step of establishing a protocol for droplet-based single-nuclei sequencing of WAT. In order to get a solution of isolated nuclei we used the protocol explained in the initial DroNc-seq publication “Massively parallel single-nucleus RNA seq with DroNc-seq” (Habib et al., 2017). The first attempt of nuclei isolation was done using the same protocol as the DroNc-seq publication, and using young (5 months) mice under chronic AL feeding. Nuclei were stained with DAPI in order to distinguish them from the background.

Although, we observed nuclei but also a lot of them were clumped together (**Figure 3-2 A**), which is problematic as they might be encapsulated together and thereby confound the single cell transcriptomic profiles. Another issue was the high amount of lipid droplets floating in the solution (**Figure 3-2 B**) which could negatively affect the encapsulation process since it is based on a flow of different lipid droplets.

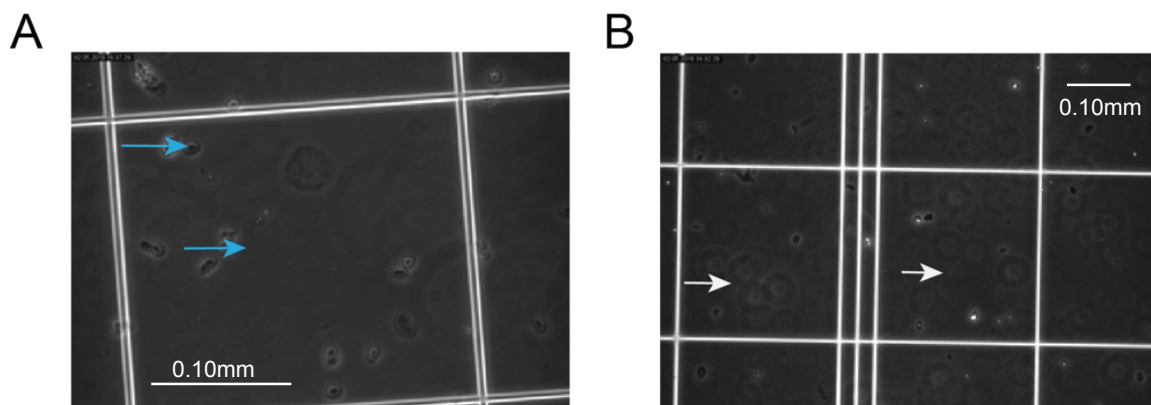


**Figure 3-2 Nuclei isolation based on the unmodified DroNc-seq protocol**

**A** – Representative image of isolated nuclei in solution, clumped nuclei are designated by blue arrows. **B**- Representative image of isolated nuclei in solution, lipid droplets are designated by white arrows.

Additionally, we observed that the nuclei should have been condensed in a pellet following centrifugation and incubation in the lysis buffer, but there was also a layer of floating fat remaining (**Figure 3-3**). We then repeated the protocol on both fractions

separately to see if nuclei were also contained in the fat layer and therefore would be lost for the analysis.

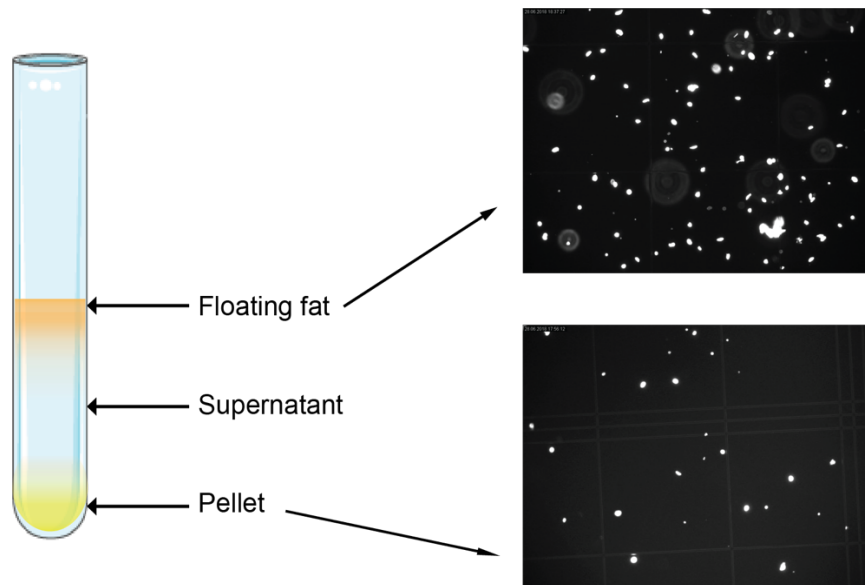


**Figure 3-3 Nuclei solution after cell lysis and centrifugation**

*Schematic representation of nuclei solution after cell lysis and centrifugation with 3 fractions from up to bottom, a layer of floating fat, the supernatant, and the pellet where nuclei are concentrated. Representative image of isolated nuclei DAPI stained from the layer of floating fat (top) and pellet (bottom).*

We noticed the presence of nuclei in both fractions, the fat fraction having more clumps and lipid droplets compared to the pellet. To get the nuclei from the fat fraction, one option was to process each fraction separately and pool them together at the end of the protocol but this could have created a bias depending on how both fractions were handled. Instead, we tested several incubation times with the lysis buffer right after the tissue homogenization with a douncer. This was to see if a longer incubation time could enable the nuclei of the fat layer to be collected in the pellet with the rest of nuclei. Nuclei were incubated for 30 and 20 min before centrifugation (**Figure 3-4.A**) In the test with 30min incubation there was no nuclei left from the fat fraction, but the nuclei collected in the pellet were either clumped or with altered shaped, and presence of lipid droplets in the solution (**Figure 3-4.B**). In contrast, after 20min incubation, we observed few nuclei in the fat fraction and a lot more in the pellet fraction (**Figure 3-4.C**). After counting using a cell counting chamber, 95% of the nuclei were from the pellet, and more importantly nuclei were well isolated and lipid droplets were not noticeable.

Using this modified protocol additional adjustments were made to optimize the final solution of nuclei. An additional washing steps was done to remove most of the lipid droplets and fat in the solution. At the end, nuclei were resuspended in a solution of PBS, RNase inhibitor and BSA at 0.01% which prevented clumping of nuclei. Finally, the last parameter to adjust was the initial quantity of tissue used for the experiment, since a certain concentration of nuclei is required for droplet-based sequencing. Not enough tissue could lead to an insufficient number of nuclei, while a too much would increase the clumping of nuclei since they tend to stick together and create large clumps. After several test with different amount of fat tissue, an amount of 0.2g was used for the following experiments.

From the initial Dronc-seq protocol, after several testing experiments, we adapted the protocol to the WAT, to collect most of the nuclei present in the tissue, remove lipid droplets and in a limited time to avoid potential alteration and stress of nuclei.

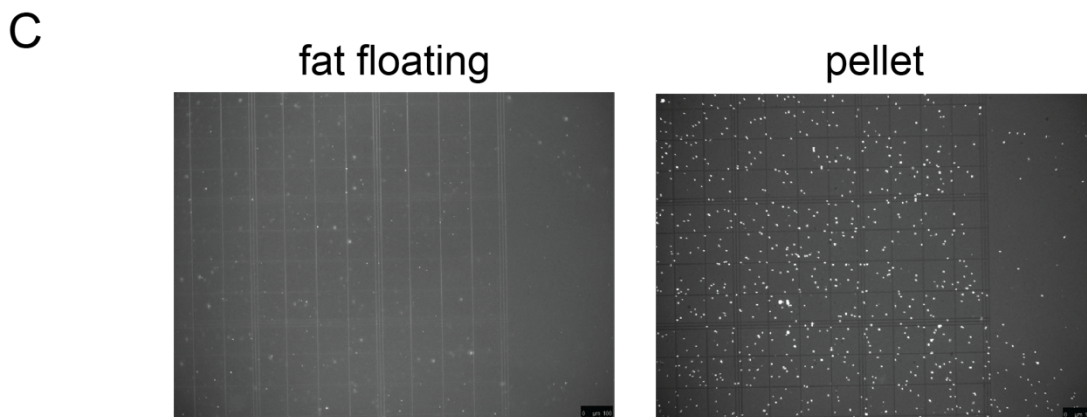
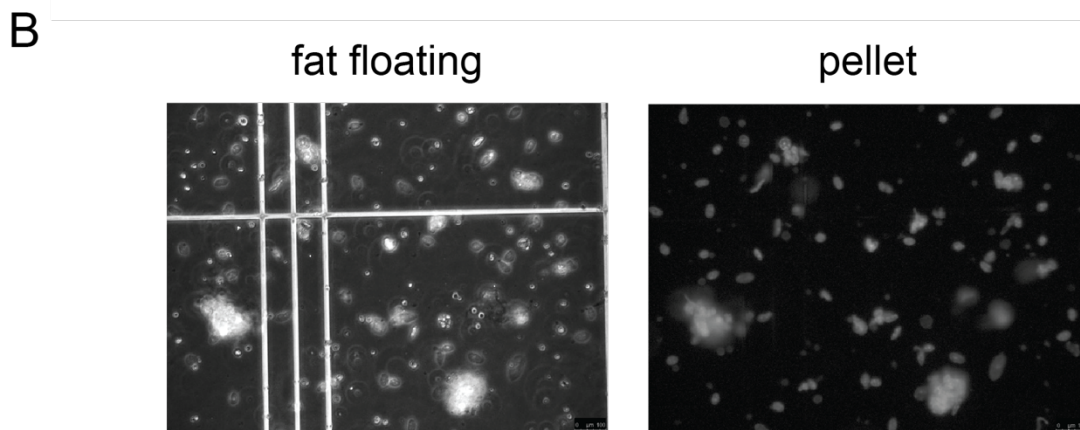
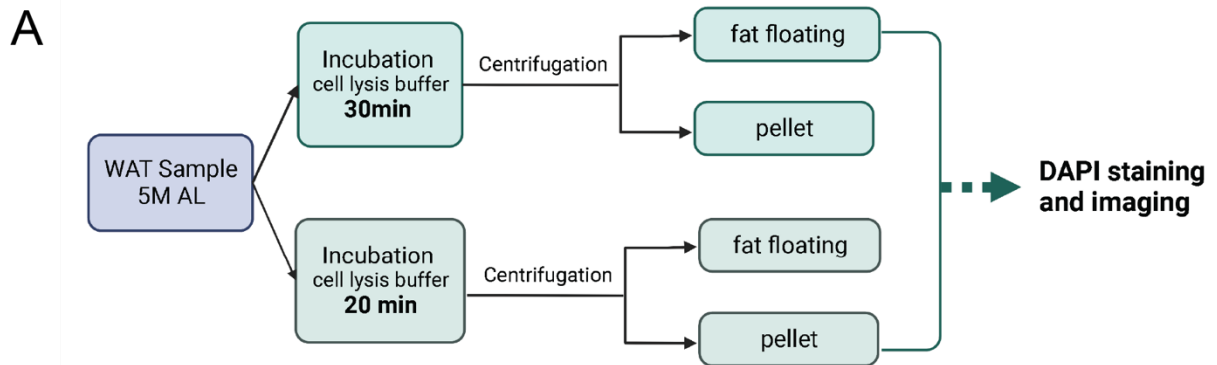


**Figure 3-4 Testing protocol to extract all nuclei from fat layer**

**A** – Schematic diagram of the test protocol with 2 incubation times and nuclei imaging from both fractions, fat and pellet, in each case. **B**- Representative images of isolated nuclei in solution, from fat floating fraction and pellet after 30min incubation in cell lysis buffer. **C**- Representative images of isolated nuclei in solution, from fat floating fraction and pellet after 20min incubation in cell lysis buffer.

### 3.2.1.2 *Benchmarking of dropletisation platforms*

#### 3.2.1.2.1 10X Chromium test-run with adipose nuclei

After establishing the protocol to obtain a comprehensive representation of nuclei from white adipose tissue, we tested two dropletisation platforms, Nadia Instrument of Dolomite bio and Chromium Controller from 10X Genomics. Both instruments are used to generate droplet in which cells or nuclei transcriptomes are captured on beads with a unique tag, generating specific transcriptomes. The first goal was to assess which platform would provide the best results but also which one was the most balanced option to have an extensive experimental design that would answer our biological question while keeping a reasonable cost. The initial plan was to use the same samples to do nuclei isolation and process half of the nuclei on both instruments so that only technical parameters would influence the results. Technical issues prevented the realization of this experiment, so instruments were tested with different nuclei isolation solution but from the same conditions, young AL and DR.

For the first try with the 10X Chromium, the nuclei were loaded in the instrument after isolation. The cDNA concentration was low in both samples when compared to other type of tissue samples, so additional PCR cycles were needed to have enough cDNA and make libraries. After further amplification, 5ng was collected for AL sample and 15ng for DR samples. Libraries can be done with 2ng, so both were processed to make libraries and were sequenced shallowly with 10 million reads per sample, to detect if there was presence of cells and if they had biological relevance to our samples.

From the first quality assessment with FastQC (Andrews, 2010) on the raw reads, we detected several issues, low quality on the two last bases of the UMI, which would impact the quantification of gene expression, and high levels of duplication levels either caused by the additional PCR cycles or error in measurement of duplication because of faulty UMIs. After mapping reads with Cellranger software (Zheng et al., 2017) to generate expression matrices, 12209 genes were detected in 2308 estimated cells for DR and 10611 genes in 990 estimated number of cells for AL. Cellranger displayed several warnings, notably the percentage of reads mapped to the genome and the fraction of reads in cells being low. Approximately 40% of the reads were mapped to the genome and 30% of the reads would be associated to cells in both

conditions. Those numbers showed that a lot of cDNA that was amplified didn't bring any biological meaningful information.

From the expression gene matrices, more filtering steps and downprocessing analysis were done with the R package Seurat (Hao et al., 2021). After filtering to remove doublets cells, cells with low number of genes detected, and high percentage of mitochondrial genes which is an indicator of apoptosis, the number of cells estimated dropped to 360 for AL and 666 for DR. Also, the number of genes detected in cells decreased to 1224 in AL and 1641 in DR.

Despite the low quality of the data, further analysis was done to see if there was a biological link between the nuclei collected and the conditions of each sample. To do so, gene expression data from each sample were first analyzed using UMAP and unsupervised Louvain clustering method, so that cells with similar profiles would be clustered together. From those clusters, gene markers are extracted as genes that were positively differentially expressed in one cluster compared to all others, making those genes specific signatures of those clusters that can be potentially be associated to a cell-type.

We detected 4 clusters in AL and 3 in DR (**Figure 3-5.A**). In DR the two largest clusters were almost merged, while AL clusters were well separated. From the gene markers collected, we could identify that the main cluster in AL, cluster 0, would represent adipocytes, from high expression of *Ghr* (Ran et al., 2019), *Tshr* (Lu et al., 2012), *Slc1a3* (Krycer et al., 2017) that are genes found in mature adipocytes (**Figure 3-5.B**). Similarly, the clusters 0 and 1 in DR seemed to have the same gene markers, suggesting that those clusters would be mature adipocyte as well. In AL the next larger cluster, cluster 1 had upregulation of genes that are found in fibroblasts or adipocyte progenitors, cluster 2 had also some markers of fibroblasts but the cell-type profile wasn't specific enough to be assigned, and the last cluster, cluster 3 displayed upregulation of genes found in myeloid cell, such as *Myo1f* (Piedra-Quintero et al., 2019) or *Runx1* (Himes et al., 2005). Cluster 2 in DR had also markers of fibroblast but again not specific enough to be attributed a cell-type.

For this first try, with really low-quality data, and shallow sequencing, we could observe the capture of transcriptome from mature adipocytes, but also differences between conditions, notably presence of immune cell-type in AL and not in DR, and the capture of nuclei from mature adipocytes. This information motivated the optimization of the

protocol to improve capture of reads that would map to the genome and belong to specific cells.

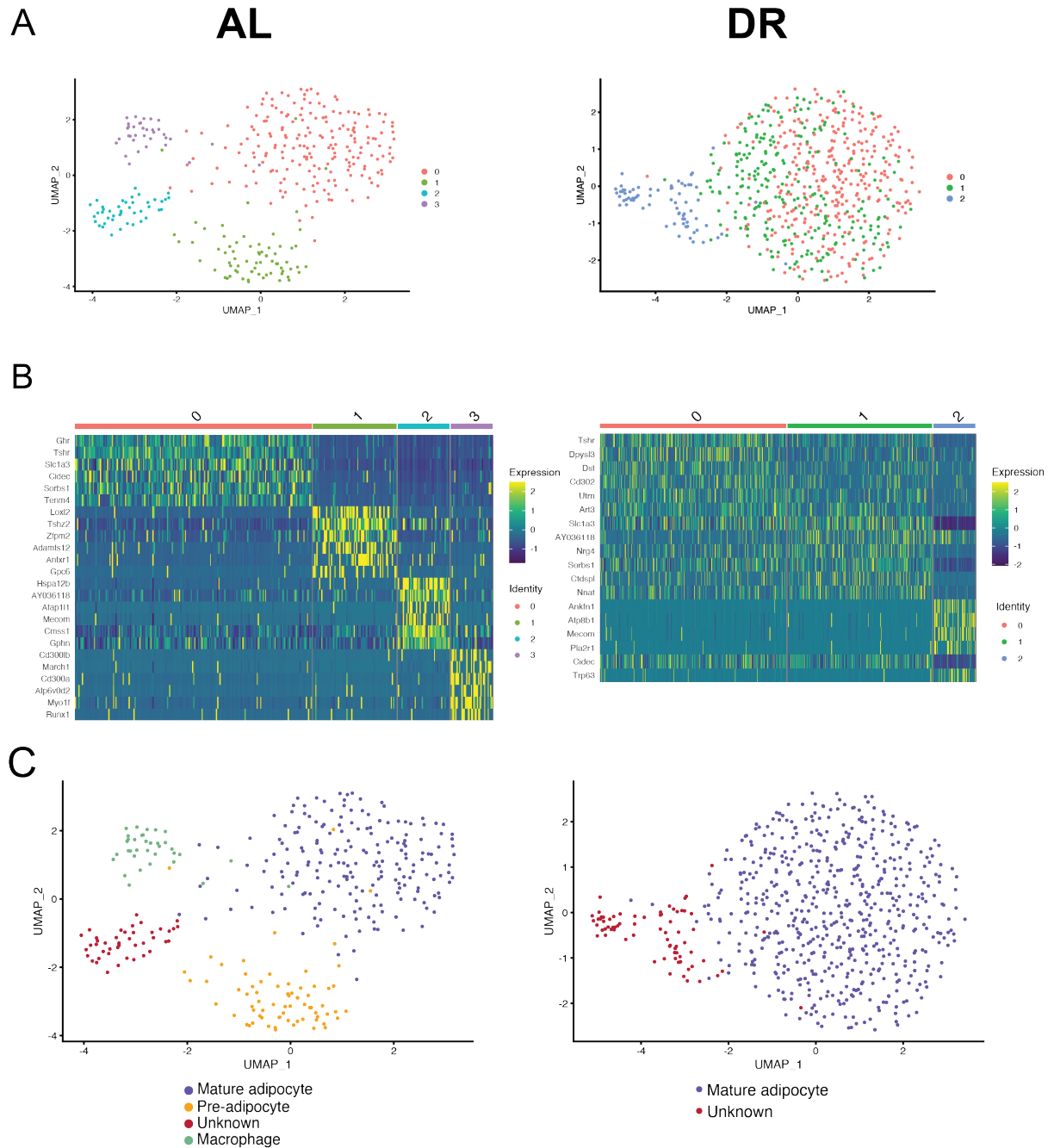


**Figure 3-5 SNuc-seq dataset of young AL and DR from 10X Chromium**

**A** – Uniform manifold approximation and projection (UMAP) two-dimensional map from unsupervised Louvain clustering, of nuclei from AL and DR condition at young age (5 months)

**B**- Heatmap showing the gene expression of the top six differentially expressed genes in nuclei per cluster in AL and DR condition at young age (5 months). Nuclei are represented in columns and genes are represented in rows. Colored bars indicate clusters assigned to both

cells and genes. **C-** Uniform manifold approximation and projection (UMAP) *two-dimensional map of nuclei with cell-type assigned, from AL and DR condition at young age (5 months)*

#### 3.2.1.2.2 Nadia Instrument test-run with adipose nuclei

The alternative option to 10X Chromium was to use the Nadia Instrument. One advantage of the Nadia Instrument is the transparency of the protocol, adjustment can be done during the encapsulation phase and afterwards, which enable to design a specific protocol for a specific experiment. The downside compare to 10X chromium, is the difficulty of execution of the protocol to obtain libraries, and in addition, the bioinformatic processing of the data is more challenging since there is no dedicated pipeline to do it. To compare both platform similar biological conditions were used, AL and DR from 5 months mice. After dropletisation, additional PCR cycles were required, like in the experiment with 10X chromium, to generate enough cDNA to build libraries. To obtain the most of those libraries, each sample was sequenced for 40 million reads. From the first quality assessment with FastQC, a lot of duplicate reads were detected, which might have come from the deep sequencing and over-amplification, but the overall quality of the reads was good. After processing the raw reads with a customized pipeline to create the gene expression matrices, Seurat was used to pre-process the data and estimate the number of nuclei and genes detected. For DR sample, 641 nuclei were estimated with 4418 genes detected, and 703 nuclei with 4388 genes for AL sample (**Figure 3-6.A**). After dimension reduction analysis with UMAP and unsupervised clustering using Louvain method, 4 clusters were found in each condition. The genes markers detected for each cluster were less informative than the ones found with 10X chromium data. Most of the gene markers were not linked to a specific cell-type but were found in the nucleus regardless of the cell-type, which made the identification of clusters difficult. In AL the larger cluster, cluster 0 had no positive gene markers associated, meaning that no genes were significantly upregulated in this cluster compared to other clusters (**Figure 3-6.B**). Because of the lack of gene markers, cluster 0 was not associated to a potential cell-type. The second cluster, cluster 1 showed upregulation of genes unspecific to cell-types but also *March1* (Galbas et al., 2017), which is enriched in macrophages, which could indicate a cluster of immune cells. Cluster 2 had positive upregulation of unspecific genes located in the nuclei such as *Rbm25* or *Luc7l3* but also immune related genes such as *Zeb2* upregulated in macrophages from immune response (Scott et al., 2018). That

information might also suggest the presence of immune cell clusters, however this assumption cannot be supported by the lack of several robust immune cell gene markers. The last cluster, cluster 3, which has the less nuclei, had positive markers of mature adipocytes such as *Ghr*, *Nnat* (Ka et al., 2017) or *Sorbs1* (Yang et al., 2003). In DR cluster 0 had a similar profile as cluster 1 in AL, and could be associated to immune cells. Cluster 1 had gene markers associated to adipocytes while cluster 2 gene markers of pre-adipocytes. Finally, the last cluster, had gene markers unspecific of cell-types and was not associated to a particular cell-type.

The overall results from the Nadia were not convincing, with 4 times deeper sequencing than with 10X chromium, the results were not more informative. The number of nuclei collected increased for both conditions and the number of genes detected, but most of the gene markers for the clusters were not cell-type specific but expressed in the nuclei, which didn't help for cell-type identification. Overall, the data quality was not good enough to do further analysis and extract any biological information. For example, the small population of adipocyte and absence of pre-adipocyte in AL didn't seem to fit with the observation made with the 10X data or previous publication of drop-seq (Tabula Muris et al., 2018).

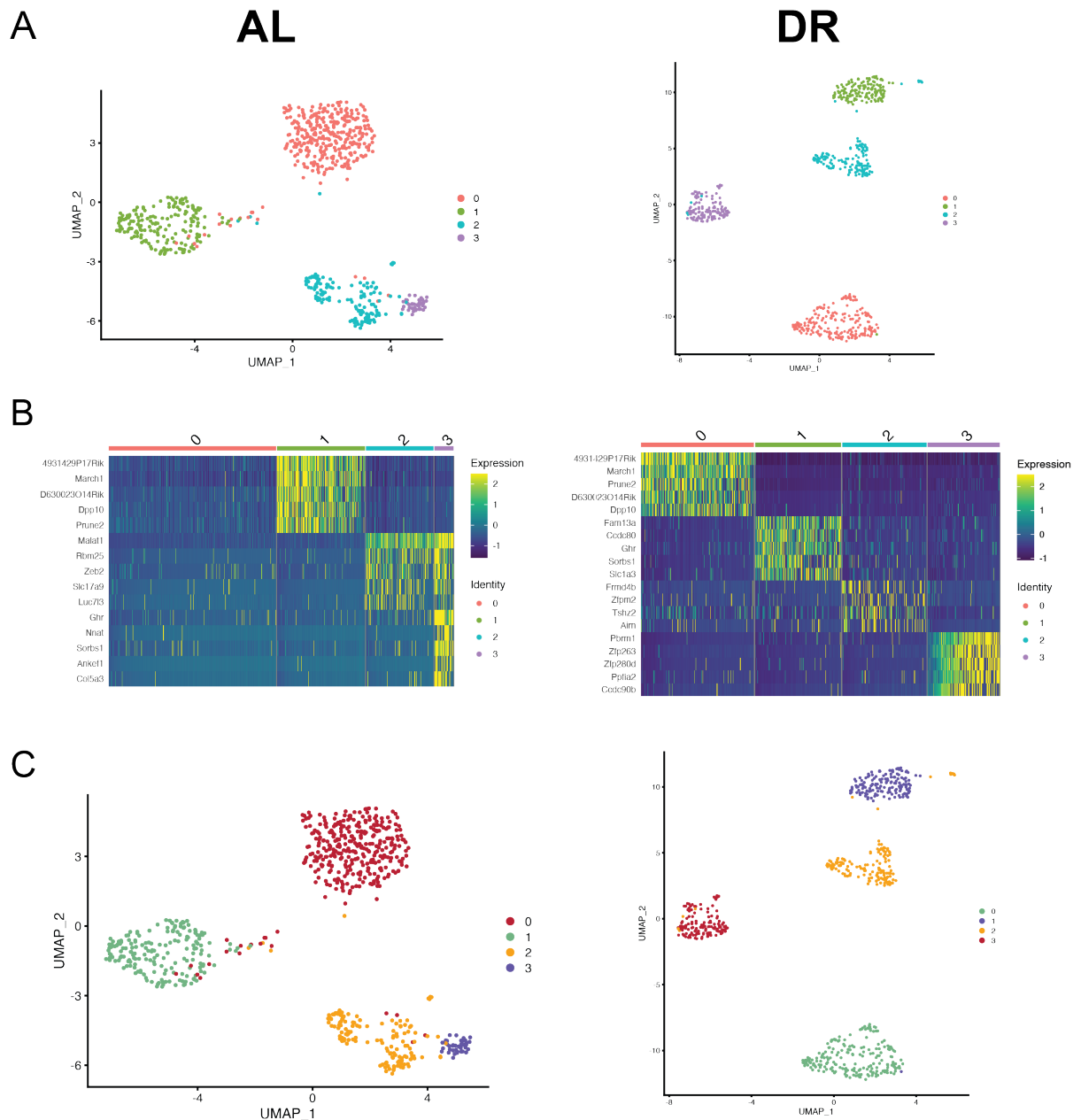


**Figure 3-6 SNuc-seq dataset of young AL and DR from Nadia Instrument**

**A** – Uniform manifold approximation and projection (UMAP) two-dimensional map from unsupervised Louvain clustering, of nuclei from AL and DR condition at young age (5 months)

**B**- Heatmap showing the gene expression of the top five differentially expressed genes in nuclei per cluster in AL and DR condition at young age (5 months). Nuclei are represented in columns and genes are represented in rows. Colored bars indicate clusters assigned to both cells and genes.

**C**- Uniform manifold approximation and projection (UMAP) two-dimensional map of nuclei with cell-type assigned, from AL and DR condition at young age (5 months)

### 3.2.1.3 *FACS improves purification of single nuclei solution*

The poor results from Nadia sequencing made us focus on the 10X platform, since with less reads the results were of similar quality, and even more relevant biologically. Also, there was possibility of improvement with 10X chromium with deeper sequencing and modification of the experimental protocol before encapsulation. The main issue from the first try was that a lot of reads were actually unused because there were neither mapping to the genome or linked to specific nuclei. A lot of cDNA was uninformative, which could come from ambient RNA present in the solution that would be attached on the beads and reverse transcribed. To prevent this issue, it was suggested by the technical support of 10X Chromium to sort the nuclei using fluorescence activated cell sorting (FACS). Nuclei can be stained with DAPI regardless of their cell types which preserved the unbiased way of the approach. The nuclei were directly sorted in the solution for dropletisation with absence of debris, ambient RNA and any lipid floating. Since the nuclei would be sorted for a small amount, smaller fat pads were used, which avoided clumping of nuclei. Another test-run was done on the same conditions with FACS and 10X Chromium to assess if adding this step was beneficial and not detrimental to the nuclei, since nuclei should be kept for a short time in solution or they could enter in apoptosis phase.

We repeated the test experiment by taking AL and DR WAT from young animals and did the same nuclei isolation protocol. Nuclei were stained with DAPI and were collected using FACS directly in the solution used in 10X chromium protocol. During the sorting, gates were designed to select single nuclei, discard doublets and debris (**Figure 3-7.A**). A number of 8000 nuclei were collected per sample, in order to retrieve around 3000 nuclei after sequencing. When observed under the microscope the nuclei isolation solution was cleaner, without debris or nuclei clumping together (**Figure 3-7.B-C**). After dropletisation, the initial tapestation results showed low cDNA concentration, but this was be expected since a small number of nuclei were incorporated to make the libraries. Interestingly, compared to the first experiment with 10X, the amount of cDNA for AL sample increased nine times, while for DR it lowered to half (**Table 3-1**). Since the amount of cDNA was low, further amplification was done, and libraries were sequenced only at 10 million reads per sample in order to measure if there was any improvement compared to without FACS.

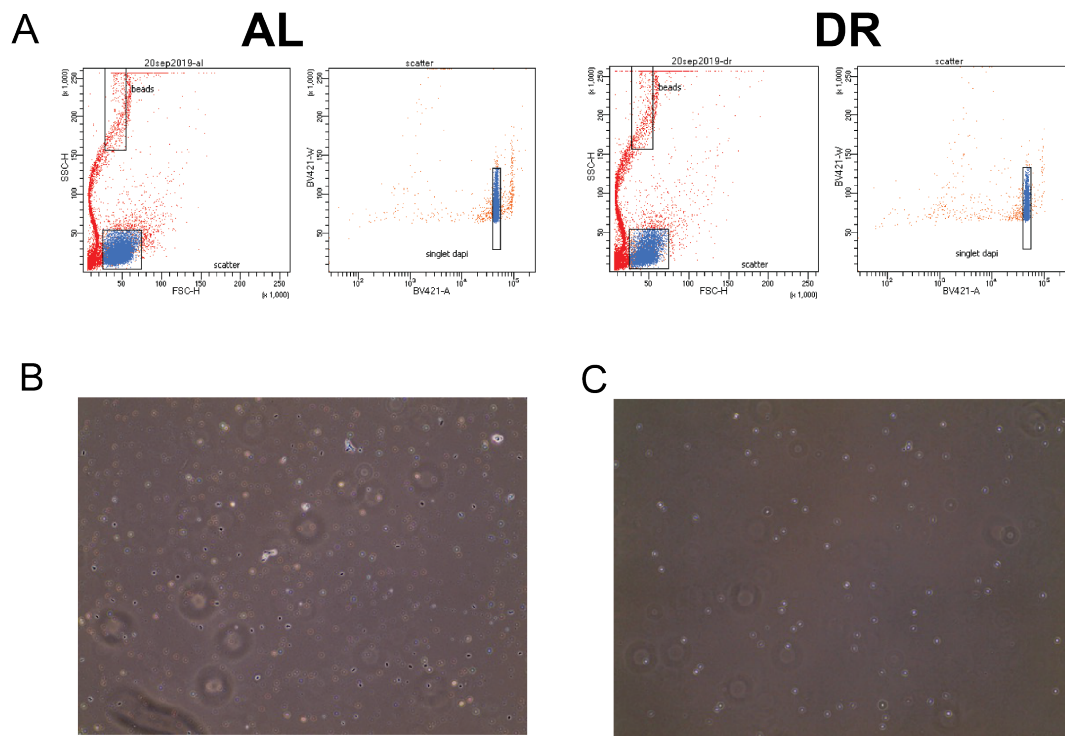


**Figure 3-7 FACS of nuclei after isolation protocol**

*A – Flowjo representation of gate to select singlet nuclei from AL and DR sample B- Representative image under microscope of isolated nuclei solution before FACS C- Representative image under microscope of isolated nuclei solution after FACS*

**Table 3-1 cDNA concentration of libraries of AL and DR sample, with or without FACS step**

	AL (pg/mL)	DR (pg/mL)
<b>Without FACS (-)</b>	46.9	249
<b>With FACS (+)</b>	396	100

**Table 3-2 Comparison between all data based on metrics after pre-processing with Seurat package.**

Platform	AL			DR		
	10x		Nadia	10x		Nadia
FACS	∅	+	∅	∅	+	∅
Number of cells	688	<b>1018</b>	589	1113	<b>1190</b>	644
Median genes/cell	114	<b>113</b>	92	81	<b>105</b>	87
Median count/cell	316	<b>152</b>	115	132	<b>131</b>	111
Total genes detected	5194	<b>8480</b>	4647	5566	<b>8260</b>	4421
Cell types detected	4	<b>6</b>	4	4	<b>6</b>	4

**Table 3-3 Comparison between 10X data with or without FACS sorting based on Cellranger metrics.**

Platform	AL		DR	
	10x		10x	
FACS	∅	+	∅	+
Number of cells	990	<b>2016</b>	2308	<b>3324</b>
Median genes/cell	64	<b>63</b>	57	<b>49</b>
Median reads/cell	12018	<b>5904</b>	5677	<b>3388</b>
Fraction of read in cells	36.7	<b>61.6</b>	29.5	<b>64.2</b>
Total genes detected	10611	<b>13013</b>	12209	<b>13999</b>

From Cellranger mapping results we saw improvements, firstly the read quality and tags were accurate, so reads could be attributed to nuclei, and gene level expression was correctly assessed from UMIs. Furthermore, the amount of reads that were effectively associated to cells doubled (**Table 3-3**), providing more information to characterize the cell type landscape of both samples. Other parameters showed improvement such as the number of cells estimated for both conditions and the number of genes detected (**Table 3-2**).

After quality filtering we obtained 922 nuclei and 3399 genes detected in AL and 951 nuclei with 3156 genes for DR. From the dimensionality reduction analysis and clustering, we observed that in both conditions more clusters were present (**Figure 3-8.A**). In AL based on gene markers, following clusters were identified in decreasing size: mature adipocytes, pre-adipocytes, myeloid cell, unknown, progenitor and endothelial cells (**Figure 3-8.C**). In DR, mature adipocytes, pre-adipocytes, unknown, myeloid cell, progenitors were identified (**Figure 3-8.C**).

We then merged both datasets to assess if same cell-types in both conditions clustered together, or if they would be differences due to the diet (**Figure 3-9**). Interestingly similar cell types merged together, but only mature adipocyte seemed to be separated based on the diet (**Figure 3-9.A**). This suggested that after 2 months, adipocytes would have different transcriptome based on their diets and those differences were observable at young age (**Figure 3-9.C**). When looking at proportions, DR showed a larger population of mature adipocyte while AL had more pre-adipocyte and immune cells (**Figure 3-9.D**).

Only from 10 million reads this last dataset showed promising information, highlighting biological differences only 2 months after diet switch. This acted as a catalyst for developing a complete experimental design that investigates the effects of nutrition and aging on the white adipose tissue.

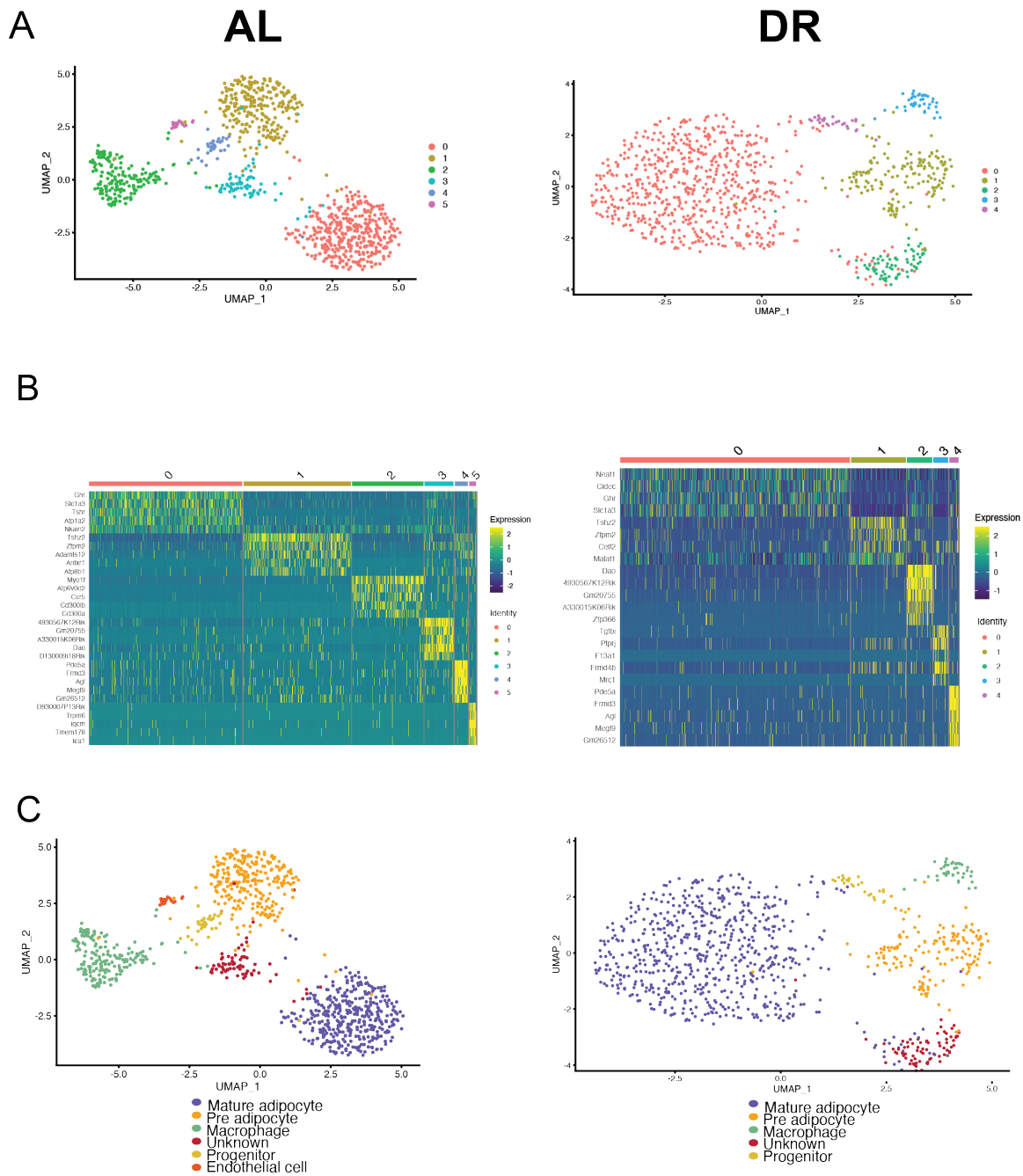


**Figure 3-8 SNuc-seq dataset of young AL and DR using FACS and 10X Chromium**

**A** – Uniform manifold approximation and projection (UMAP) two-dimensional map from unsupervised Louvain clustering, of nuclei from AL and DR condition at young age (5 months)

**B**- Heatmap showing the gene expression of the top five differentially expressed genes in nuclei per cluster in AL and DR condition at young age (5 months). Nuclei are represented in columns and genes are represented in rows. Colored bars indicate clusters assigned to both cells and genes. **C**- Uniform manifold approximation and projection (UMAP) two-dimensional map of nuclei with cell-type assigned, from AL and DR condition at young age (5 months)

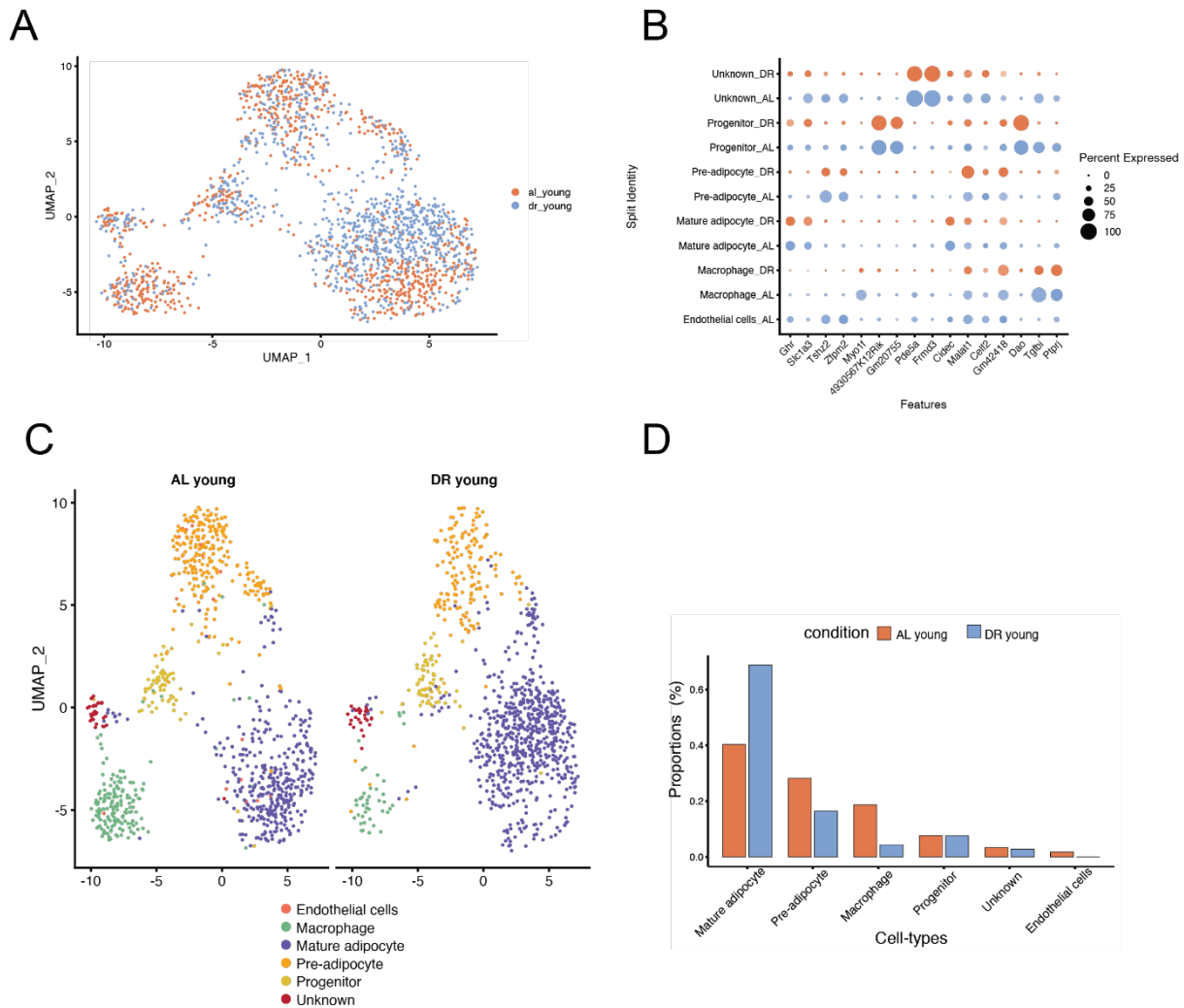


**Figure 3-9 Merged SNuc-seq dataset of AL and DR young using FACS and Chromium 10X**

**A** –UMAP of merged nuclei from AL and DR condition at young age (5 months) **B**- Dotplot showing the gene expression of the top two gene markers per cluster in AL and DR condition at young age (5 months). Only common genes of the merge data were represented. Size of the dot represent the percentage of cells in the cluster expressing the gene. **C**- UMAP of merged nuclei split by diet. Clusters are colored by cell-type assignment before merging. **D**- Proportions of cell types in percentage per diet.

## 3.2.2 Understanding changes in cell type composition with deconvolution analysis

### 3.2.2.1 *Weighted Deconvolution methods show better prediction than Cibersort*

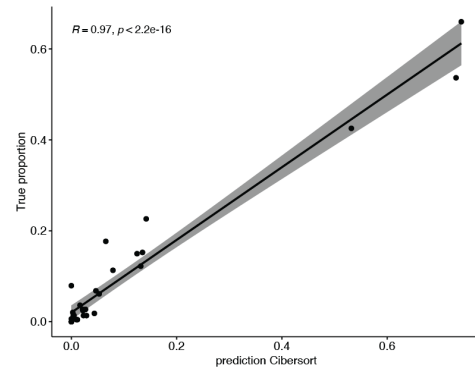
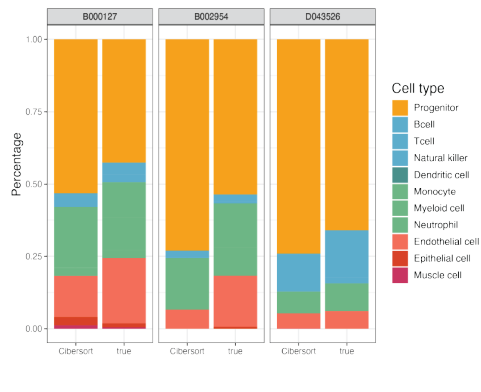
Deconvolution methods are useful tools to get a better insight of cell-type composition of a tissue while avoiding the generation of single-cell data. With a bulk RNA-seq dataset it is possible to infer cell-type proportions based on the gene expression data. From previous benchmarking study (Avila Cobos et al., 2020) we selected 3 methods to compare, Cibersort, SCDC, and MuSiC to select the one that would provide the most accurate results with using single-nuclei data from WAT.

First, their performance in predicting cell-type proportion from known single-cell and single-nuclei datasets was compared. To do so, Tabula Muris data of WAT (Tabula Muris et al., 2018) was used as reference for single-cell, and the data of ALDR16 condition from our SNuc-seq dataset was used as reference for single-nuclei data. In both case pseudobulk datasets were generated from the original data single cell or nuclei, so that we knew the true proportion of each cell types. The pseudobulk datasets were deconvoluted using the single-cell or single-nuclei data as reference with each method.

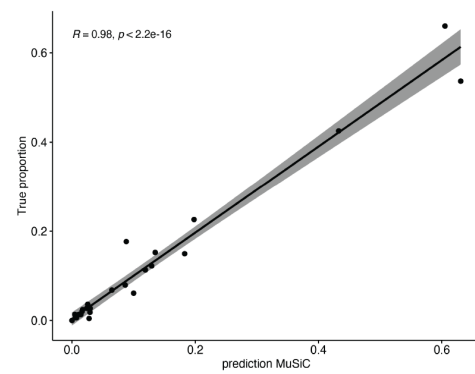
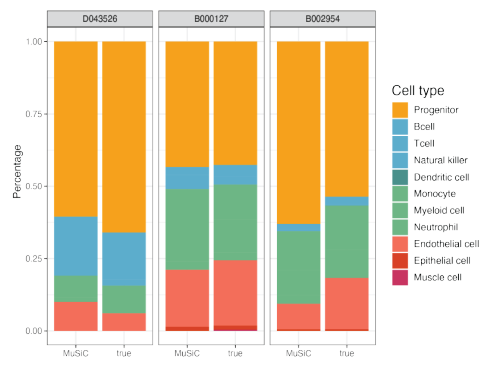
Tabula Muris single-cell data were used to compare the methods. Therefore, data were filtered to only keep single-cell data obtained through FACS of adipose tissue of female mice. The dataset was composed of 777 cells across 3 samples, with expression data in 23433 genes. Those cells were divided across 11 different cell-types, the main one being adipocyte progenitors, followed by immune cells and tissue support cells (**Sup.Figure 6**). The prediction results of each method were compared to the true proportions by samples, summarized by Pearson correlation coefficient and the associated p-value. Cibersort, SCDC, and MuSiC showed almost perfect prediction of cell-type composition, with Pearson correlation coefficient between 0.97 and 0.98, and associated p.value  $<2.2e-16$ , indicating significant correlation between predictions and real values (**Figure 3-10.A-C**). Furthermore, when we compared directly the methods predictions between them, SCDC and MuSiC actually were positively correlated together with a Pearson coefficient of 1, showing that the two

methods provided really close predictions in this case (**Figure 3-10.D**). As a last comparison, we used the root mean square error (RMSE) for each sample and combined it per methods (**Figure 3-10.E**). SCDC and MuSiC had the lowest values, so the smallest margin of error between their prediction and the true values. Despite those results showing MuSiC and SCDC as slightly more accurate in their predictions than Cibersort, the difference was not significant (Kruskal-Wallis test, p.value=0.18).

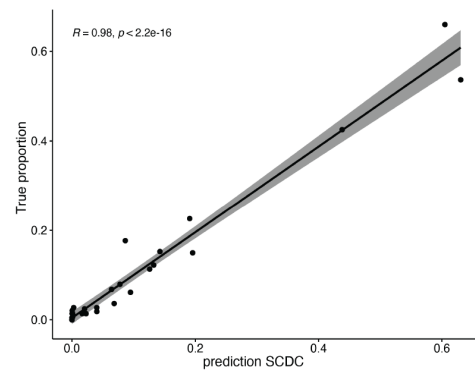
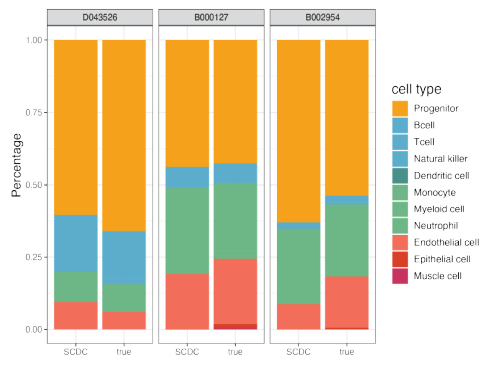
A



B



C



D



E

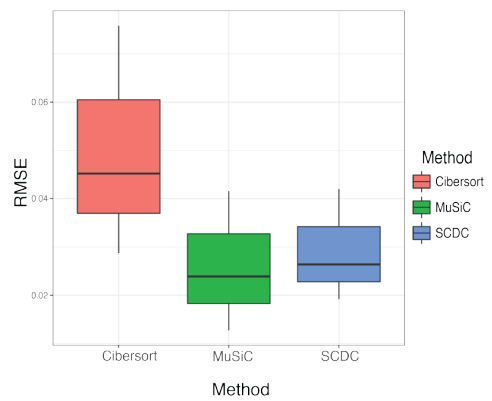
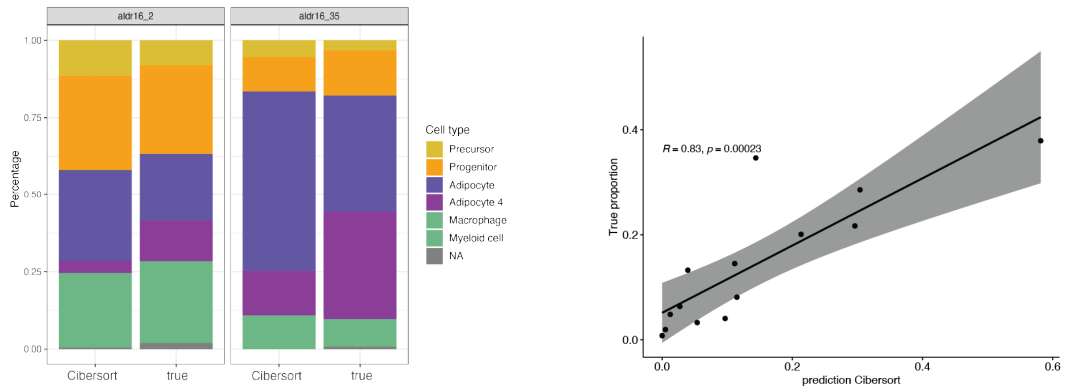


**Figure 3-10 Comparison of deconvolution methods using Tabula Muris single cell data from adipose tissue**

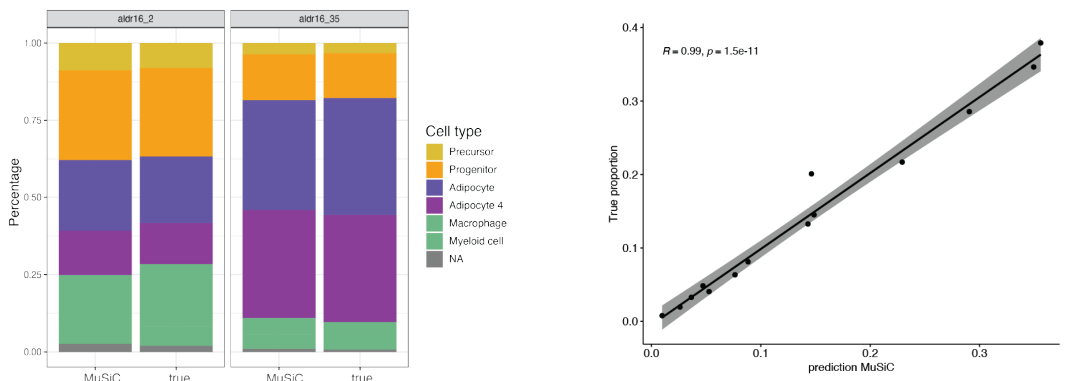
**A –C.** Stacked barplots of cell-type proportions predicted by Cibersort, MuSiC and SCDC methods compared to the true proportions. Prediction of 3 samples for each method. Correlation plots between predicted and true proportions with Pearson correlation coefficient ( $R$ ) and associated  $p$ .value. **D-** Correlation plot of prediction results from all methods. **E.** Barplot of RMSE per sample for each method (Kruskal-Wallis test  $p$ .value=0.18)

The methods were then tested to see if they also perform well when using single-nuclei data as input. The same testing workflow was used on ALDR16 single-nuclei data composed of 2896 nuclei across two samples, with 7694 genes expressed. This dataset was selected to see how the methods would perform with less genes and nuclei available, and if they could discriminate two subtypes of a similar cell-type, adipocytes 1 and 4. In this case, SCDC and MuSiC predicted almost perfectly the proportions of the different cell-types ( $R=0.98$  and  $R=0.99$  respectively), Cibersort was less accurate where prediction and actual values were correlated with  $R=0.83$  (**Figure 3-11.A-C**). Cibersort couldn't predict well the proportion of adipocyte 4 (**Figure 3-11.A**), showing struggles to predict accurately different type of a similar cell-type. Then all results were compared together through a correlation plot, where SCDC and MuSiC were again highly correlated between each other and with the actual true values (**Figure 3-11.D**). Finally, by looking at the RMSE data for each method, we could appreciate that Cibersort perform worst, yet the difference was not statistically significant (Kruskal-Wallis,  $p$ .value=0.16).

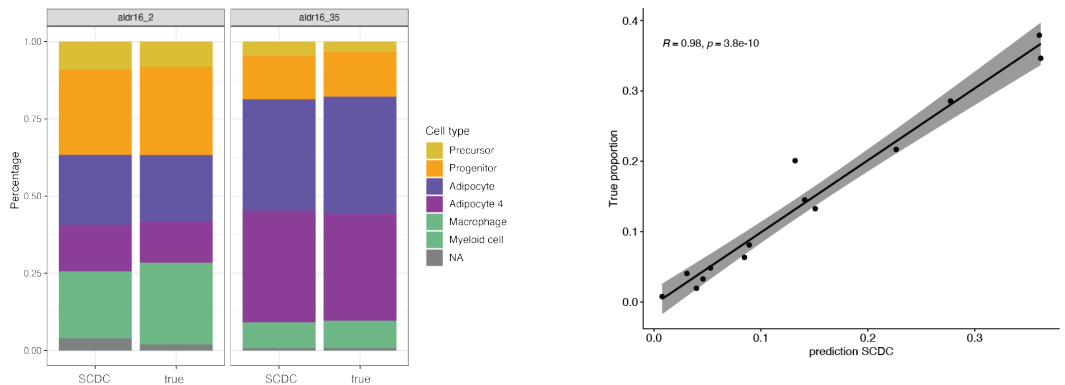
A



B



C



D



E

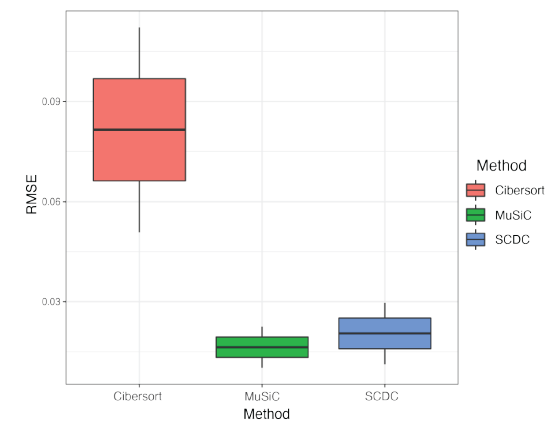


Figure 3-11 Comparison of deconvolution methods using single-nuclei as reference

**A –C.** Stacked barplots of cell-type proportions predicted by Cibersort, MuSiC and SCDC methods compared to the true proportions. Prediction of 2 samples for each method. Correlation plots between predicted and true proportions with Pearson correlation coefficient ( $R$ ) and associated  $p$ .value. **D-** Correlation plot of prediction results from all methods. **E.** Barplot of RMSE per sample for each method (Kruskal-Wallis,  $p$ .value=0.16).

### 3.2.2.2 Weighted Deconvolution methods difference in prediction accuracy using single-cell or single-nuclei data

The nearly perfect prediction of SCDC and MuSiC led us to focus on them despite the non-significant difference in prediction between Cibersort and SCDC, MuSiC. The initial benchmarking test was done to see how the method is performing in perfect conditions: same genes expressed and same cell-types in the data to deconvolute and the reference. But it is not always the case, more often, deconvolution methods are used when the single-cell data are not available, so it is necessary to find a single-cell reference matching the data to deconvolute. In the case of the WAT, it can be an additional challenge since most datasets focused on the stromal vascular fraction of the adipose tissue and discarded mature adipocytes. We tested SCDC and MuSiC performance when a cell-type is missing or a reference is incomplete.

To test both methods, we used different datasets for the pseudo-bulk data to deconvolute and reference dataset. Among the WAT single-nuclei datasets available, one has mature adipocyte in addition to cells of the SVF fraction (Emont et al., 2022). This dataset, designated by Emont dataset, has 4 samples, for a total of 16659 nuclei with 28727 genes expressed, spread among 14 different cell-types and was used to generate pseudo-bulk data to deconvolute (**Sup.Figure 7**).

Firstly, Tabula Muris was used as reference data to see how SCDC and MuSiC would predict cell-types proportions using another dataset. Both methods can take into account a list of common cell-types between the test data and the reference data to deconvolute. In this case, Tabula Muris and Emont datasets had in common 8 cell-types: Progenitor, Endothelial cell, B cell, T cell, Monocyte, Muscle cell, Natural Killer, Neutrophil. Using those cells profiles to predict Emont proportion in each sample, correlation profiles of predictions and true values were plotted as correlation plot for each method (**Figure 3-12**). Both methods didn't perform well in this case especially

MuSiC (**Figure 3-12.A**), having a correlation  $R=0.36$ , and SCDC (**Figure 3-12.B**) with a better coefficient but still poor results  $R=0.64$ , both being statistically significant ( $p.value=0.046$ ,  $p.value=8.1e-05$ ). Interestingly in both cases, endothelial cells proportion was overestimated by both methods, while MuSiC underestimated the proportion of progenitors, explaining the even poorer prediction result (**Figure 3-12.A-B**).

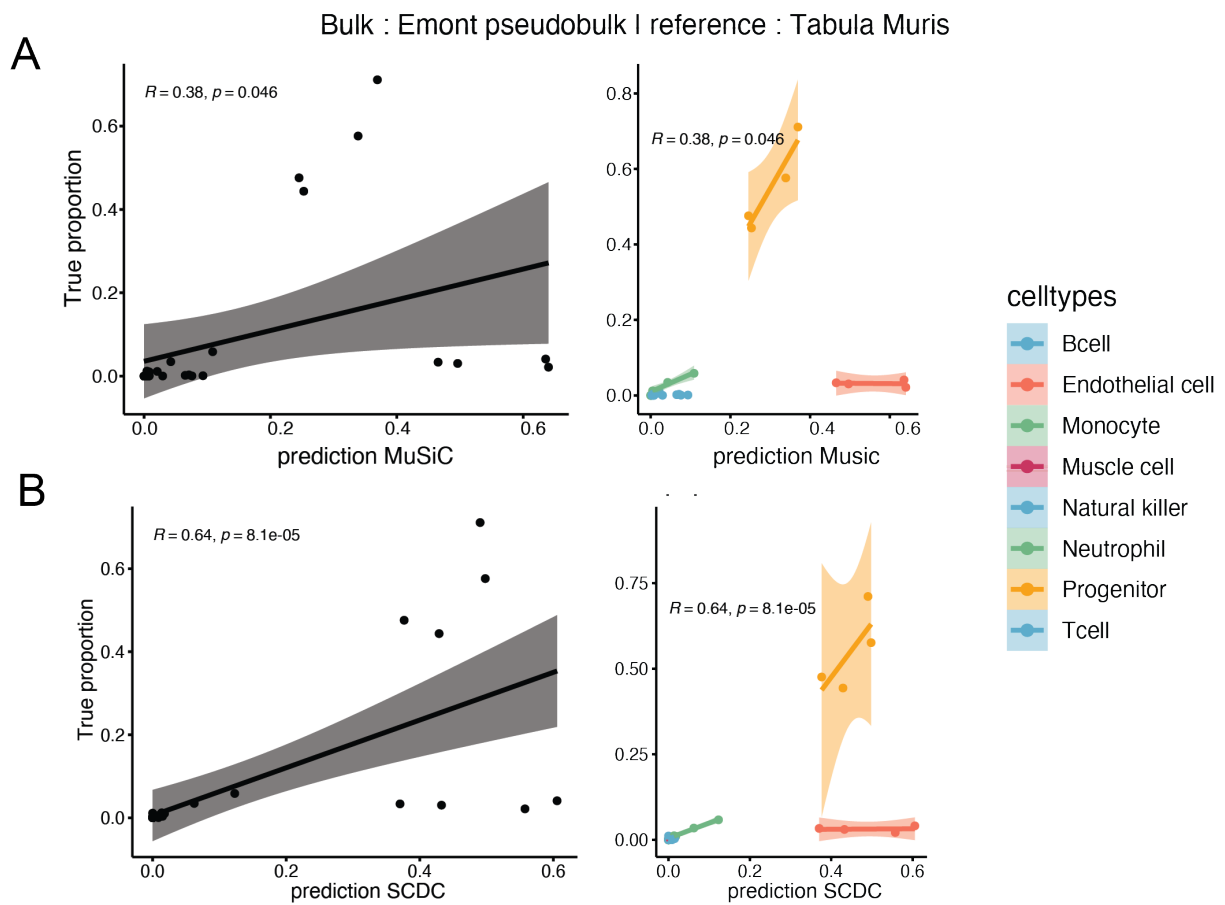


**Figure 3-12 Deconvolution results of Emont pseudobulk using Tabula Muris as reference**

**A-MuSiC method:** Correlation plots between predicted and true proportions with Pearson correlation coefficient ( $R$ ) and associated  $p.value$ . **B- SCDC method:** Correlation plots between predicted and true proportions with Pearson correlation coefficient ( $R$ ) and associated  $p.value$ .

Then ALDR16 dataset was used as the reference, in that case we could test the performance of both methods using single-nuclei data to predict proportions of another dataset. Single-nuclei data being sparse, with less nuclei and genes, only 3 cell-types

were found common: adipocytes, progenitors and macrophages. Despite the few common cell-types, predictions results were more accurate, with  $R=0.81$  for MuSiC and  $R=0.83$  for SCDC with associated significant  $p$ .value=0.0015 and  $p$ .value=9e-04 (Figure 3-13.A-B). Interestingly, both methods predicted correctly progenitors, but less accurately adipocytes.

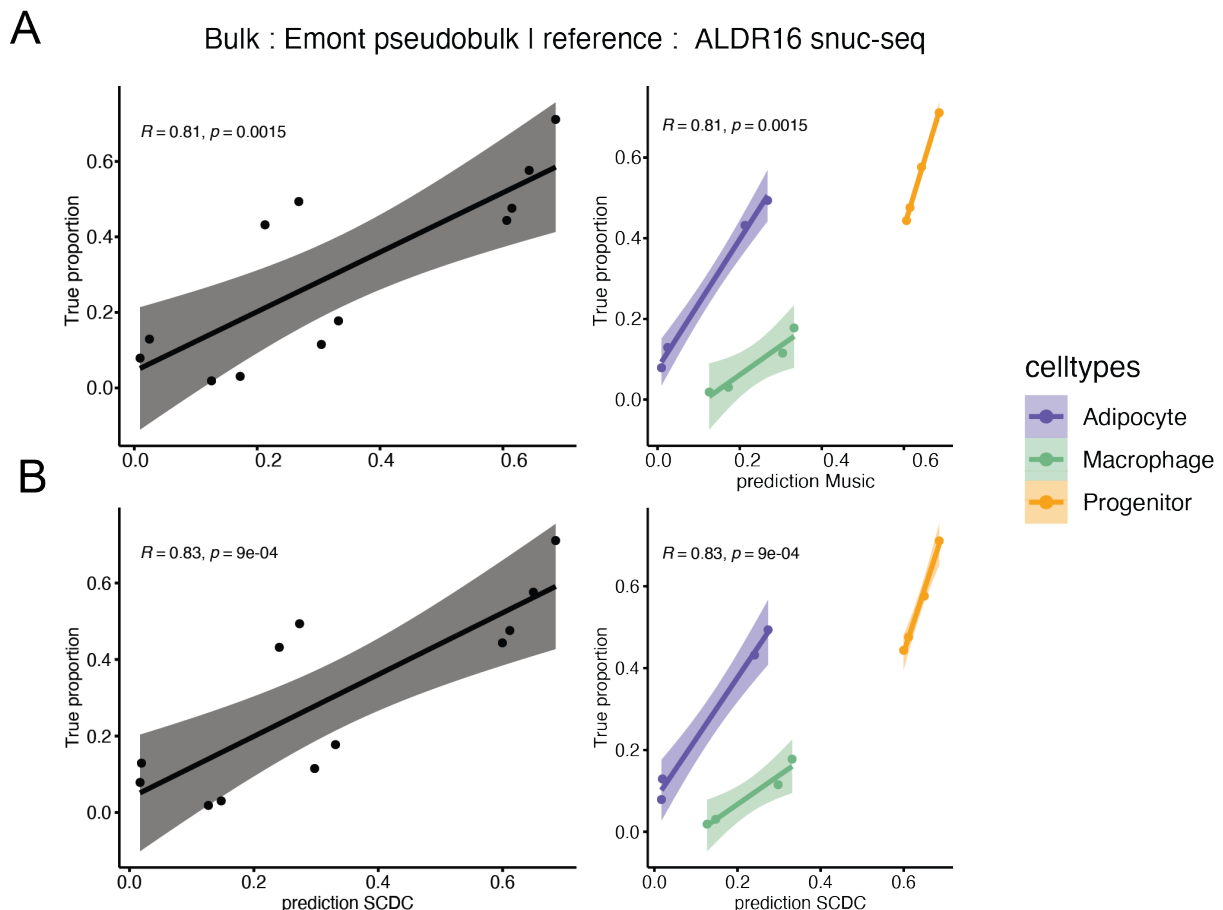


**Figure 3-13 Deconvolution results of Emont pseudobulk using ALDR16 sNuc-seq as reference**

**A-** MuSiC method: Correlation plots between predicted and true proportions with Pearson correlation coefficient ( $R$ ) and associated  $p$ .value. **B-** SCDC method: Correlation plots between predicted and true proportions with Pearson correlation coefficient ( $R$ ) and associated  $p$ .value.

A final parameter was tested in order to potentially improve prediction of the deconvolution methods in the case of using single-nuclei data as reference. Previously nuclei data from ALDR16 was used to deconvolute profiles from Emont dataset, that has three times more genes expressed. We hypothesized that non common genes

could add noise instead of informative data for the methods, while taking a subset of genes that are common between both datasets could improve the prediction. Emont dataset was filtered to retain only common genes with ALDR16. Interestingly in both cases, the predictions were slightly improved,  $R=0.85$  for MuSiC and  $R=0.86$  for SCDC with associate significant  $p.value=5e-04$  and  $p.value=0.00035$  (**Figure 3-14.A-B**). The change was observable in prediction of macrophage that were previously overestimated when using the full dataset to deconvolute (**Figure 3-13.A-B**).

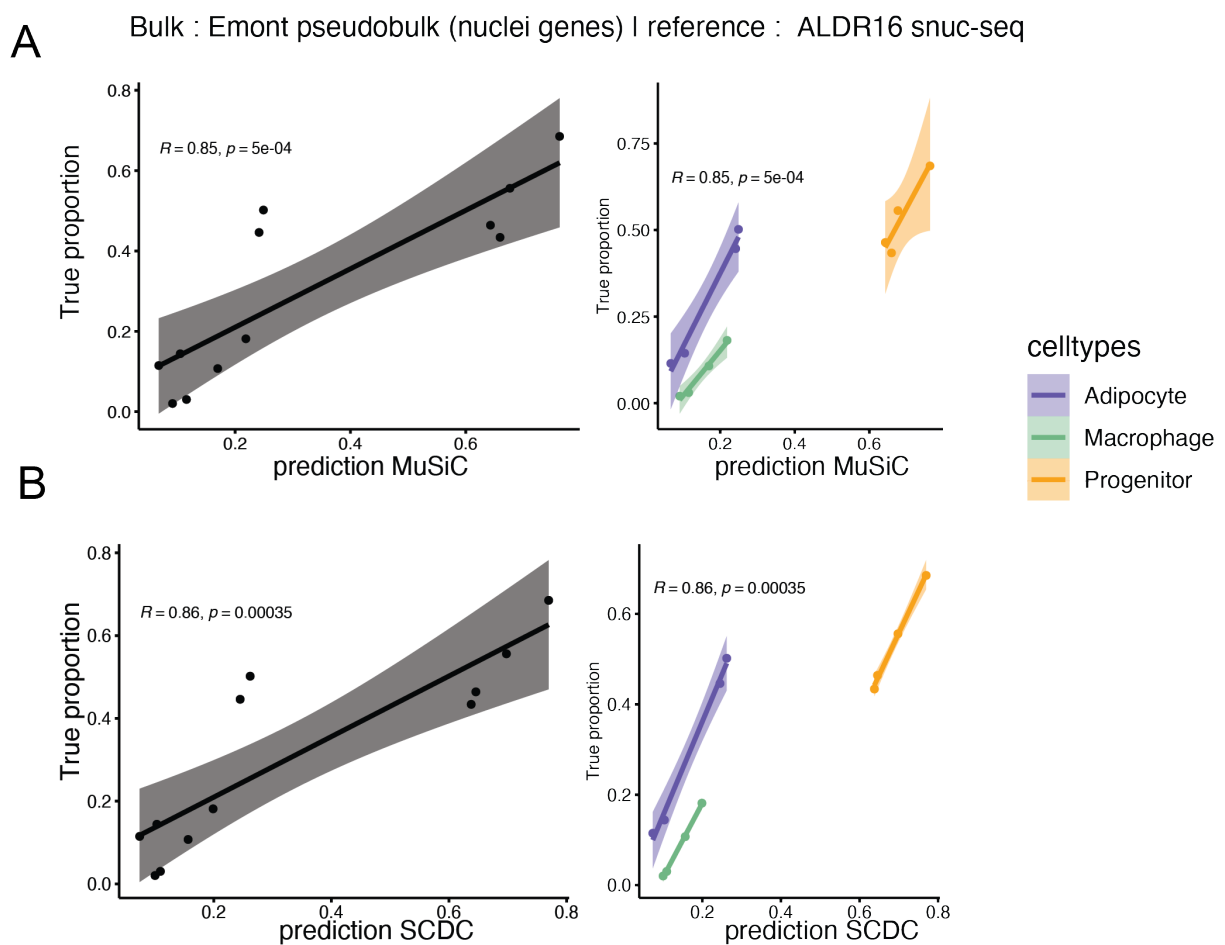


**Figure 3-14 Deconvolution results of Emont pseudobulk (filtered for nuclei genes) using ALDR16 sNuc-seq as reference**

**A-MuSiC method:** Correlation plots between predicted and true proportions with Pearson correlation coefficient ( $R$ ) and associated  $p$ .value. **B- SCDC method:** Correlation plots between predicted and true proportions with Pearson correlation coefficient ( $R$ ) and associated  $p$ .value.

Results of prediction cross-datasets were summarized with RMSE plot, showing the predictions errors across reference datasets, either Tabula Muris for single-cell or ALDR16 for single-nuclei and methods, SCDC and MuSiC (Fig. 3-14). Regardless of the reference dataset, SCDC performed better having lower prediction errors (Anova,  $p$ .value=0.019). Even if the results using single-nuclei data as reference didn't discriminate the methods, the poor performance of MuSiC with Tabula Muris as reference made the difference.

Results between using the full dataset and only common genes between the input data and the reference were summarized with RMSE analysis (**Figure 3-15.B**). Even if the predictions were slightly more accurate using only common genes just based on correlation across samples, the difference was not significant (Anova  $p$ .value=0.94).

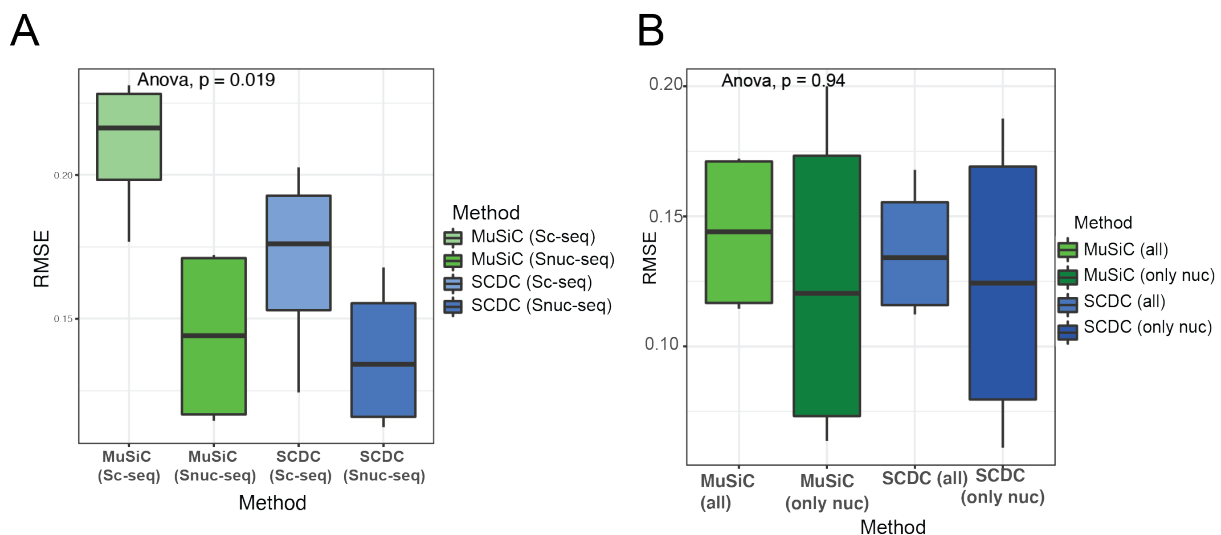


**Figure 3-15 Comparison of prediction results between methods using single-cell or single-nuclei as reference**

**A-** Barplot of RMSE per sample for SCDC (blue) and MuSiC (green) predictions. Comparisons between using single-cell (Sc-seq) or single-nuclei (SNuc-seq) as reference. Anova,  $p=0.019$ .

**B-** Barplot of RMSE per sample for SCDC (blue) and MuSiC (green) predictions. Comparisons between using all genes in pseudobulk data (all) or genes only expressed in ALDR16 (only nuc). Anova,  $p=0.94$ .

Since SCDC provided more robust results along the testing, it was used in a last test. SCDC can take multiple references datasets as input, so that if one dataset is missing some cell-types it can be completed with another dataset. Since our ALDR16

reference was missing quite some cell types, we combined it with AL\_24 sNuc-seq dataset that has 2 samples and more additional cell types, especially immune ones. Combining ALDR16 and AL\_24, more cell types were found common with Emont pseudobulk data: progenitor, adipocyte, macrophage, dendritic cell and endothelial cell. Predictions from SCDC were more accurate using this combined reference dataset, with  $R=0.97$  and  $p=4.2e-13$  (**Figure 3-16**). Not only SCDC showed better performance along all tests but the possibility to combine datasets is a major improvement in the case of incomplete reference datasets.

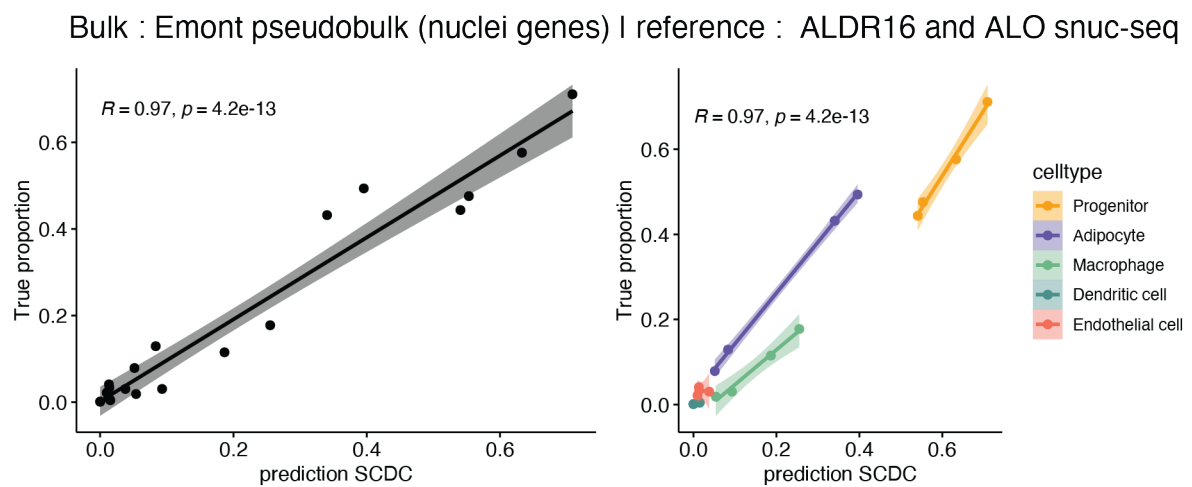


**Figure 3-16 Deconvolution results of Emont pseudobulk using ALDR16 and AL\_24 sNuc-seq as reference**

*SCDC method: Correlation plots between predicted and true proportions with Pearson correlation coefficient ( $R$ ) and associated  $p$ .value.*

### 3.3 Discussion

#### 3.3.1 10X Chromium with FACS provided better data quality for WAT

To generate single-nuclei data from WAT, since no protocol and method were available for this tissue at the beginning of the study, it was necessary to develop a suitable protocol. Starting with the nuclei isolation, where several rounds of experimentation were needed to obtain a nuclei solution free of fat floating and debris while avoiding a potential dissociation bias. To do the droplet sequencing two platforms were accessible, Nadia Instrument and 10X Chromium. Nadia Instrument has the advantages of customizable protocols and relatively lower in cost compared to 10X Chromium which is the most use platform despite being on the expensive side. Thanks to its strong performance and high data quality it is widely used and has well developed analysis pipelines but its protocol is not modifiable, which could limit its application for difficult tissue like the WAT.

To compare both platforms, a benchmarking experiment was done where each instrument would generate data based on the same samples. To do so we selected WAT from 5-month-old mice of AL and DR diet.

The first run on 10X Chromium provided poor results, where a lot of reads were duplicated, not associated to cells because of faulty barcodes and also not mapped onto the genome, indicating a lot of contaminant RNA. Despite the shallow sequencing, we could still identify relevant cell-types to the tissue especially mature adipocytes. Most papers studying fat at this point only looked at progenitors and SVF fractions (R. B. Burl et al., 2018) (Schwalie et al., 2018) or used targeted approach to study at adipocytes (Boumelhem et al., 2017). This motivated further improvement of the protocol; aiming to increase the number of reads mapped to the genome, and gain more insightful transcriptomic information.

In comparison the results of the Nadia Instrument were even less informative despite a deeper sequencing. From the low number of cells or genes detected, most genes being specific to nuclei but not to a specific cell-type making the data redundant.

In addition, the entire pipeline was challenging to execute, from the library making to the analysis of the data. The bioinformatic workflow had to be fully adapted, making the analysis more time consuming. Lastly, in addition to poor quality data, since our biological question needed a more extensive experimental design and the wet-lab protocol was hard to perform, it was concluded that the Nadia Instrument wasn't a suitable option for our project.

The 10X Chromium protocol had to be optimized by getting rid of nonspecific RNA and possible debris or lipid in solution that might hindered the results. Using FACS, nuclei were stained with DAPI and sorted, regardless of their cell-type to maintain the unbiased approach of the experiment. The results improved, from the number of cells and genes detected, but most importantly the fraction of number of reads in cells doubled in both condition. With the same amount of reads we gained relevant information, characterized more cell-types, and even detected biological differences between samples. Increased proportion of immune cells in AL compared to DR, suggested immune infiltration as it was observed in histological data (Lisa F. Drews, 2021). Interestingly, DR samples always had better quality results regardless of the platform. One possible explanation is coming from the nuclei solution that is less contaminated by fat, and so less lipids and debris contaminating the solution.

In conclusion, the promising results from a shallow sequencing using 10X Chromium with FACS gave us confidence to set up the full experimental design to answer our biological questions

### 3.3.2 Evaluation of deconvolution methods for WAT

Cell-type composition is an important factor to understand metabolic function of a tissue. Early single-cell studies showed that for a lot of tissues, cell-types or sub-cell types were unknown, or that specific condition could change the cell-type landscape and affect tissue homeostasis. For example, presence of inflammatory cells in a tissue can be a sign of disease and can help to understand the dysfunction of normal metabolic processes in the tissue. Since single-cell methods are not always accessible, because of the experimental challenge or cost, deconvolution is a great

alternative to estimate cell-types proportions using RNA-seq bulk data. A lot of methods are now available, and selecting the adequate method based on the available data is essential to obtain valid results. In our case we wanted to find the most accurate method to predict cell-type proportions from bulk of WAT. Since this tissue is difficult to profile with single-cell methods, a lot of single-cell datasets of WAT are incomplete, missing mature adipocytes or even additional cell-types. To obtain an unbiased view of the tissue, we used a single-nuclei approach to generate data. Knowing that droplet-based sequencing methods can add technical bias, we wanted to validate the cell-type proportions observed in the single-nuclei dataset we generated by using deconvolution methods on RNA bulk samples of the same conditions. This was an additional parameter to take into account, whether prediction based on cell or nuclei profile be similarly accurate. It was necessary to find a method that could work with single-nuclei data, taking into account multiple samples and possibly incomplete reference dataset.

We tested 3 methods, Cibersort, SCDC and MuSiC with pseudo-bulk data generated from annotated single-cell datasets in order to have known proportions of the cell-types. Using Tabula Muris WAT data to predict proportion from its pseudobulk dataset provided great predictions for all 3 methods, especially SCDC and MuSiC that almost predicted perfectly the tissue composition. Similar results were observed for SCDC and MuSiC when the same test was done with ALDR16 data while Cibersort gave a less accurate prediction. One reason could be that Cibersort is using a signature matrix as reference, constructed from the single-cell or single-nuclei data provided, which discard the variability information from multiple samples. Additionally, single-nuclei data is sparser, with less genes expressed, while the dataset from Tabula Muris is from full cells and from FACS which in general provide more robust and complete data.

From those results, SCDC and MuSiC were selected to be tested with different datasets for reference and data to deconvolute. Usually, deconvolution methods would be used in the case of having only bulk data and trying to infer cell-types proportions using another single-cell dataset available of the same tissue or condition. Depending on the tissue, datasets can be similar if the tissue is homogeneous or if the tissue is complex, dataset might represent a fraction of it. For example liver has a small number of well characterized cell-types (Ding et al., 2016), while tissue like the brain (Mu et al., 2019), or the WAT are harder to get a full depiction of all cell types present in them.

To test SCDC and MuSiC accuracy in the case of different dataset between reference and data to deconvolute, we used a large single-nuclei dataset of WAT having 14 different cell-types including mature adipocyte (Emont et al., 2022). First Tabula Muris was used as reference and for both methods, predictions were not accurate, whereas using ALDR16 gave positive correlation between predictions and actual proportions of ~80%. This showed that using single-nuclei as reference can outperform single-cell data, the most important factor being that the main cell-types are found in the reference and the data to deconvolute. Even if in Tabula Muris, 8 cell-types are overlapping with Emont dataset, mature adipocyte are missing, which influence importantly the results, like MuSiC overestimating the proportion of endothelial cells. On the contrary even if ALDR16 data is from single-nuclei and had only 3 cell-types in common, the fact that those 3 cell-types, mature adipocytes, progenitors and macrophages are among the most important ones, it gave accurate predictions.

We wanted to assess if using genes commonly expressed between the reference dataset and the data to deconvolute could improve prediction since additional genes could add noise. A study showed actual improvement by removing genes non expressed in nuclei in the data to deconvolute when using sNuc-seq data as reference (Sutton et al., 2022). In our case the correlation was better between prediction and actual proportion but the difference was not significant. Finally, SCDC was used with multiple datasets as references, to complete possible missing cell types, and got the most accurate prediction.

Among the three methods tested, SCDC showed the most accurate and robust results. If MuSiC and SCDC usually performed similarly, it is because they use the same type of approach, a weighted non-negative least squares (W-NNLS) regression framework. Yet SCDC was able to perform better when using a different reference dataset and even by combining datasets to have a comprehensive reference. SCDC is giving more weight to expression profiles of the reference data that correlates positively with the data to deconvolute, and is discarding potential cells that are wrongly annotated (Dong et al., 2021).

Those results highlighted the importance of having a comprehensive reference to have accurate prediction results, which can be challenging when the tissue of interest is not fully characterized or single-cell or nuclei datasets are not yet available. Nevertheless, new methods like SCDC seemed to be a suitable alternative by combining multiple

reference datasets to get profiles of all potential cell-types and provide valid prediction results.

4 Single nuclei RNA profiling of white adipose tissue under dietary restriction reveals decreasing responsiveness with age

## 4.1 Introduction

Dietary restriction (DR) one of the most successful anti-aging strategies, has been demonstrated to slow down the aging process in a variety of animal models, including primates and worms (Balasubramanian et al., 2017). Dietary restriction affects nutrient sensing pathways, gene expression, cellular repair systems, and metabolic functions to promote longevity (Most et al., 2017). The metabolism must be able to adjust to the nutritional alteration in order to profit from the DR treatment. This ability to adapt appears to be fading with age, as it was previously demonstrated in mice where the effect of late onset dietary restriction on mortality and gene expression was investigated (Hahn et al., 2017). This study showed that with age, the white adipose tissue (WAT), one of the most metabolically active organs, is unable to adapt to the DR condition. The WAT transcriptome of young animals was able to rapidly adapt to the DR conditions, suggesting that transcriptional nutritional memory is established later in life.

In order to narrow down the interval when the metabolism loses the ability to benefit from DR, mice were switched from ad libitum (AL) to DR at 12, 16, 20, 24 months of age in a follow-up study (Lisa F. Drews, 2021). The lifespan results suggested that the phenocritical period in which DR can positively affect survival ends between 16 and 20 months of age. Thus, comparing the molecular response in the WAT to DR between 16 and 20 months might help to identify the molecular basis of the dietary memory and whether this contributes to the survival phenotype. Because the WAT is a highly heterogeneous tissue with a variety of cell types, bulk sequencing is insufficient to completely comprehend the dynamics of gene expression in this tissue (Hwang et al., 2018). Recent developments in single-cell RNA sequencing methods enable to capture the transcriptome of multiple cells from an unbiased and high throughput approach. Mature adipocytes are the main functional cell type of WAT but by accumulating lipids and their fragile nature, it presents a challenge for usual single-cell droplet-based methods (Hagberg et al., 2018). Targeting nuclei instead of cells is an alternate method to capture single transcriptomes from WAT as it was successfully shown in recent studies on adipose tissue of mice and human subjects (Emont et al., 2022).

In this study we used sNuc-seq to capture in an unbiased way transcriptome profiles and proportions of specific cell-types in WAT subjected to different diet strategies and ageing. We compared single cell gene expression between 5 and 24 months for chronic diets, AL and DR, and found DR prevents age-related immune infiltration in the WAT. We identified a specific sub-cluster of mature adipocytes in the earlier switch at 16months, showing increased activation of de-novo lipogenesis pathway, similarly to chronic DR adipocytes. Collectively our results identify targets to better understand the metabolic flexibility of the WAT in the light of ageing but also nutrition and as a result contributes to the research on age related diseases such diabetes or cardiovascular disease.

## 4.2 Results

### 4.2.1 Generating a cell-type landscape from young and aged murine white adipose tissue under dietary restriction

To study the flexibility of WAT gene expression in response to age and diet, gonadal fat pads from female mice were used for sNuc-seq and bulk RNA-seq (Lisa F. Drews, 2021). DR was started at 12 weeks of age by feeding the DR animals 60% of the food consumption of AL controls. Late-onset DR was introduced at 16 (ALDR16) and 20 months (ALDR20) of age (**Figure 4-1 A**). We obtained unbiased gene expression profiles from single nuclei using droplet-based sNuc-seq from the optimised method adapted to the WAT (see section 3.2.1 Optimization of single nuclei sequencing protocol for WAT). Chronic AL (AL\_5) and DR (DR\_5) WAT were sampled at 5 months, while at 24 months chronic AL (AL\_24), DR (DR\_24), and the two DR switches at 16 months (ALDR16) and 20 months (ALDR20) were included. Three individuals were pooled for each sample in order to reduce biological inter-sample variability and two samples were used per condition. After isolation, nuclei were stained with DAPI and filtered with FACS to limit unspecific RNA contamination (**Figure 4-1 C**). Purified nuclei were processed with the 10X Genomics Chromium system (Zheng et al., 2017),

generating single-nuclei transcriptomes for 12,044 cells after quality control. Using known marker genes, fifteen cell groups were found after unsupervised clustering of data from all conditions (**Figure 4-1 B**). These fell into three super clusters: adipocytes, immune cells, and stromal-vascular fraction (**Sup.Figure 8-F**). For instance, we detected markers specific to mature adipocytes in multiple clusters, evidence of several sub-type of mature adipocyte. *Slc1a3* is a gene marker that is expressed in all adipocyte sub-clusters and maintains a steady import of acidic amino acids into adipocytes (Krycer et al., 2017).

Immune cells were also clustered together and shared markers expressed in myeloid and lymphoid cells, such as *Runx1* (North et al., 2004). We could distinguish a large cluster of macrophages expressing *Ptprj*, a regulator of macrophage adhesion and spreading (Dave et al., 2013), and dendritic cells expressing gene markers such as *Myo1f* and *Alcam* (Oh et al., 2019). Finally, among immune cells, we identified lymphoid cells, expressing lymphocyte markers such as *Bank1* (Aiba et al., 2006) and *Inpp4b* (Srivastava et al., 2013).

The final super cluster was made up of heterogeneous cell-types from the stromal vascular fraction, such as progenitors, pre-adipocytes, endothelial cells, or muscle cells (Han et al., 2015). *Zfp2* is significantly higher expressed in fibroblasts or preadipocytes in comparison with adipocytes (**Sup.Figure 8-E**) (Oger et al., 2014) and *Lama2* is a regulator promoting adipogenesis (Zhu et al., 2020). Both are top gene markers for the first cluster identified as pre-adipocyte cluster. Interestingly *Adamts1* seems to be highly expressed in adipose stem cells (T. Wang et al., 2020), indicating that the cells of this cluster are earlier in the adipogenesis process and so referred as progenitors. Another cluster of pre-adipocytes was separated by the expression of fibrogenic and inflammatory markers such as *Fndc1* (Hepler et al., 2018). Additional small clusters could be identified, such as endothelial cells expressing *Ptprb*, or muscle cells expressing *Dmd*. In summary our unsupervised analysis of all merged data could identify a diversity of cell types reflecting the biological complexity of the white adipose tissue. This analysis also enabled to capture the variability coming from different conditions, emphasizing the impact of age and diet on the cell-type landscape.

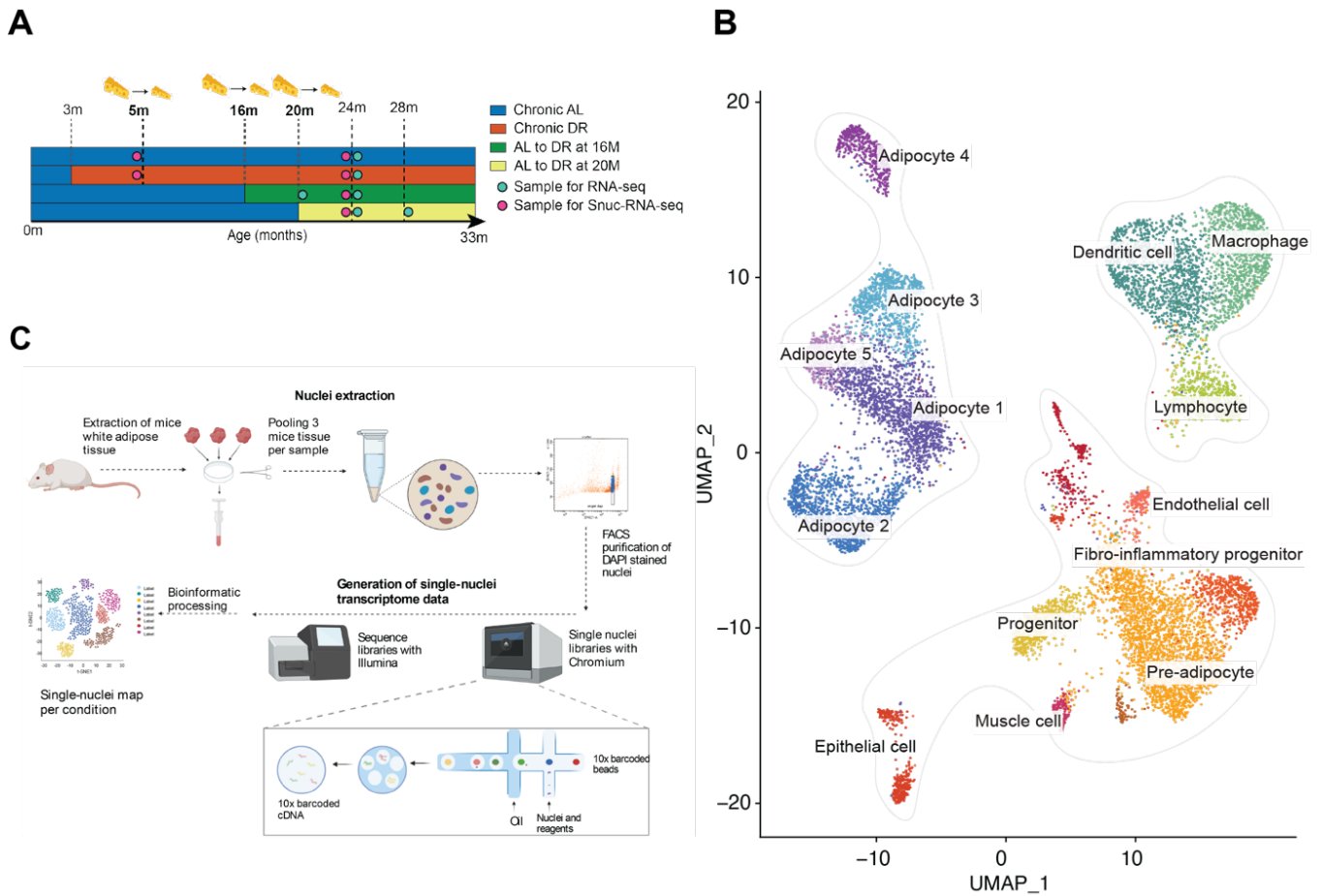


**Figure 4-1 Single nuclei transcriptomic analysis of young and old murine adipose tissue, under AL and DR feeding and diet switch**

**A**, Schematic diagram of experimental design **B**, Uniform manifold approximation and projection (UMAP) two-dimensional map from unsupervised Louvain clustering, of nuclei from all merged conditions showing 3 super-clusters of adipocytes, immune cells and stromal vascular fraction **C**, Schematic diagram of the experimental pipeline, from tissue to single-nuclei data. After nuclei isolation, DAPI-stained nuclei from mice white adipose underwent FACS to remove debris and then were encapsulated into droplets with the Chromium platform. The resulting libraries were sequenced on an Illumina platform, and the raw data were processed with Cell Ranger to obtain expression matrices. The downstream analysis was done R using mainly the Seurat package to get single-nuclei maps of each biological condition.

## 4.2.2 Cell-type landscape changes with age and DR

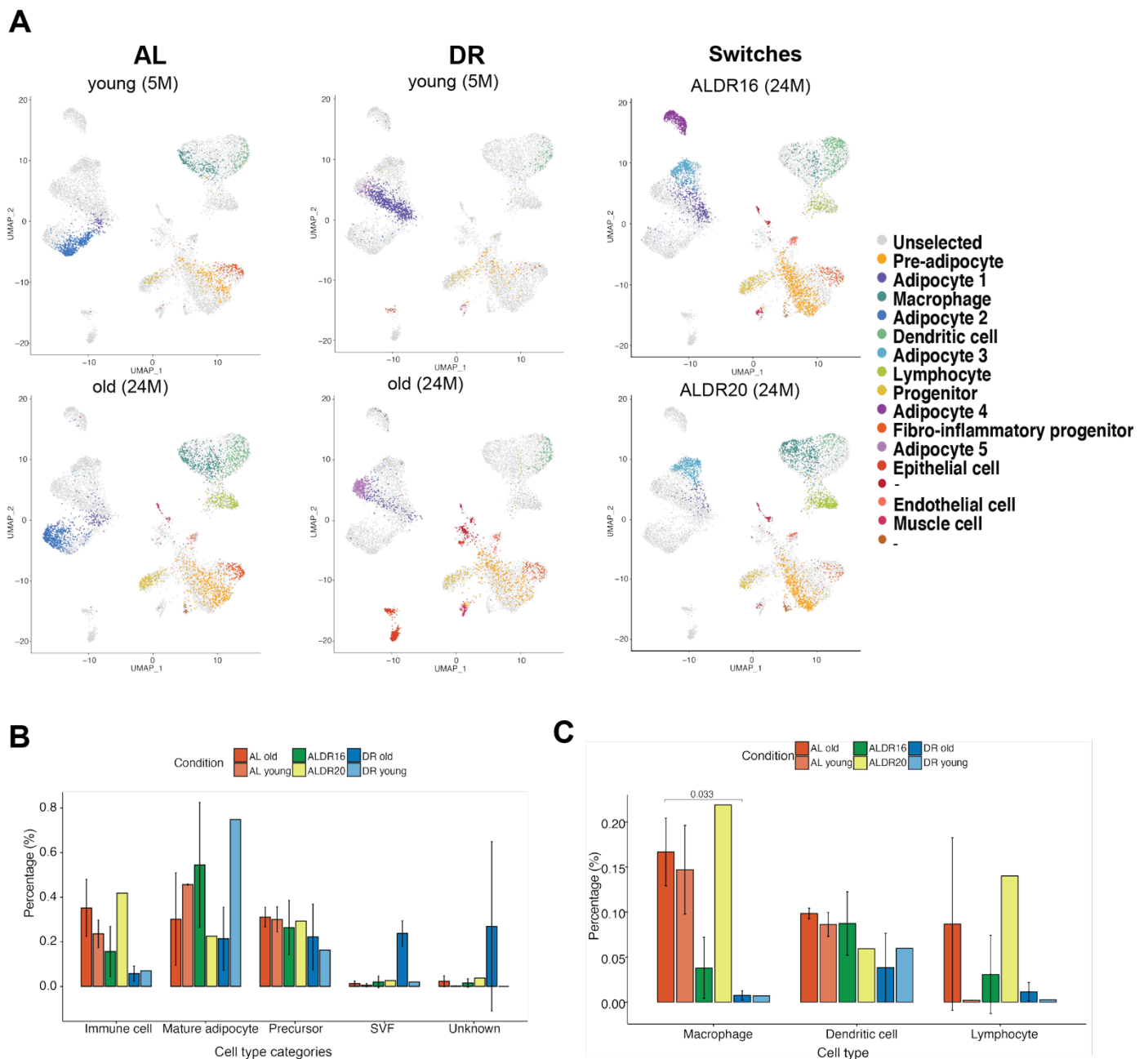


**Figure 4-2 Compositional and transcriptional changes in the murine adipose tissue in function of age and diet**

**A**, Uniform manifold approximation and projection (UMAP) plots showing highlighted nuclei coming from each single condition. **B**, Cell-type composition differences between different conditions of single-nuclei samples quantified as proportions over cell types. Cell-types were divided in 5 categories. Data are plotted as mean  $\pm$  s.e.m. **C**, Immune cell-type proportion differences between different conditions of single-nuclei samples. Proportions were transformed using arcsin square root. Data are plotted as mean  $\pm$  s.e.m. T-test was used to calculate p-values. Benjamini and Hochberg false discovery rates were used to account to multiple testing of cell types/clusters.

To examine the effects of age and diet on the cell-type landscape, we highlighted the nuclei from each age and diet condition in the merged UMAP (**Figure 4-2.A**). The heterogeneity of the cell-type landscape was highly affected by both age and diet. Cell type diversity increased with age in AL fed animals, and more differentiated cells appeared with age, including endothelial cells and lymphocytes. There was also an increase immune cells with age from 20% to 35% of all cells present in AL (**Figure 4-2B**). Macrophages representing more than 15% in AL\_24 and 20% in ALDR20 (**Figure 4-2 C**). Previous studies showed macrophage infiltration in adipose tissue under high fat diet, generating local inflammation in the tissue (Russo & Lumeng, 2018). Lpl is upregulated in dendritic cells in AL\_5 and AL\_24, this gene contributes to lipid accumulation in the dendritic cells and causes their dysfunction, which leads to tumour evasion and growth (Gao et al., 2015). Lymphocytes in white adipose tissue, particularly T-cells, recruit and encourage the formation of M1, pro-inflammatory macrophages. Lymphocytes were found only in AL\_24 WAT, consistent with an age-related immune infiltration already demonstrated by previous studies on obese WAT (Surmi & Hasty, 2008) (DeFuria et al., 2013).

Age had less effect on WAT composition of DR animals, especially an absence of immune infiltration. The macrophage population represented a small proportion of all cell-types at young age, less than 5% and did not increase with age (**Figure 4-2C**). Additionally, no lymphocytes were detected in DR WAT, consistent with the hypothesis that DR has a protective role against age-related tissue inflammation of the WAT (Ishaq et al., 2018). The switch conditions showed as well differences in immune infiltration with intermediate profile for ALDR16, where we found presence of macrophage and dendritic cell but not to the level of AL\_24 and very little lymphocytes. On the contrary, the later switch, ALDR20, displayed similar profile to AL\_24 with presence of large population of immune cells including lymphocytes (**Figure 4-2C**). These results suggest that only the earlier switch, at 16 months, had a protective effect against immune infiltration.

Among the other cell-types we saw less differences in proportions with the exception of DR\_24 having a lot of cell-types from the stromal-vascular fraction other than immune cells. The fact that DR\_24 mice have a small fat pad and surrounding tissues may have been caught during dissection could explain why they had more cell kinds

of support, such as epithelial cells or muscle cells. The number of precursors was fairly similar in all condition even if pro-inflammatory progenitor were found in almost all condition but DR\_5, once again a sign of the inflammation of the tissue. The main cell-type of the adipose tissue are adipocyte and, in our case, we could see that they were subdivided with age and diet influencing the clustering (**Sup.Figure 8A-B**). In relative proportions, surely because of the lack of differentiated cell types in young samples, we observed larger cluster of adipocytes compare to the old samples. The different conditions produced sub-clusters of mature adipocytes but not the other cell-types, demonstrating how age and diet impacted the metabolic activity of adipocytes which highly influence the tissue's main functionality.

#### 4.2.3 Adipocytes exhibit greater variety in relation to nutrition and age

To further understand what caused the split between the various sub-clusters of adipocytes, we focused initially on the chronic diet conditions AL and DR. Before evaluating the effects of a late-onset diet switch, it was essential to know how chronic DR differs from AL and how aging affects the metabolic activity of the tissue. Datasets from old and young AL and DR were merged together and after unsupervised clustering we obtain 4 subclusters of adipocytes (**Figure 4-3 A**). Those 4 clusters were divided based on their age and diet conditions (**Figure 4-3 B**). We compared them using differential gene expression analysis and looked at the enriched hallmarks from the enrichment analysis using on Msigdb Hallmarks (Subramanian 2005).

Firstly, we looked at the ageing effect in both diet conditions (**Figure 4-3 C-D**). In DR, hallmarks of adipose tissue metabolic activity were upregulated with age (**Figure 4-3 C**). Among interesting genes upregulated with age we noted some genes being linked to the de-novo-lipogenesis (DNL) pathway, like *Lipe* which hydrolyses stored triglycerides to free fatty acids, *Fasn* which catalyses the synthesis of palmitate from acetyl-CoA and malonyl-CoA, in the presence of NADPH, into long-chain saturated fatty acids, *Acs11* synthesizes long chain fatty acid. The upregulation of this pathway under DR has been showed previously (Solinas et al., 2015) and observed in the previous bulk study (L. F. Oliver Hahn 2019). DNL would contribute to maintain a flow of long fatty acids, either for mitochondria biogenesis or to act as adipokines and

activating transcription factors sustaining a healthier metabolic homeostasis (Song et al., 2018)

In the case of AL feeding, similarly genes linked to metabolic activity of the WAT were upregulated with age but not the same genes as DR (**Figure 4-3 D**). Insulin linked genes such as *IRS1*, *IGF1* or *PParg* are essential transcriptome factor for lipid metabolism and were upregulated in AL\_24, demonstrating their crucial role for adipogenesis. This could be explained by the fact that in AL, with age, there is a need for a constant supply of mature adipocytes to stock new lipids. Interestingly *Sorbs1*, an insulin sensitive gene, that has been reported to contribute to adipose tissue inflammation and linked to obesity and diabetes (S. J. Kim et al., 2014) was upregulated in both AL\_24 and DR\_24 compare to their young conditions.

Then we took interest in the difference between the transcriptome profile of mature adipocytes in AL\_24 and DR\_24. Even if both conditions had a similar ratio of mature adipocyte at old age (**Figure 4-2 B**), they showed the most differences between all cluster's comparisons. In DR\_24 we noticed the upregulation of Mtorc1 signalling hallmark, and notably the genes *Acsl1*, *Acaca*, *Acly* which are all enzyme essential to DNL. DR\_24 showed lower levels of expression of the *Rora* gene compared to AL\_24 (**Figure 4-3 E**). *Rora* is linked to hypoxia and it has been suggested that the expansion of the WAT during obesity leads to a lack of oxygenation of the tissue. This has consequences on adipocytes, inducing insulin resistance, inflammation related adipokines secretion, and eventually contribute to tissue fibrosis (Trayhurn, 2013). This would explain why *Rora* and additional genes linked to tissue remodelling were downregulated in DR\_24 compared to AL\_24 since the WAT doesn't increase as much under limited feeding. For example, in the angiogenesis hallmark, *App* was downregulated in DR\_24 compared to AL\_24 (**Figure 4-3 E**). A previous study showed that *App* was increased in obese phenotype promoting hypertrophy of adipocyte (Min et al., 2017). Furthermore, several collagen genes, which are promoting differentiation into mature adipocytes to increase stockage capacity of lipids (Cho et al., 2019), were found downregulated between DR\_24 and AL\_24 in the epithelial transition hallmark. In young conditions, comparing DR\_5 to AL\_5, angiogenesis was downregulated with genes like *Vegfa*, which promotes proliferation of endothelial cells to enable oxygenation of the tissue (Herold & Kalucka, 2020)(**Figure 4-3 F**). AL expanding faster than DR could require more remodelling of the tissue even at young age, explaining

the downregulation of collagen genes in DR (**Figure 4-3 F**). DR\_5 had lower expression of adipogenesis genes compared to AL\_5, such as *Fabp4* and *Lpl* (Gonzales & Orlando, 2007) that are acting on maturation of adipocyte and lipid stockage.

With age, AL and DR adipocytes showed upregulation of different metabolic pathways, some differences being visible at young age such as the specific upregulation of DNL genes in young and old DR (**Figure 4-3 C,E**). AL diet driving adipocytes to activate pathways that would promote the proliferation of new adipocytes in order to stock more fatty acids and angiogenesis to remodel and maintain oxygenation of the tissue (**Figure 4-3 D,F**).

From the UMAP clustering to the enrichment results, adipocytes were divided in 4 clusters showing the impact of age and diet (**Figure 4-3A**). Even if DR is known to have a healthier phenotype even at old age, old DR adipocytes were not similar to young DR adipocytes (**Sup.Figure 10**). WAT under DR is subjected to less mechanical stress and immune infiltration which preserves the metabolic homeostasis of the tissue, yet ageing is still affecting the transcriptome profile of the tissue. This raises the question of when ageing prevents DR from having a beneficial impact on the metabolic activity of the WAT.

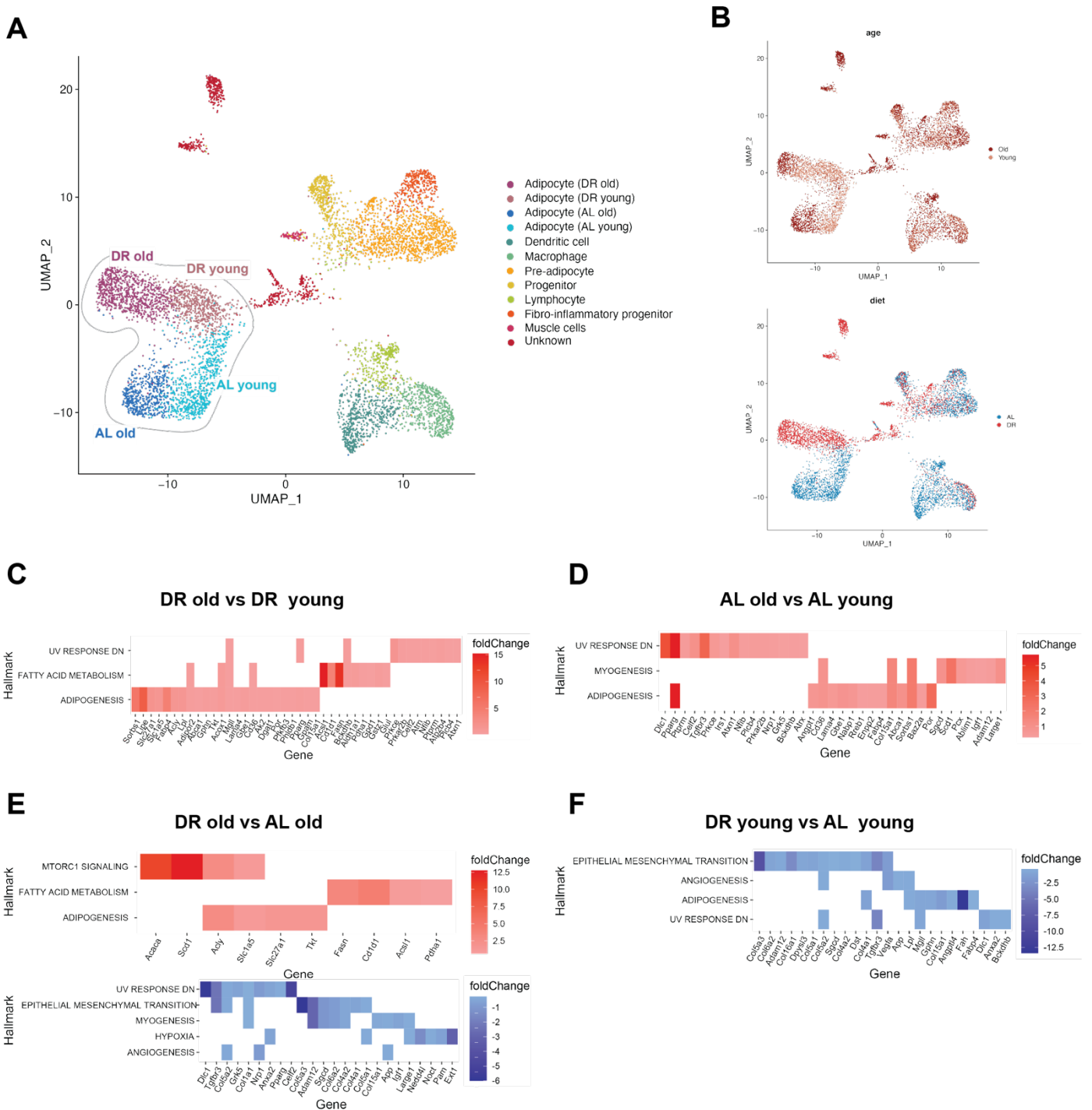


**Figure 4-3 Adipocytes show subtypes depending on diet and age**

**A**, UMAP of nuclei from all chronic conditions, AL young (5M), old (24M), DR young (5M), old (24M), from unsupervised louvain clustering, showing separation of adipocytes in 4 clusters in function of age and diet. **B**, UMAPs showing nuclei derived from young (5M) and old (24M) or from chronic conditions AL and DR coloured by age or diet. **C-D**, Hallmark enrichment analysis of differentially expressed genes between old and young adipocytes for DR and AL (ageing effect). Only significant enriched hallmarks are represented ( $P < 0.05$ , after correction with Benjamini-Hochberg). Corresponding genes of the enriched hallmark are red (upregulated) or blue (downregulated). **E-F**, Hallmark enrichment analysis of differentially expressed genes between DR and AL adipocytes at young and old age (diet effect). Only

*significant enriched hallmarks are represented ( $P < 0.05$ , after correction with Benjamini-Hochberg). Corresponding genes of the enriched hallmark are red (upregulated) or blue (downregulated)*

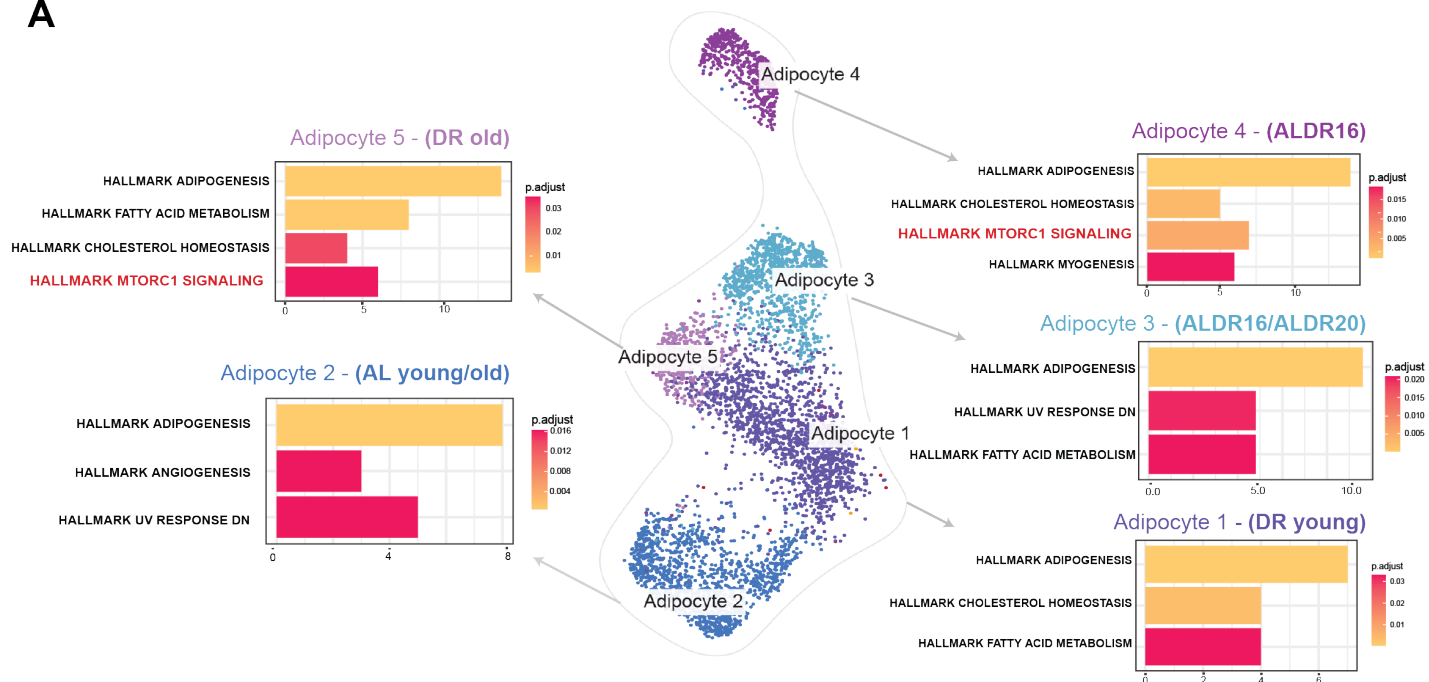
#### 4.2.4 A specific type of mature adipocyte emerges from the switch of DR at 16M

Chronic diets conditions showed gradient of sub-types of adipocytes separated based on age and diets, with giving evidence for metabolic differences observed between AL and DR increasing with age. To determine where the diet switch adipocytes were distributed among the sub-cell types of adipocytes, diet switch conditions were taken into consideration during the analysis. From the lifespan data, the switch done at 16 months showed lifespan extension similar to chronic DR while the later switch at 20 months was not extending lifespan (Lisa F. Drews, 2021). We investigated if we could see potential differences at the single-cell level between those two diet switches, especially among the sub-clusters of adipocytes. Five sub-clusters were observed when all conditions were merged together (**Figure 4-4 A**). Adipocytes 1 cluster was made of DR\_5 and part of ALDR16, while adipocyte 2 cluster was made of adipocyte from AL\_5 and AL\_24. Adipocyte 3 included ALDR20 and part ALDR16, and the two last clusters were from only one condition, ALDR16 for Adipocyte 4 and DR\_24 for Adipocyte 5. Only from the unsupervised clustering, AL young and old adipocytes (adipocyte 2) were separated from the others conditions. The DR young and old adipocytes, ALDR20 and part of the ALDR16 were overlapping while some ALDR16 (adipocyte 4) were completely detached from the other adipocytes.

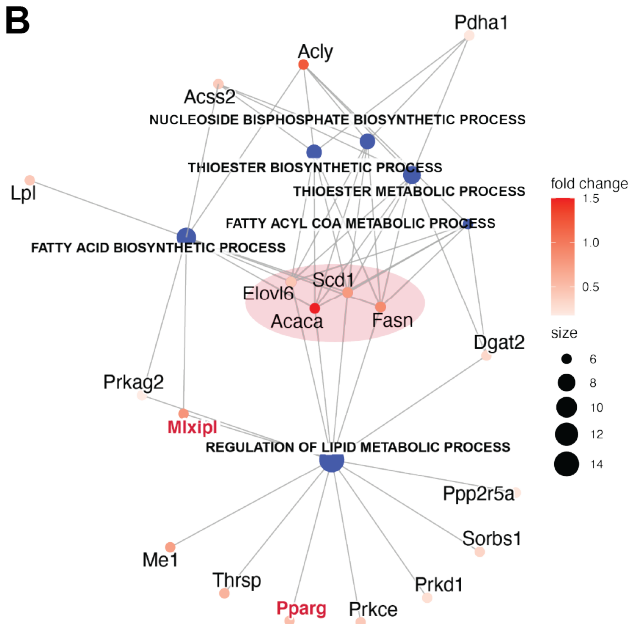
The two clusters made by a single condition, adipocyte 4 (ALDR16) and 5 (DR\_24) showed the most interesting profiles based on the enrichment analysis of their specific gene markers. Apart from upregulation of fatty acid metabolism hallmark, we noticed the significant upregulation of the hallmark mtorc1 signalling for both clusters (**Figure 4-4 A**). *Acaca*, *Acly*, *Elovl6* or *Me1* are among the genes enriched in this hallmark, and as it was already mentioned, they are connected to metabolic pathway of de novo lipogenesis. Interestingly, not all adipocytes of ALDR16 were in Adipocyte 4, only half of them, this cluster being metabolically similar to DR\_24, while the rest was merged in adipocyte 3 and 1. Given that it was present in both replicates (**Sup.Figure 8C**), it showed the consistency of this subpopulation of adipocytes with an unique metabolic

profile. To get more precise information on metabolic changes in that cluster, enrichment with GO term was also done. For this analysis the genes of that cluster were compared to all the other clusters in the tissue, and a network plot was used to represent relations between the different genes and GO terms (**Figure 4-4 B**). Again *Acaca*, *Fasn*, *Elovl6*, *Scd1* were significantly upregulated, and are central in the network showing the importance of long fatty acid synthesis. Two genes linking the GO term “regulation of metabolic process” and “fatty acid biosynthetic process”, *Prkag2* and *Mlxipl* are regulators of de novo lipogenesis process, ChERBP (*Mlxipl*) being strongly upregulated and actively promoting DNL as a transcription factor. We analysed the expression levels of the relevant genes across all clusters (**Figure 4-4 C**), particularly across Adipocyte 4 and 5. *Scd1*, the enzyme that transform saturated fatty acid in unsaturated fatty acid to be incorporated in membranes or act as lipokines, was highly in expressed in DR\_24 compared to ALDR16. On the contrary the other genes of DNL and the transcription factor ChERBP were highly expressed in ALDR16. Adipocyte 5 (DR\_24) and 4 (ALDR16) clusters showed similar upregulation of DNL, but with a difference in some key gene regulators, suggesting that some adipocytes are responding to the change of diet in the earlier switch at 16 months. Given that this is only seen in ALDR16, age may be a factor in response capability following diet switch.

**A**



**B**



**C**

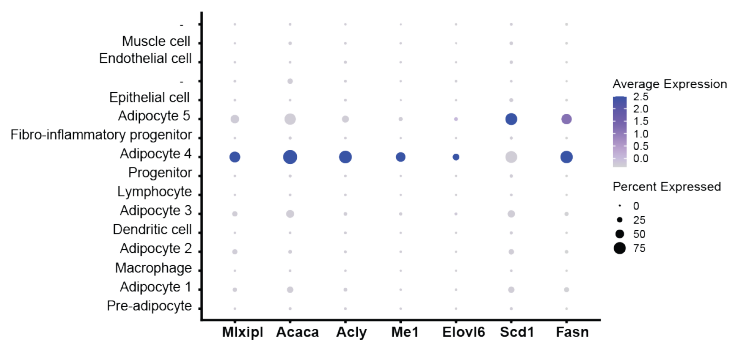


**Figure 4-4 A specific type of mature adipocyte emerges from the switch of DR at 16M**

**A**, Schematic representation of all adipocyte clusters from all merged data, with corresponding Hallmarck enrichment. Hallmark enrichment analysis of signature genes of each adipocyte cluster. Only significant enriched hallmarks are represented ( $P < 0.05$ , after correction with Benjamini-Hochberg). **B**, Gene-Concept Network showing linkages of genes and enriched GO categories (Biological Process). Blue node represents significantly enriched GO term ( $P < 0.05$ , after correction with Benjamini-Hochberg). Red nodes represent significant signature genes of the cluster, from light to dark red, showing the level of upregulation of the gene in the cluster compared to the rest of the dataset. **C**, Average expression of De-Novo-Lipogenesis genes in all clusters.

#### 4.2.5 With aging, the metabolic flexibility of WAT is impaired

To assess if age was an important factor in WAT ability to change its metabolic profile, we sequenced bulk RNA-seq samples of 3 replicates of the same conditions as the ones of the sNuc-seq experiment, and added ALDR16 at 20 months (ALDR16\_20) and ALDR20 at 28 months (ALDR20\_28) (**Figure 4-5 A**). The raw data from bulk RNA-seq samples were processed and normalised using Deseq2 (Love et al., 2014). Quite some variability was observed among samples of the same conditions, where conditions were overlapping in the PCA analysis (**Sup.Figure 12 A**). This could be due to the advanced age of the mice since variability is increasing with age, while in sNuc-seq variability might have been lowered by pooling 3 mice per sample. Some samples considered as outliers from the PCA analysis were identified, sample 1059 for DR\_24 and 1012 for ALDR16\_20. Interestingly by looking at the level of expression of some inflammation markers (**Sup.Figure 12**), sample 1059 of DR\_24 had higher expression of inflammation markers Cd68, Infgr1, Myo1f compare to other replicates, and the lowest expression of Cd163 which is anti-inflammatory (Chen et al., 2019). On the contrary, sample 1012 of ALDR16\_20 had higher expression for Cd163 but the lowest expression level for the pro-inflammatory markers compared to other replicates. And this was confirmed in the deconvolution results where sample 1012 had the smallest proportion of immune cells in all ALDR16\_20 samples and sample 1059 had the largest proportion among samples of DR\_24 (**Sup.Figure 12**). Inflammation seemed to play an important role in the variability observed among samples of the bulk analysis, where some replicates of the same conditions were not subjected to the same level of immune infiltration.

Despite the variability between replicates, since we wanted to specifically monitor the DNL signal specific to DR and some ALDR16 adipocytes (adipocyte 4), we focused on first on DNL gene expression across conditions. The PCA analysis was done this time only with DNL genes (**Sup.Figure 12 B**), and we could observe that based on the PC1 (61.43% of the variability), conditions were spread from DR\_24 to ALDR16\_20, ALDR16\_24, AL\_24 and ALDR20\_24, ALDR20\_28. Hence, DNL genes could separate the conditions following the trend observed in the SNuc-seq data, where DNL was upregulated in ALDR16 and DR\_24.

We then looked at the log normalised gene expression of DNL genes in all conditions (**Figure 4-5 B**). The same trend was observed regardless of the gene: compared to chronic AL the same genes in ALDR16 had higher expression levels 4 months after the switch (ALDR16\_20), following by a decrease after 8 months (ALDR16\_24). Similar observation was made for ALDR20 but the expression levels were lower than for ALDR16 as it was also observed in RTqPCR (**Sup.Figure 11. C**). Additionally, when compared to chronic conditions, ALDR16 at 20 and 24 months had similar levels of expression of DNL genes to DR\_24 while ALDR20 at 24 months matched AL\_24. ALDR20 at 28 months had the lowest level of expression for all DNL genes showing that ALDR20 expression of DNL genes did not recapitulate ALDR16's level even after a longer time frame (**Figure 4-5 B**).

To measure the relative proportions of adipocyte 4 (ALDR16) in all conditions (**Figure 4-5 D**) we performed tissue deconvolution analysis on the bulk data. We used the package SCDC (Dong et al., 2021) to do the analysis using combined SNuc-seq ALDR16 and AL\_24 dataset as reference (described in 3.3.2 Understanding changes in cell type composition with deconvolution analysis). All bulk RNA-seq samples were deconvoluted to evaluate proportions of different cell-types in each condition. Combining replicates samples together we could observe that the largest proportion of adipocyte 4 was observed in DR\_24 and ALDR16\_20 (**Figure 4-5 E**). ALDR20 proportion of adipocyte 4 was lower and decreased with age, fitting the previous trend observed with DNL gene markers (**Figure 4-5 B**).

Finally, another important factor linked to the diet and age is the level of inflammation of the tissue, and as it was previously mentioned, immune cell-type populations increased with age but also under AL. We looked at expression level of different immune cell markers (**Figure 4-5 C**), particularly 3 macrophage markers, *CD68*, *CD86*, and *CD163* (Chen et al., 2019). *CD68*, a pan macrophage marker, increased expression with age for ALDR20, while remain the same for ALDR16. *CD86* is an M1 macrophage marker, which promotes inflammation in the tissue. *CD86* increased with age for both switches and had higher level of expression in ALDR20. On the contrary, *CD163* an M2 macrophage marker, which is anti-inflammatory, showed decreased expression with age but was expressed at a higher level in ALDR16 compare to ALDR20. *Myo1f* which expression is linked to inflammatory response and *Ptprj* which is highly expressed in macrophage-enriched tissue, showed a similar trend where expression increased with age for switches, with ALDR20 having higher levels of

expression compared to ALDR16. This trend was also observed in the deconvolution results, where both switches showed increased percentage of immune cell types with time, with ALDR20 (52%) having a larger proportion compared to ALDR16 (45%) 8 months after the switch. Those results showed that inflammation of the WAT increased with age for both switches but ALDR16 expressing more anti-inflammatory macrophages, and lesser levels of pro inflammation markers compared to ALDR20 (**Figure 4-5 C**).

As a whole, those results showed that adipocytes with upregulation of DNL were more expressed in DR\_24 and ALDR16, while ALDR20 expressed lower level of DNL genes markers. In addition, ALDR20 showed a stronger decrease in expression of those markers 8 months after the switch while it remained similar for ALDR16. Even after the same time period, ALDR20 had a different metabolic profile compared to ALDR16, having less of the adipocytes 4 and an overall more inflamed status.

As a final validation we used the previous dataset of bulk RNA-seq with diet switch (Hahn et al., 2019) to do a deconvolution analysis with the same parameters (**Sup.Figure 13 E**). In this case the switch was done at old age (24 months) and transcriptomic profiles were measured 2 months later at 26 months. This short late-on switch didn't show as strong signals as the earlier switch from our study but some trends were still observable. Notably adipocyte 4 proportions were similar for young samples of AL and DR, but only AL proportion decreased at old age (**Sup.Figure 13 F**). Regarding the switches, DRAL that was under DR for a longer time had more adipocyte 4 compared to ALDR, putting in evidence again the link between restricted feeding and the subtype of adipocyte 4 upregulated for DNL expression.

Despite the variability in the bulk dataset, we observed similar trends in the sNuc-seq data and the bulk dataset. Those datasets were generated from different mice of the same cohort, showing consistency in the observed trends. Even an older dataset from another switch study hinted at similar patterns of impact of DR on the cell type landscape. Taken altogether those results suggest that switching to DR is affecting the metabolic function of some adipocytes, displaying a similar profile to DR. The earlier the switch to DR, the more effective is the change of metabolic activity to have the benefits from DR. ALDR20 diet switch was not able to recapitulate ALDR16 profiles after the same amount of time and even showed that late diet switch could trigger even more immune response compared to AL. This loss of flexibility of the WAT with age has been previously characterized as a memory effect of the bulk transcriptome as

described in (Hahn et al., 2019). Using a the single-nuclei approach, we could show that dietary memory is stronger in ALDR20 compare to ALDR16 that displayed a new sub-type of adipocyte adapting to DR. This observation was also validated through the bulk RNA-seq by looking at gene markers expression level and deconvolution analysis. We then investigated if the dietary memory was only coming from the mature adipocyte or if other cell types in had also a role in transcriptional flexibility of the WAT.

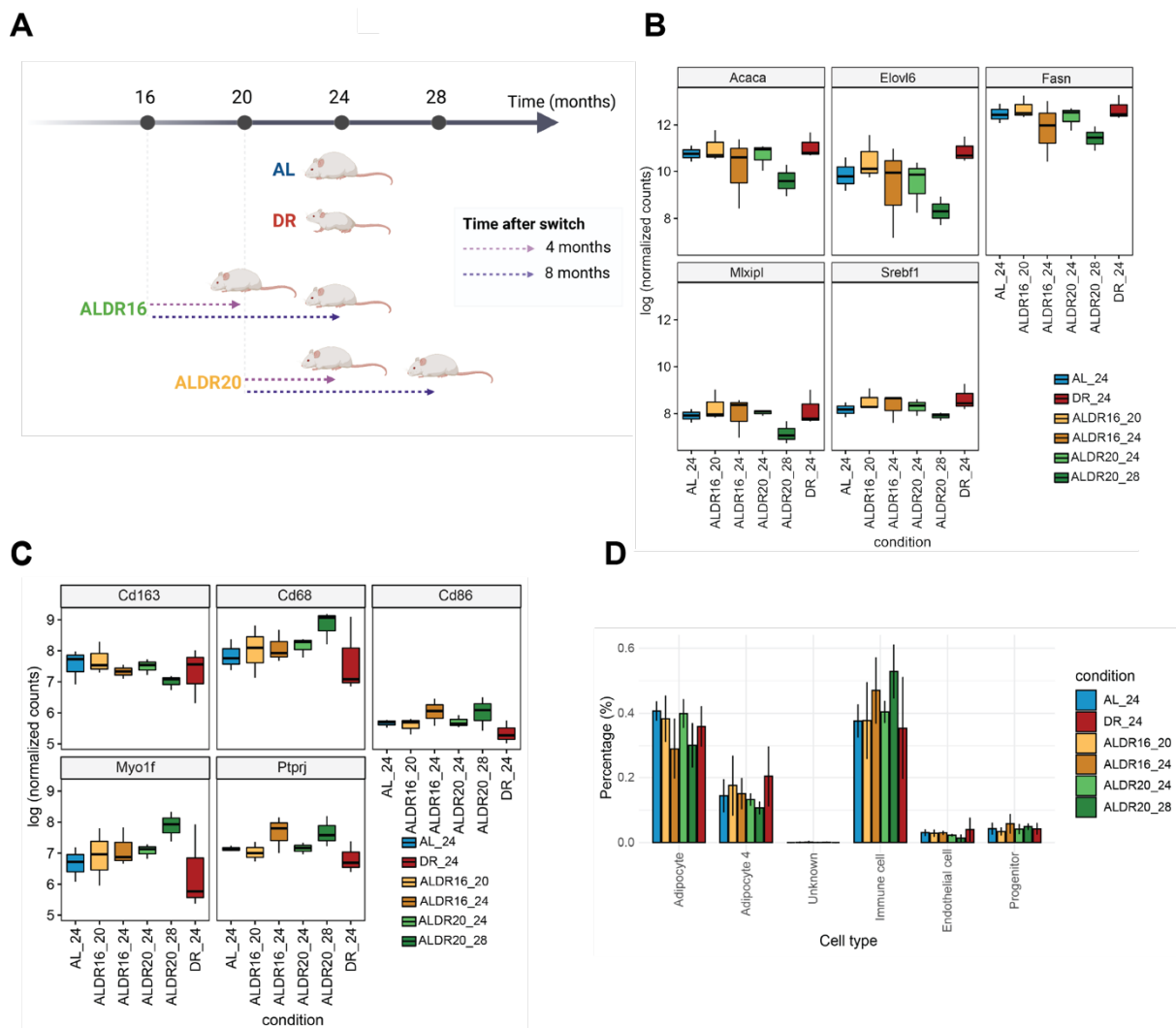


**Figure 4-5 Age is a key a factor in the metabolic flexibility of the WAT**

**A**, Schematic of experimental design for RNA bulk sequencing. **B**, Expression level (log of normalized counts using median of ratios methods) of DNL genes for all conditions. **C**, Expression level (log of normalized counts using median of ratios methods) of immune marker genes for all conditions. **D**, Percentage of cell-type categories per samples based on deconvolution analysis with SCDC. Data are plotted as mean  $\pm$  s.e.m.

#### 4.2.6 The transcriptional memory of the WAT is caused by gene expression changes in mature adipocytes and cell type composition of immune cells

The previous study on late-on diet switch used bulk RNA-seq data to compare transcriptomic profiles of liver and WAT before and after DR switch (Hahn et al., 2019). They looked at differentially expressed genes between DR and AL (DR/AL), and between DR and ALDR (AL/ALDR). If the number of differentially expressed genes between DR/ALDR was low, it would have meant that ALDR had a similar profile like DR and so fully adapt to the switch of diet. Nevertheless, the overlap of differentially expressed genes between DR/AL and DR/ALDR was comparably large, 1978 genes were found common, meaning that ALDR had a profile similar to AL in the WAT and did not fully adapt to DR. These 1978 genes were designated as memory genes, since their transcriptome profiles were not affected by the change of diet and remain similar as being under AL feeding.

Thanks to the single-nuclei dataset we were able to add information on where this memory effect is coming from in the tissue. We initially investigated the cell types expressing these memory genes. We selected memory genes that were commonly expressed in both bulk and all merged sNuc-seq data, in total 718 genes. We took the 30 memory genes that had the highest expression in the sNuc-seq data and looked in which cell types they were mostly expressed (**Figure 4-6 A**). We could see that they were found mainly in the different adipocytes' subtypes (adipocytes 3,4,5) but also in some immune cell types such as macrophages and dendritic cells. Looking at the top 30 genes, some genes found in adipocytes are genes of the DNL pathway such as *Acaca*, *Acs11* or *Acly*. In macrophage we noted *Zeb2* and *Ptprj* that are gene mainly expressed during immune response. We looked at the repartition of all 718 genes in the different cell-types and summarized the results in (**Figure 4-6 B**). It validated what we observed, 67% were expressed in adipocytes and 21% in immune cell types. It seemed that if a lot of memory genes from the bulk were coming from adipocytes, it could come from difference in gene level expression, especially as we saw upregulation of DNL pathways in DR\_24 compared to AL\_24 (**Figure 4-3 E**) but also from differences in proportion of sub-type of adipocytes such as the adipocyte 4. On the contrary genes found in immune cells seemed to not come from a difference in

gene expression but from different proportions between conditions. We didn't capture subtypes of macrophages depending on the condition, their transcriptomic profiles remained similar, whereas their proportion changed with immune infiltration (**Figure 4-2 B**). Immune cells were found to represent approximately 40% of cells for AL\_24 and ALDR16 but only 5% for DR\_24. This could explain why gene markers of macrophages and in general immune cells would be found differentially expressed in the bulk RNA-seq dataset. If the memory effect seemed to come from both differential gene level expression and changes in proportions in the cell-type landscape, we then focused on the adipocytes, being the main cell-type found in the memory analysis.

We did a similar analysis as the one in bulk, to define memory genes from the sNuc-seq data in adipocytes. Both switches were used to define memory genes, finding 108 refractory genes for ALDR16 and 73 for ALDR20 (**Figure 4-6 C**). More genes were differentially expressed between DR\_24 and ALDR16 compared to DR\_24 and ALDR20. Looking at the top genes downregulated in DR\_24 compared to ALDR16 in adipocytes, we found all genes from DNL pathway and ChREBP (**Table 5-2**). On the contrary, genes that were upregulated in DR\_24 compared to ALDR16 were insulin sensitive such as Sorbs1 (Yang et al., 2003), Fam13a (Wardhana et al., 2018), anti-inflammatory genes like Nnat (Ka et al., 2017) or genes involved in thermogenesis like Ctcflos (Bast-Habersbrunner et al., 2021) or Adbr3 (Rayanne B. Burl et al., 2018)(**Table 5-1**).

We then compared those memory genes to the ones found in bulk and commonly expressed in both datasets. In both cases, almost half of the sNuc-seq memory genes were found in the bulk ones, 46% and 41% for ALDR20 and ALDR16 respectively (**Figure 4-6 D**). Hallmark enrichment analysis was done on the genes found common between bulk, ALDR16 and ALDR20 memory genes (19 genes) (**Figure 4-6 E**). Fatty acid metabolic processes were found enriched, including genes of the DNL pathway, Acaca, Acsl1, Acly. Then genes found in memory only for the ALDR16 genes were used for hallmark enrichment (**Figure 4-6 F**), and among the terms enriched lipid metabolism terms were found but RNA splicing as well. All lipids' enriched terms were linked by Mlxipl (ChREBP) as previously observed upregulated in adipocyte 4 (**Figure 4-4 B**), a transcription factor which activates DNL pathway.

Single-nuclei data helped to better characterize the memory effect observed in the bulk dataset, showing that the memory genes found were present mostly in adipocytes but also in immune cells. The refractory genes would come from both non adaptation

of gene level expression but also change in cell type proportions in the tissue. Furthermore, we analyzed the single-nuclei dataset in the same way to define memory genes from both switches and compared it to the bulk. Only half of the memory genes for both switch were found in the bulk, and common genes were linked to fatty acid metabolism notably the specific upregulation of DNL in DR. Interestingly only in specific memory genes of ALDR16 was found the transcription factor ChREBP, emphasizing its important function for adaptation to DR. Thanks to the single-nuclei data we collected additional data to better understand which cells are the main actors of the transcriptional flexibility of the WAT and which metabolic pathways are involved in the process.

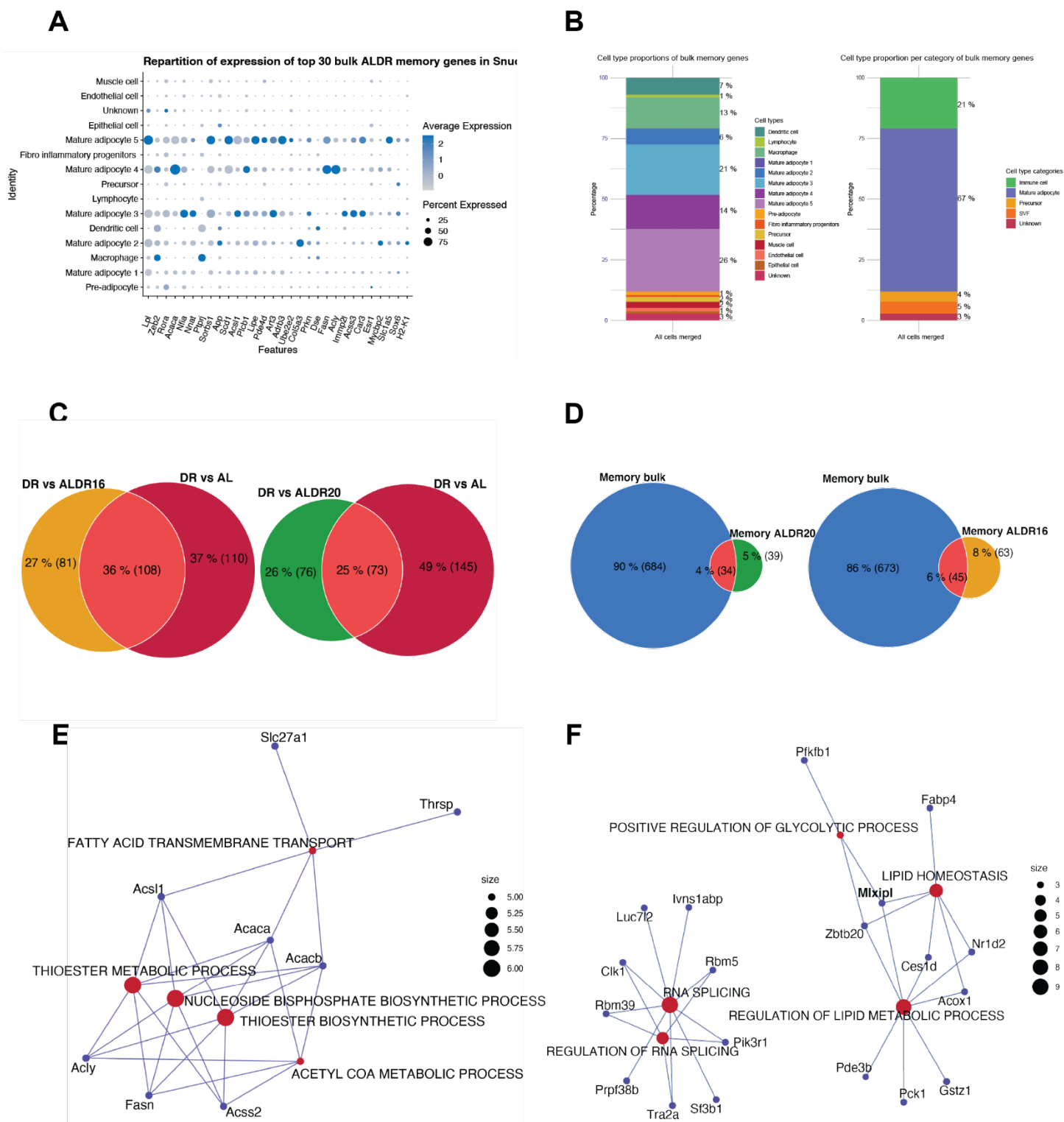


**Figure 4-6 Memory genes analysis from bulk and single-nuclei data**

**A**, Dotplot of the cell type repartition of top 30 expressed memory genes from bulk in the all merged single-nuclei dataset. **B**, Stacked bar plot of the repartition of all memory genes from bulk in all cell types, and by cell type categories. Each memory gene was associated to the cell type where it was the most expressed. Proportions are based on the amount of memory

genes per cell type, or summarized in cell type categories. **C**, Venn diagram of single nuclei memory genes analysis. Memory genes are the overlap between differentially expressed genes of DR/AL and DR/ALDR16, and DR/AL and DR/ALDR20. **D**, Venn diagram of comparison between memory genes from bulk and SNuc-seq data. **E**, Network plot of hallmark enrichment of memory genes common to bulk, ALDR16 and ALDR20 (19 genes). **F**, Network plot of hallmark enrichment of memory genes unique to ALDR16 (63 genes).

## 4.3 Discussion

DR increases health and lifespan in diverse organisms including primates (Balasubramanian et al., 2017). In humans, short term interventions with moderate caloric restriction also improve health, by decreasing the prevalence of age-related pathologies like diabetes, cardio-vascular diseases and cancer (Redman & Ravussin, 2011). However, maintaining a DR diet over long periods is challenging for most humans, which is also reflected in higher withdrawal rates of participants following the DR regime in the corresponding clinical trials. Reducing the time period in which humans have to practice DR should make it more applicable to a wider part of the population and might also reduce negative side effects. Thus, the timing of the DR treatment and whether late-life DR can positively affect health and survival in humans are important questions, that are currently underexplored. In mice, DR is only effective in extending lifespan, when initiated earlier in life (Hahn et al., 2019). Mice lose their ability to respond with lifespan extension to DR between 16 and 20 months of age (Lisa F. Drews, 2021). A previous study looked into the transcriptome of liver and WAT, highly active metabolic organs, and found that at old age, the white adipose tissue (WAT), is unable to adapt to the DR condition (Hahn et al., 2019), indicating a nutritional memory of gene expression in the WAT. However, the molecular basis of this memory and the cell types in the WAT that contribute to memory formation were unknown. In my PhD thesis, I addressed these questions by performing single-nuclei sequencing of the ageing WAT under DR conditions.

### 4.3.1 The effects of age and diet on the cell-type landscape of the WAT

I generated a dataset of 12044 nuclei in total from 6 different conditions, divided in 16 clusters after non-supervised clustering, showing how the cell-type landscape is modified by age and diet. We noticed that the cell-type diversity increased with age, mainly driven by immune infiltration, especially in chronic AL and in the late switches. Comparison of lean and obese human phenotypes with single-cell also confirmed the presence of larger immune population in obese patients (Hildreth et al., 2021). Each condition had either different cell-types or in different proportions, but interestingly only mature adipocytes displayed sub-cell types in function of age and diet. The importance

of mature adipocytes could not be characterized in bulk RNA-seq and they were usually missed out in single-cell studies because of their large size, but thanks to a single-nuclei approach, we got specific transcriptomic profiles from sub-clusters of adipocytes. We investigated their transcriptional activity starting by comparing the chronic diet AL and DR diets at young and old age. The diet type shaped the metabolic profile of adipocytes from young age, and with age an increased fatty acid metabolic activity was observed. DR\_24 adipocytes showed upregulation of both Mtorc1 signaling and genes linked to DNL which was previously associated to insulin sensitivity (Collins et al., 2010). On the contrary AL\_24 adipocytes showed upregulation of pathway linked to tissue expansion such as angiogenesis, myogenesis, epithelial mesenchymal transition but also hypoxia. Hypoxia has also been linked to the crown-like structure of macrophages surrounding dead adipocytes (Hasty 2008). This was also observed in mice from the same cohort of this study. AL\_24 mice and ALDR16, ALDR20 shortly after switching diet, had an increase of crown structures in the WAT (Lisa F. Drews, 2021).

Although pathways associated with a healthy phenotype were upregulated in mature adipocytes old DR animals, they were not similar to adipocytes from young AL or DR animals, indicating that DR induces a specific transcriptional profile and is not just slowing down age-related gene expression. Consistent with this hypothesis, the expression profiles of AL and DR adipocytes were already different at young age. Under AL conditions pathways involved in adipocyte expansion and lipid storage were upregulated. The hallmark "*UV Response DN*" is upregulated in AL\_5 compared to DR\_5, and is also upregulated with old age regardless of the diet. In WAT, UV exposition, modifies the expression of adipokines and can lead to macrophage infiltration (Kim et al., 2018) and inhibits adipogenic differentiation (Lee et al., 2010). The genes found in the hallmark are downregulated when exposed to UV light, and are associated to adipogenesis like *Dlc1* (Sim et al., 2017) or progenitors' proliferation such as *Tgbr3* (Petrus et al., 2018) . Upregulation of this pathway shows the need of more mature adipocytes to stock lipids, where this was observed mostly under AL feeding, but also increased with age for both diets.

Cells are communicating in a tissue, and in a heterogenous tissue such as the WAT, the diversification of cell-types with age can have an influence on the metabolic activity of the tissue. Adipocytes are interacting via adipokines secretion but also by being in contact with pro or anti-inflammatory cytokines expressed by immune cells. For

example, sub-types of pre-adipocytes have been characterized based on their spatial localization, notably fibro-inflammatory precursors being close to macrophages (Backdahl et al., 2021). Based on our observation DR did not rejuvenate the tissue, but protected it from hyperplasia and immune infiltration which dysregulate the homeostasis of the tissue.

#### 4.3.2 Late-onset DR at 16 months leads to a unique subtype of adipocyte

We then focused our analysis on mature adipocyte of the switches to determine whether mid-life onset provides the same benefits as chronic DR. Interestingly a specific sub-cluster of mature adipocytes was found only in ALDR16, and showed a similar metabolic profile like DR\_24. In fact, apart from Mtorc1 signaling and DNL pathway being upregulated like in DR\_24, we observed the upregulation of the transcription factor Mlxipl (ChREBP) specifically in that unique cluster of ALDR16. A previous study in obese humans demonstrated that increased expression of adipose ChREBP was associated to improved glucose tolerance and positively correlated to insulin sensitivity (Kursawe et al., 2013). ChREBP expression in adipose tissue is also regulated by transporter GLUT4 which is important for modulation of glycemia. Obese patients with insulin resistant phenotype displayed decreased expression of GLUT4 and lipogenic enzymes compared to non-obese subjects showing the importance of the transcription factor for metabolic health (Eissing et al., 2013). ChREBP target genes are involved in DNL, including the fatty acid elongase ELOVL6, which produces elongated fatty acid like phospholipid oleic acid (Eissing et al., 2013). Mitochondria biogenesis and DNL are both upregulated in the WAT of DR animals (Hahn et al., 2019). Accordingly, it has been suggested that long chain fatty acids might be used to supply mitochondria membrane production and the upregulation of mitochondrial activity might contribute to maintain a healthier metabolism under DR (Hahn et al., 2019). This was not observed in the sNuc-seq, since most mitochondria genes were not captured in nuclei transcriptomes.

ChREBP was not identified as a strongly regulated gene in the previous bulk data set but was identified as a highly regulated gene in the single-nuclei data set. This might be explained by the fact that there are 2 isoforms of ChREBP, ChREBP- $\alpha$  and ChREBP- $\beta$ . Only ChREBP- $\beta$  isoform has a constitutive nuclear localization, and has

elevated transcriptional activity compare to ChREBP- $\alpha$  (Herman et al., 2012). Its expression is associated to expression of DNL genes and insulin sensitivity (Eissing et al., 2013), which could explain why we saw its upregulation under DR in sNuc-seq data.

Long chain free fatty acids have been suggested to contribute to improved health by enhancing plasma membrane fluidity and improving insulin signaling (Morigny et al., 2019). Additionally, long chain free fatty acid also act as lipokines activating intracellular pathways of fatty acid metabolism. *ChREBP* activity is tightly linked to *PPAR $\gamma$* , and can activate *PPAR $\gamma$*  through endogenous fatty acid (Nicole Witte 2015). Supplementation of palmitoleic acid effectively improved insulin and glucose tolerance in dependence of *PPAR $\gamma$*  of mice on a high fat diet (Souza et al., 2020). *PPAR $\gamma$*  is a transcription factor highly expressed in adipocytes, regulating storage and adipogenesis, but its major role as modulator of lipid metabolism and insulin sensitivity makes it an important target to prevent age-associated diseases and improve lifespan. This actually fit as well with the mitochondria biogenesis hypothesis since *PPAR $\gamma$*  is an activator of the pathway, and its expression is upregulated in clusters linked to upregulation of ChREBP and DNL, like adipocytes of DR\_24 (adipocyte 5) and ALDR16 specific cluster (adipocyte 4).

A spatial transcriptomic study done on human WAT, identified 3 different types of adipocytes, and associated insulin sensitivity with marker genes linked to lipid metabolism and glucose, notably *ChREBP*, in one of the clusters. This sub-type of adipocyte showed positive correlation for insulin-stimulated lipogenesis and was also less abundant in obese subjects (Backdahl et al., 2021). Thus, in summary, these findings suggest that the sub-type of adipocytes observed in ALDR16 animals probably indicates a healthier adipocyte state.

#### 4.3.3 WAT transcriptional flexibility is impaired with age

We next enquired if the lack of responsiveness in ALDR20 was due to the short time frame, 4 months, to adapt to DR switch, when ALDR16 had 8 months. To verify this hypothesis, we generated a bulk RNA-seq dataset of WAT with the same condition as the sNuc-seq data, and ALDR16 at 20months and ALDR20 at 28 months. From expression levels of gene markers in bulk RNA-seq data, it showed that after a longer

time under DR, ALDR20 had still lower expression of DNL gene markers, and higher expression of inflammation markers. The remodeling capacity of the tissue seemed to be age dependent and this would explain why even after a longer period ALDR20 cannot benefit from the same metabolic shift as ALDR16.

One hypothesis explaining why ALDR16 still had the potential to adapt to DR could be that the pool of progenitors can differentiate in DR functional mature adipocyte compared to ALDR20. The proliferation and differentiation capacity of adipocyte progenitors is altered with age (Ou et al., 2022), so switching at an older age could be ineffective by lack of responsiveness of the tissue. Additionally, we looked at some gene markers involved in adipocyte differentiation, and at markers of full differentiated adipocytes. We observed that the sub-cluster of adipocytes observed only in ALDR16 expressed higher levels of PPAR $\gamma$  and ChREBP compared to other clusters, both being involved in differentiation (Witte et al., 2015), and lower levels of Fabp4 a marker of mature adipocytes (Arimochi et al., 2016). This might indicate that these adipocytes are younger, and differentiated after the switch to DR feeding. As the plasticity of the WAT declines with age, the late-life switch at 20 months of age might not be able to induce these changes due to a change in differentiation capacity of adipocyte precursor cells.

Finally, by comparing the results between the previous analysis done on bulk RNA-seq data (Hahn et al., 2019) and our results of sNuc-seq data, we could go deeper in characterizing the dietary memory. The list of genes from bulk RNA-seq data that were refractory to the change of diet between AL and DR, were found mostly in mature adipocytes but also in immune cells. Dietary memory could come from changes in gene expression, such as the different metabolic profiles observed in adipocytes but also from changes in cell type proportions, like immune infiltration.

It has been shown that obesity impacts negatively the metabolic activity of the WAT, with hypertrophy of the adipocytes resulting in hypoxia, which triggers the recruitment of pro-inflammatory cells (Khan et al., 2020). Because late-onset DR conditions were fed on AL for a longer period of time, they also experienced immune infiltration, which could account for the difference in immune cell count between them and DR, and the observation of immune genes in the memory genes.

The pro-inflammatory processes observed in obese phenotypes are also inducing pro-fibrotic phenotype, and impairing adipogenic potential. Progenitors differentiation potential is also affected with age, the accumulation of senescent cells affecting

adipogenesis (Tchkonia et al., 2010). This could explain the difference in gene expression profiles between adipocytes of DR and late-onset switch conditions, since after the change of diet, new progenitors might not be able to differentiate to a different metabolic profile and already matured adipocyte under AL feeding didn't adapt to DR. Interestingly in the single-nuclei memory genes, we observed more memory genes in ALDR16 compared to ALDR20, while ALDR16 had a cluster of adipocytes with upregulation of pathways similar to DR, such as DNL. Yet, looking at the DE genes in adipocytes between DR\_24 and ALDR16, it seemed that even if DNL was upregulated in both clusters, they displayed different profiles. We noted a stronger and significant upregulation of DNL and ChREBP in ALDR16 and genes linked to adipogenesis compared to DR\_24. In DR\_24 we saw upregulation of genes linked to insulin-sensitivity or thermogenesis. Being of the WAT is characterized by increased thermogenic capacity, leading to beneficial health effect since BAT is more active metabolically (Vargas-Castillo et al., 2017). Even if being of the tissue was not observed in DR mice of our study, previous study showed a link between caloric restriction and being (Fabbiano, Suárez-Zamorano, et al., 2016). In addition, DR\_24 showed upregulation of genes associated to inflammation, like *Snhg11* that recruits M2 macrophages (Shi et al., 2022). In summary those results showed that even if those two subtypes of adipocytes were enriched for DNL activity, their complete transcriptome profiles didn't overlap, as observed on the UMAP of all merged conditions. If the specific cluster of ALDR16 is made of adipocyte differentiated after the diet switch this could explain the upregulation of adipogenesis genes and absence of genes markers of inflammation.

#### 4.3.4 Conclusion, limitations and future perspectives

This project provided novel insights on the dietary memory observed in the WAT in the light of ageing and diet, however it was subjected to several limitations. The age window where mice did not respond to the change of diet could be sex-specific or specific to the mouse strain. Previous study observed different response to caloric restriction depending on the strain and sex of mice (Mitchell et al., 2016). Similar study of multiple diet switch could be done in male and other mice's strain in order to either confirm the age where transcriptional flexibility is declining, or to find a broader age

window. In addition, in the case of this study, enough tissue material was not available especially for the bulk RNA-seq experiment. Age increased the variance between mice, and particularly old mice (24M or 28M) would frequently have tumors or tissue fibrosis, which would increase the variance between samples. The lack of enough replicates prevented to do differential analysis with the bulk RNA-seq data or getting significant statistical differences between gene level expression. We could also see among replicates of the diet switches, that some mice responded well to diet restriction and would be protected from immune infiltration while some others would suffer from inflammation and were not showing sign of metabolic shifting. Understanding the causes behind the capacity or not to respond to diet restriction similarly among replicates of the same condition would be important.

The single-nuclei approach led to the discovery of new information that helped to better understand the dietary memory, although using a novel methodology can be challenging. Regarding the experimental dataset, since this is a costly method, we had to get 2 replicates for each condition, while additional replicates would have enabled to have statistical power and allow to detect smaller changes in the transcriptome. To limit the variability between replicates, we pooled 3 mice per replicate, but then we couldn't trace back which cells were coming from which mice. The small number of biological replicates per condition is not unusual in single-cell studies because of the cost and it also depends on the research question. To generate a cell atlas of a tissue, looking at a single condition, usually around 3 biological replicates are used (Emont et al., 2022) (Tabula Muris et al., 2018). When conditions are compared, usually less replicates are used. Similar to our experimental approach, a study of the epididymal adipose tissue that compare obese and lean states pooled 3 mice for both replicates in each condition (Sárvári et al., 2021).

Since the nuclei were selected by FACS, mitochondria were not found in the solution before encapsulation, so the mitochondrial DNA was not captured. This was observed in another study, where mitochondria genes were not present in single nuclei data (Lake et al., 2017). Mitochondria biogenesis being upregulated under DR was an important finding from the bulk RNA-seq dataset, and even if some mitochondrial genes are nuclear-encoded, we didn't see this signal in the sNuc-seq. Another drawback of the dataset's limited gene expression was that trajectory analysis was not feasible. This could have been used to estimate, using pseudotime trajectories

(Trapnell et al., 2014), if the subtype of adipocyte found in ALDR16 was indeed newly differentiated adipocyte after the switch to DR.

Despite those limitations, it was still possible to extract important biological information from the sNuc-seq and bulk RNA-seq datasets. They followed the same trends despite coming from different mice, which gave the results additional significance. Follow-up experiments could be done to validate the findings of this project. First, RNAScope might be used to confirm whether the new subtype of adipocytes discovered only in ALDR16 are in fact more numerous in ALDR16 compared to the other conditions (Wang et al., 2012). This technique allows visualization of single RNA molecules in individual cells directly in the tissue, using formalin fixed paraffin-embedded tissue for example. It could be used to look in the same tissue with specific markers of the new sub-type of adipocytes of ALDR16 and markers of adipocyte with an AL profile. Additionally, assessing if those specific adipocytes from ALDR16 were younger and just got differentiated could be done by using adipogenesis markers and seeing if there is a difference in maturation between the two clusters of mature adipocytes.

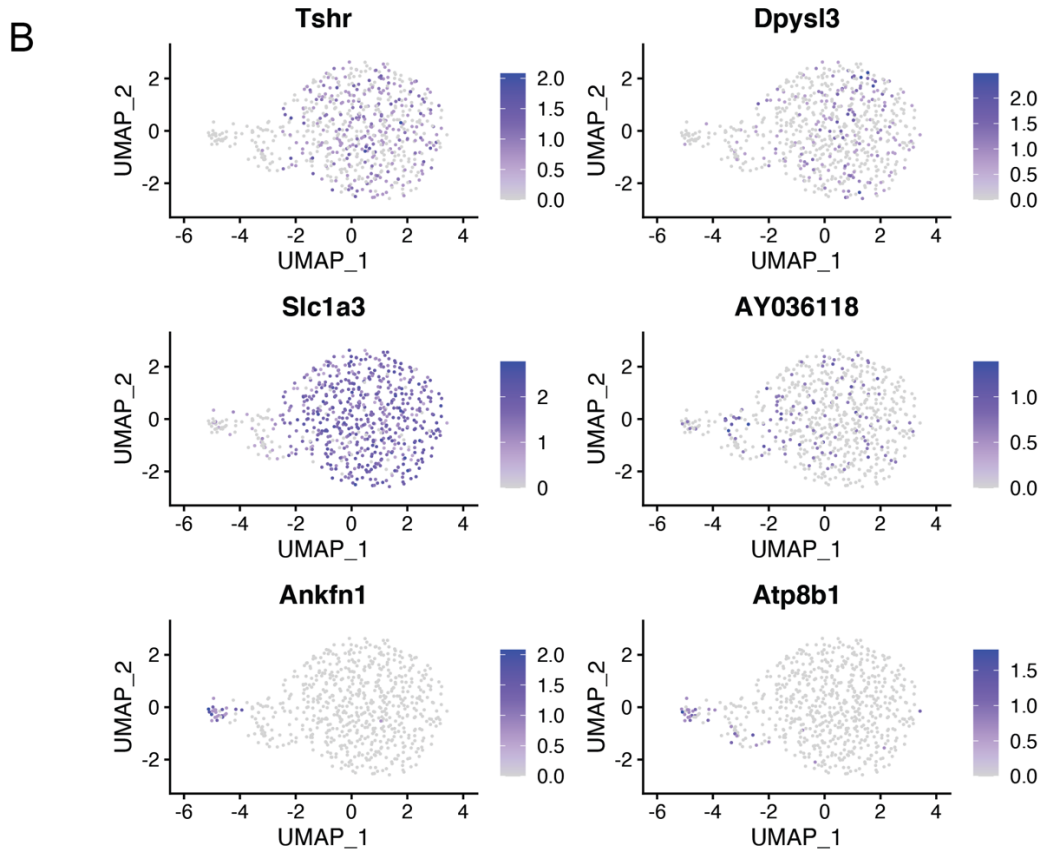
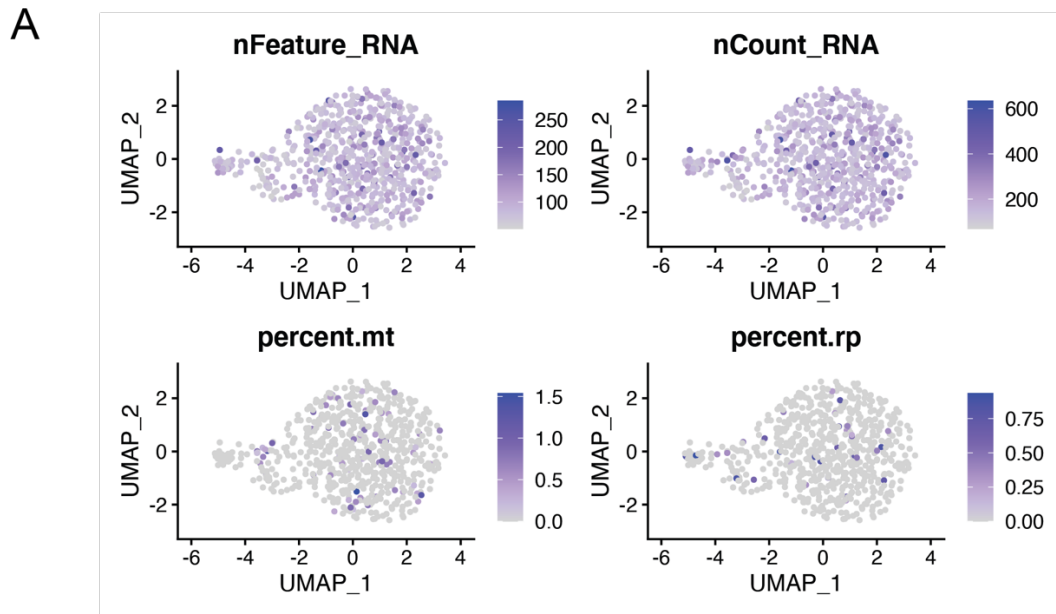
The cellular landscape is an important factor in the WAT homeostasis, it would be useful to see how those different subtypes of mature adipocytes are scattered in the tissue and which cell types surround them. Similar to the study done in human (Backdahl et al., 2021), it would be interesting to use spatial transcriptomics and assess if adipocytes respond to the diet in function of the cells surrounding them, and if the presence of macrophages or low vascularization could prevent the adaptation to DR.

Finally, one interesting finding of this study is the upregulation of the transcription factor ChREBP in the subtype of adipocyte found only in ALDR16. Palmitic acid-hydroxy-stearic acid levels are associated with ChREBP expression in adipose tissue, they have been shown to promote a healthy metabolic activity with anti-diabetic and anti-inflammatory effects (Iizuka et al., 2020). Further work is needed to understand why ChREBP is upregulated in some adipocytes under DR feeding, especially since it is activated with glucose.

In summary, our study demonstrates that DR positive effects on WAT are highly dependent on when DR is started. We showed that WAT is a highly heterogeneous tissue, its plasticity depending on the cellular landscape. With ageing, immune

infiltration increases, affecting its remodeling capacity and preventing to DR to be effective. The sNuc-seq data enabled to find a novel sub-cell-type of adipocytes, only found in the earlier switch at 16 months, showing upregulation of pathways linked to insulin sensitivity and fat tissue homeostasis. This metabolic profile is in adequation with the lifespan observations made on the same cohort, where ALDR16 was closer to DR and ALDR20 to AL. Those findings suggested that the metabolic flexibility of the tissue relied mainly on adipocyte and possibly their capacity to go through adipogenesis after the switch to DR. There is an effort in the research field to find a potential intervention preserving the differentiation potential of adipocyte progenitors. Some previous work showed promising results by blocking activin A and improving metabolic activity of senescent progenitors (Xu et al., 2015) or identifying specific gene targets maintaining differentiation capacity of adipose progenitors (Mandl et al., 2020). It would be interesting to investigate if the age at which the WAT stops responding to DR is delayed by combining an intervention that preserves the adipogenic potential of progenitors with multiple diet restriction switch time-points. Further work is now needed to find an intervention that would conjugate maintaining the plasticity of WAT in order to benefit from DR.

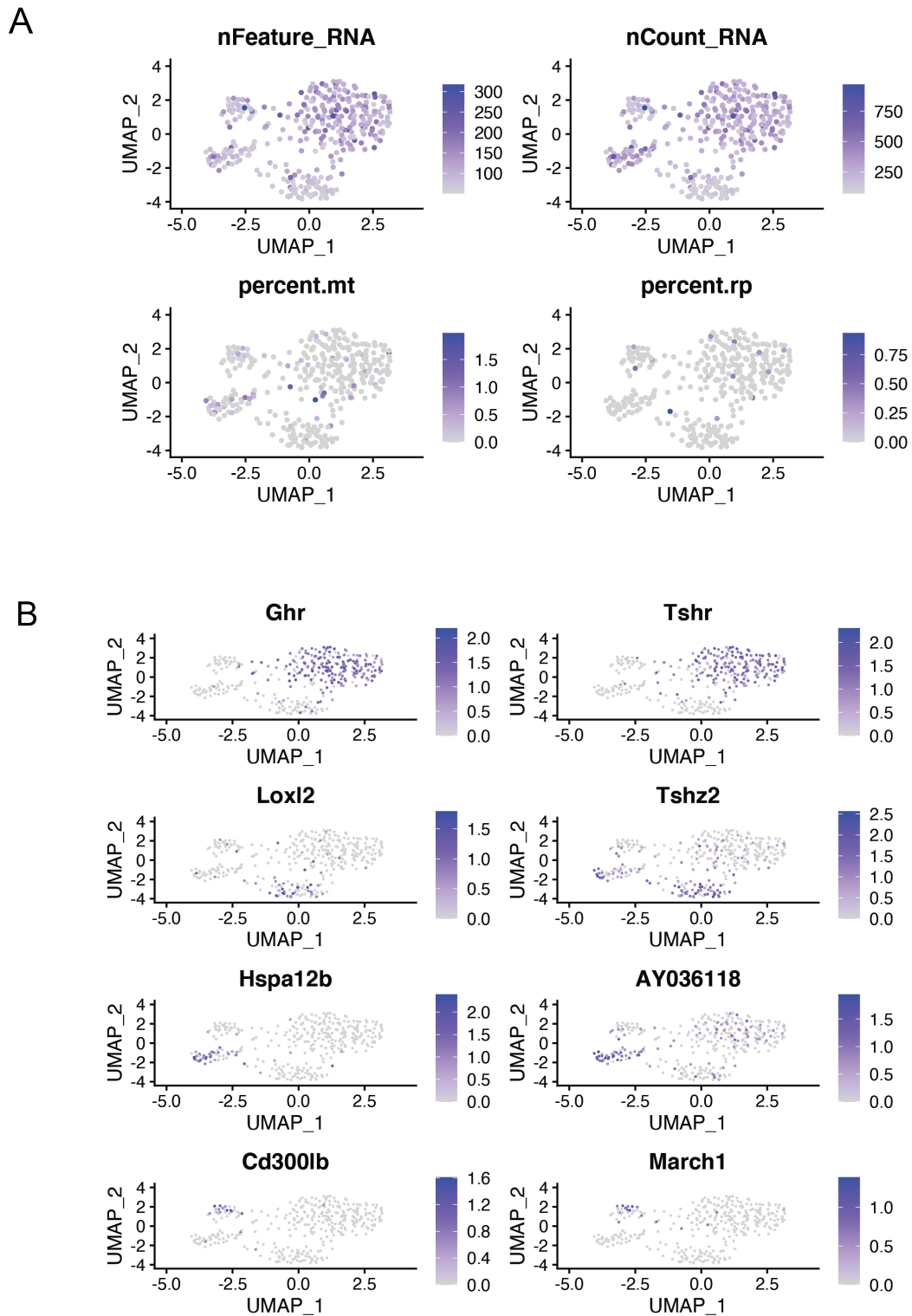
## 5 Extended data



**Sup. Figure 1 SNuc-seq data from AL young from 10X Chromium**

A, UMAP of the number of features detected, RNA molecules, percentage of mitochondria genes, ribosomal genes.

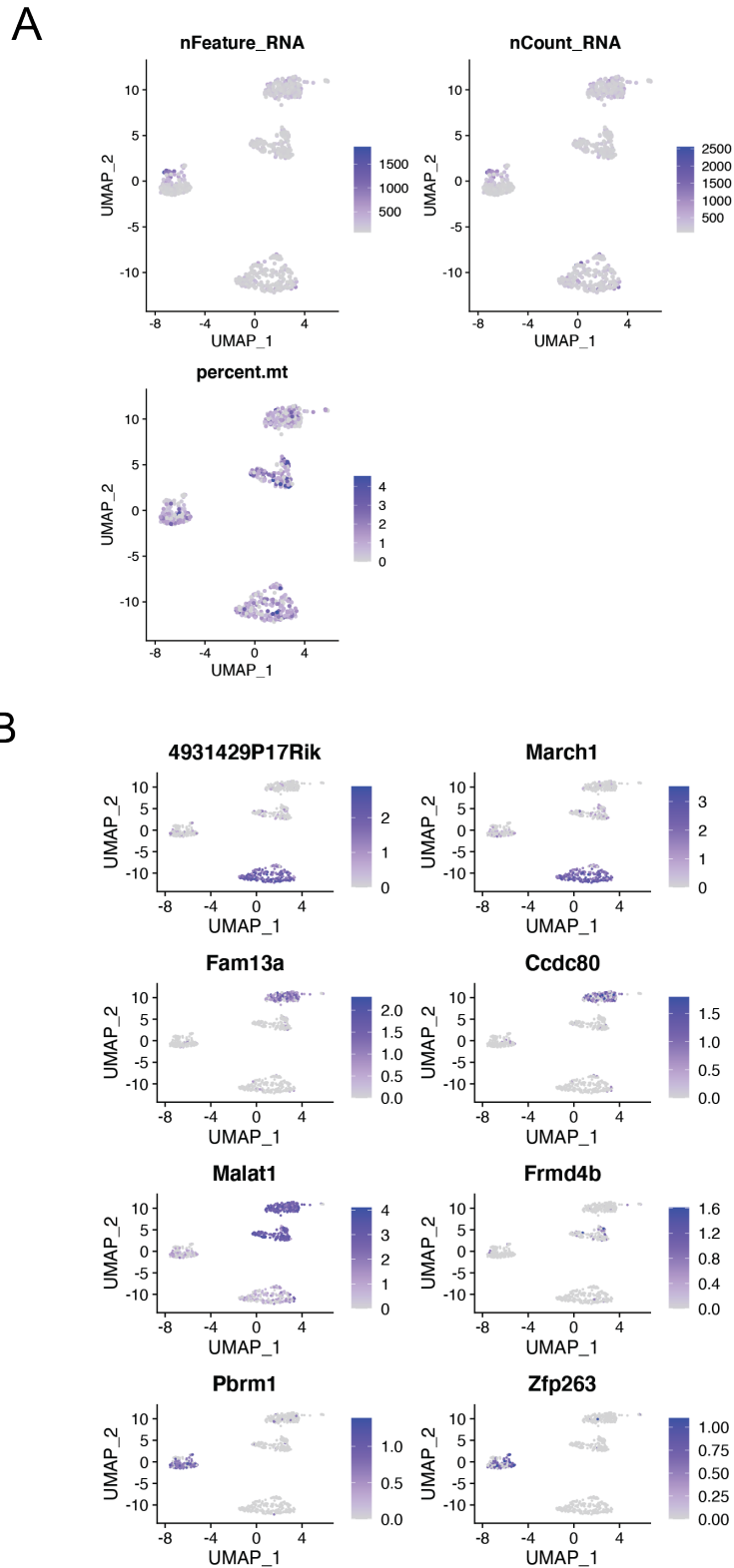
B, Selected UMAP feature plots showing RNA expression of two gene markers for each cluster



**Sup.Figure 2 SNuc-seq data from DR young from 10X Chromium**

A, UMAP of the number of features detected, RNA molecules, percentage of mitochondria genes, ribosomal genes.

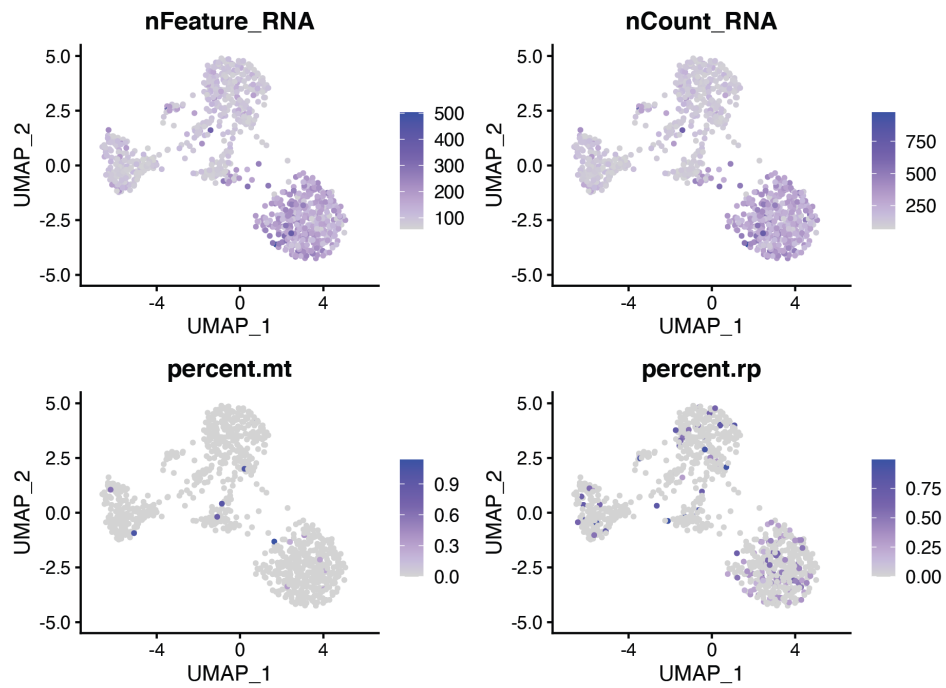
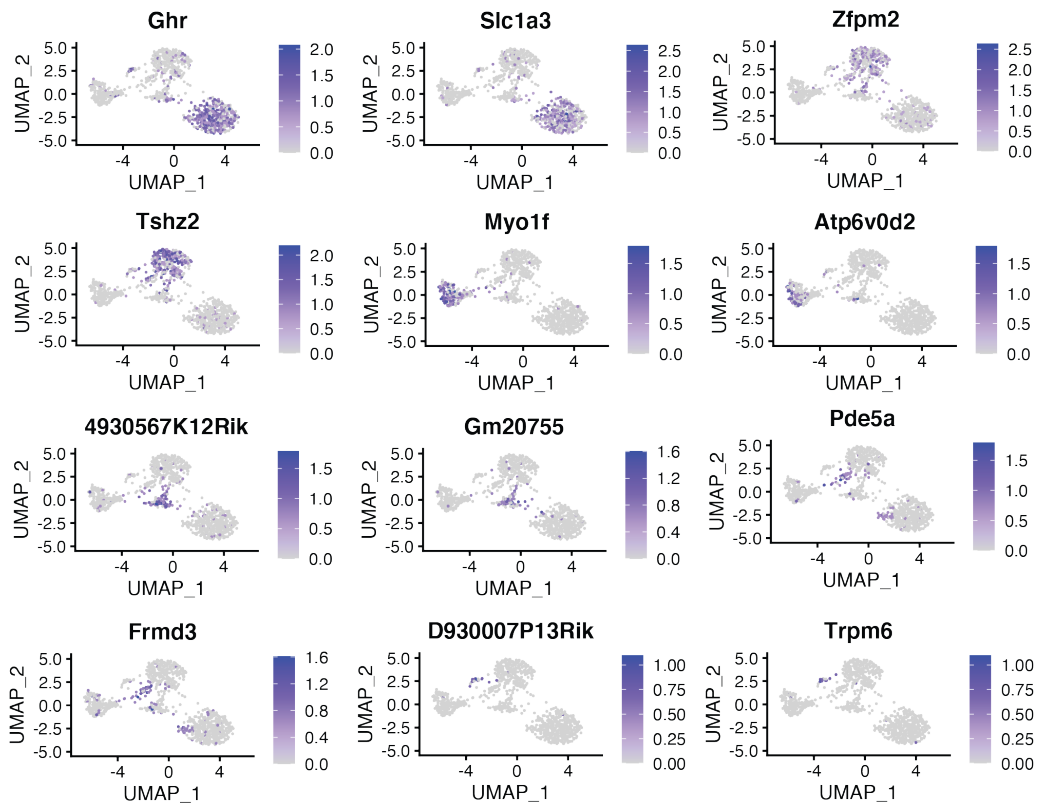
B, Selected UMAP feature plots showing RNA expression of two gene markers for each cluster



**Sup.Figure 3 SNuc-seq data from DR young from Nadia Instrument**

A, UMAP of the number of features detected, RNA molecules, percentage of mitochondria genes, ribosomal genes.

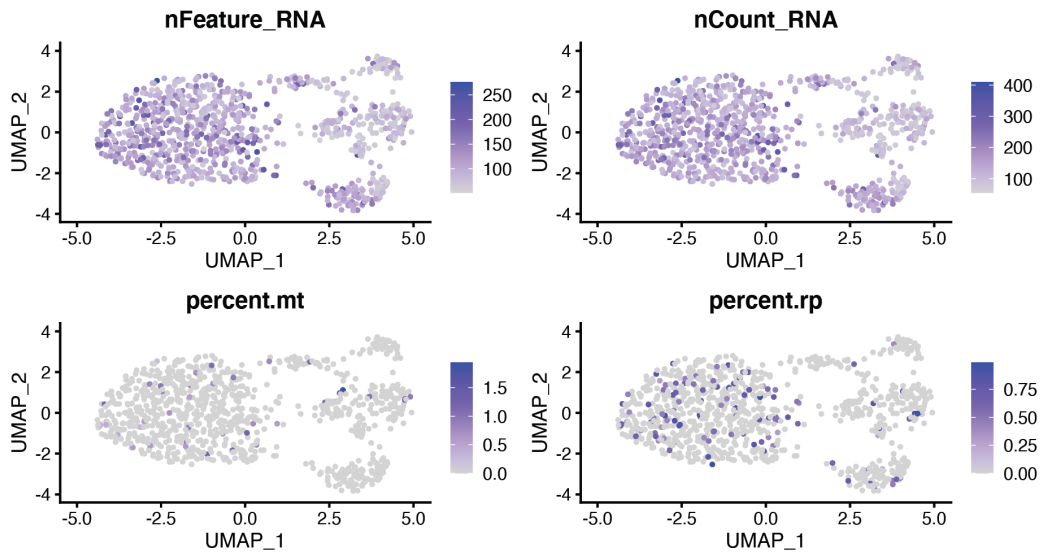
B, Selected UMAP feature plots showing RNA expression of two gene markers for each cluster.

**A****B****Sup.Figure 4 SNuc-seq data from AL young from FACS+10X Chromium**

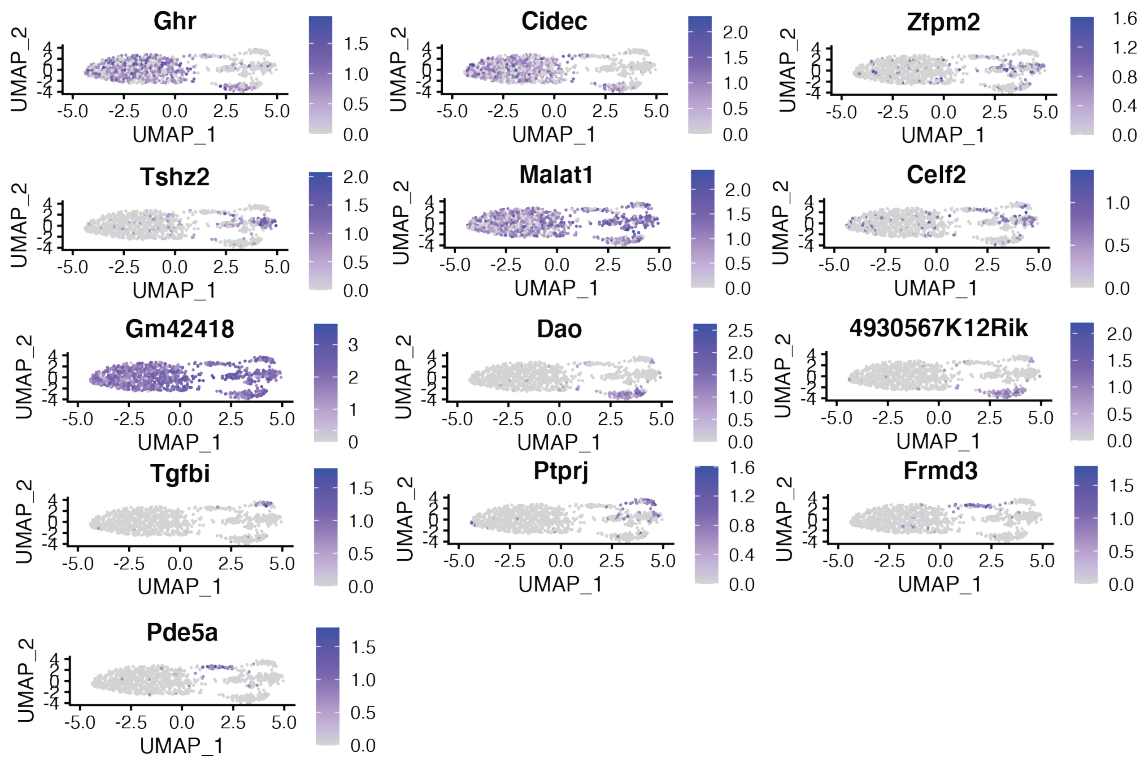
A, UMAP of the number of features detected, RNA molecules, percentage of mitochondria genes, ribosomal genes.

B, Selected UMAP feature plots showing RNA expression of two gene markers for each cluster

A



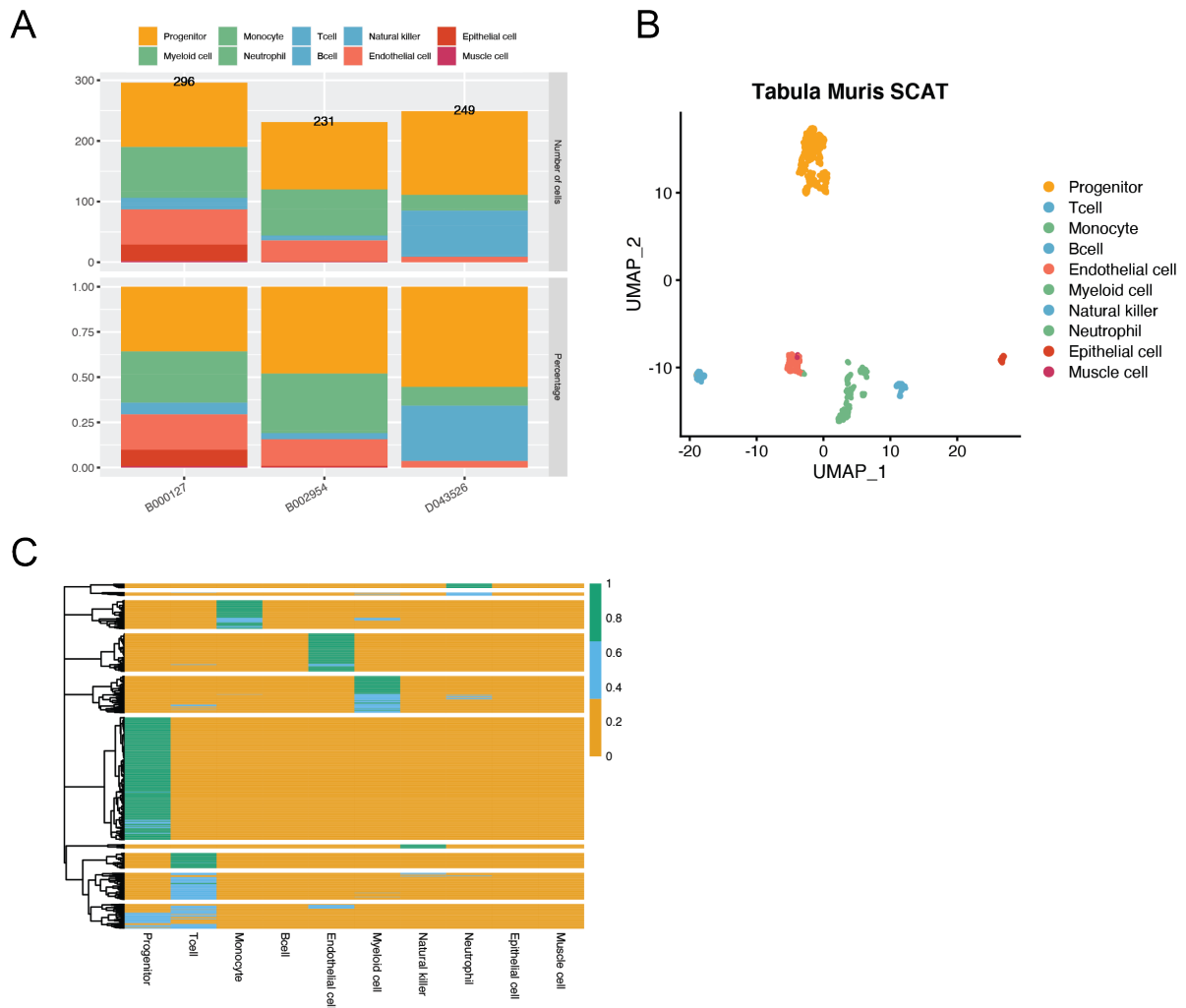
B



Sup. Figure 5 SNuc-seq data from DR young from FACS+10X Chromium

A, UMAP of the number of features detected, RNA molecules, percentage of mitochondria genes, ribosomal genes.

B, Selected UMAP feature plots showing RNA expression of two gene markers for each cluster

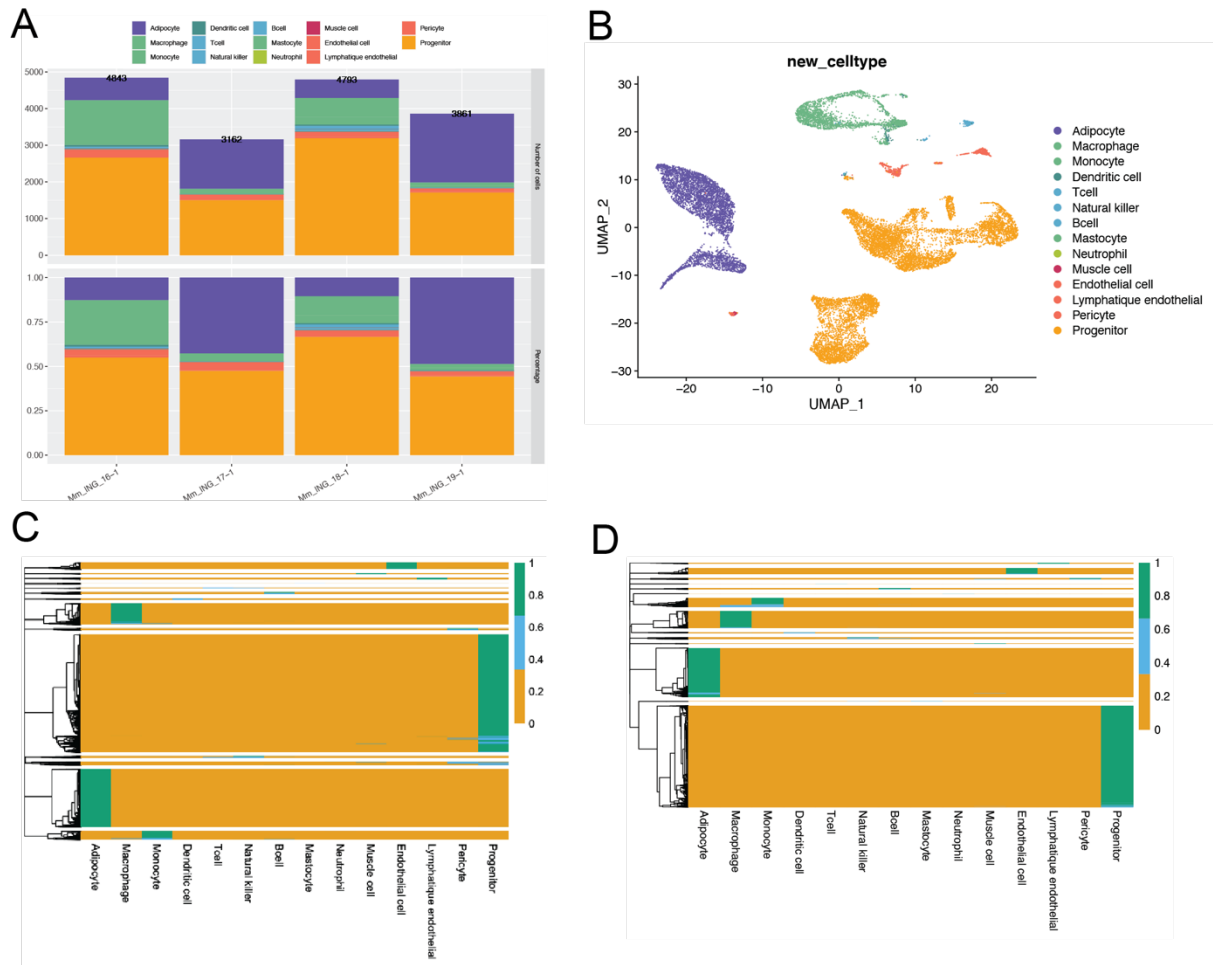


**Sup. Figure 6 Clustering of cells for Tabula Muris single-cell deconvolution reference dataset**

*A, Barplot of cell type distribution of 3 samples of sub-cutaneous adipose tissue (SCAT) from Tabula muris dataset*

*B, UMAP of the SCAT dataset*

*C, Heatmap of cells from SCAT dataset, clustered by cell-types. Cells having a similar profile to the other cells in the clusters are scored from 0.7 and above (green) and are used to construct the reference dataset.*



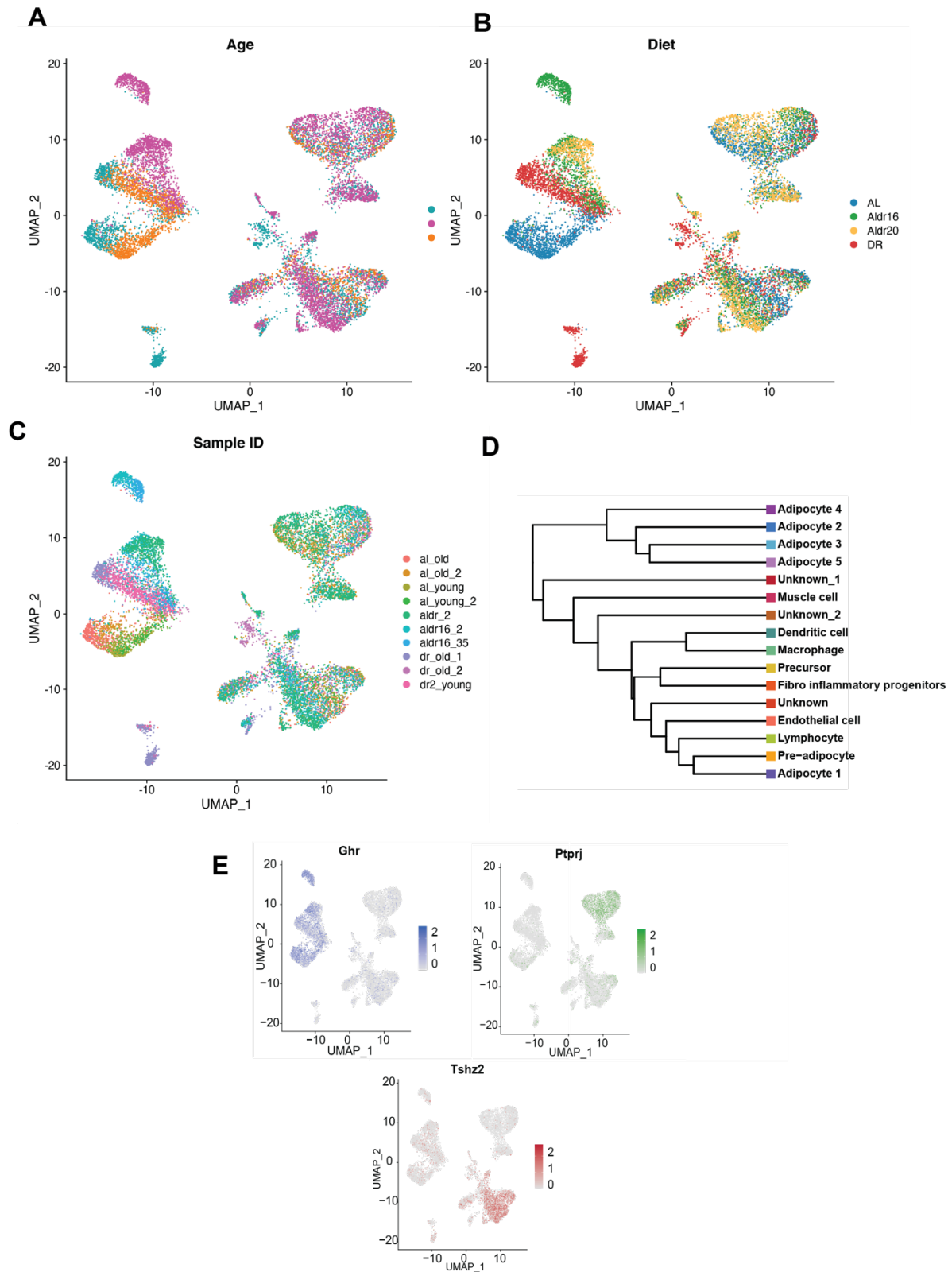
**Sup. Figure 7 Clustering of cells for Emont single-cell deconvolution reference dataset**

*A, Barplot of cell type distribution of 4 samples of Emont dataset*

*B, UMAP of the Emont dataset*

*C, Heatmap of cells from Emont dataset, clustered by cell-types. Cells having a similar profile to the other cells in the clusters are scored from 0.7 and above (green) and are used to construct the reference dataset.*

*D, Heatmap of cells from Emont dataset using only nuclei genes, clustered by cell-types. Cells having a similar profile to the other cells in the clusters are scored from 0.7 and above (green) and are used to construct the reference dataset.*



**Sup. Figure 8 Cell-type landscape of WAT in function of biological and technical parameters**

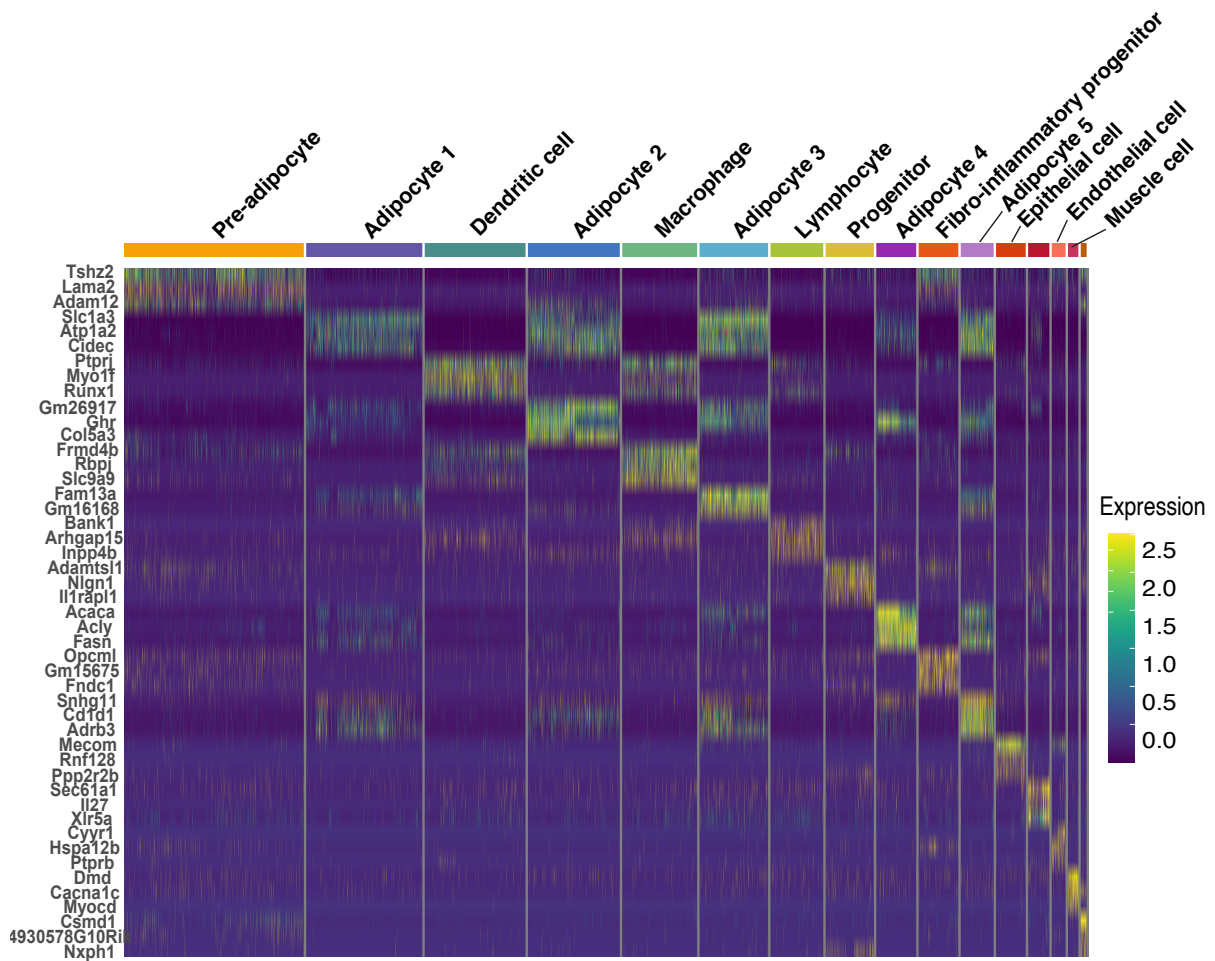
**A**, Uniform manifold approximation and projection (UMAP) two-dimensional map of nuclei from all merged conditions showing repartition by Age

**B**, UMAP of nuclei from all merged conditions showing repartition by Diet

*C*, of nuclei from all merged conditions showing repartition by Sample

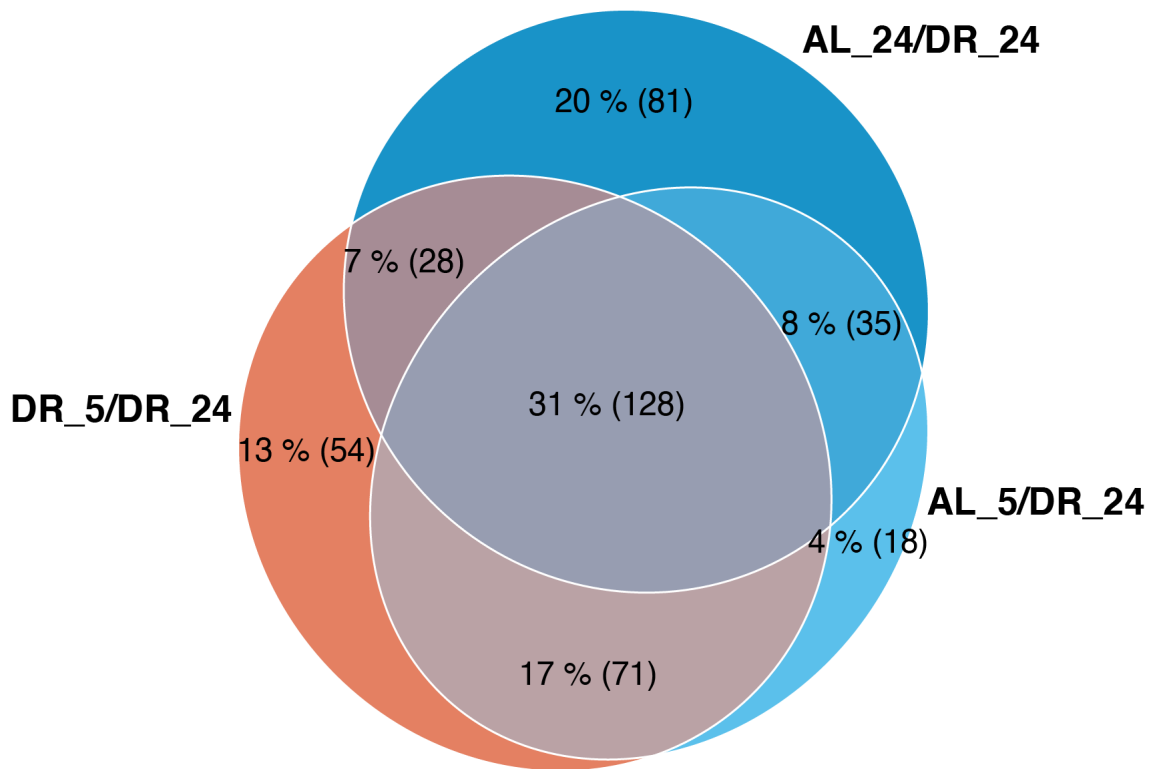
*D*, Distance tree estimated based on distance matrix between average profile of each cluster

*E*, UMAP Gene expression of *Ghr*, *Tshz2*, *Ptprj*, main signature genes markers of super clusters



### Sup.Figure 9 All gene markers from merged SNuc-seq data

*Unsupervised heatmap of the top 3 differentially expressed cluster marker genes for each cell type cluster. Cells are represented in columns and genes are represented in rows. Cluster identities are shown above the heatmap. Color saturation indicates the strength of expression*



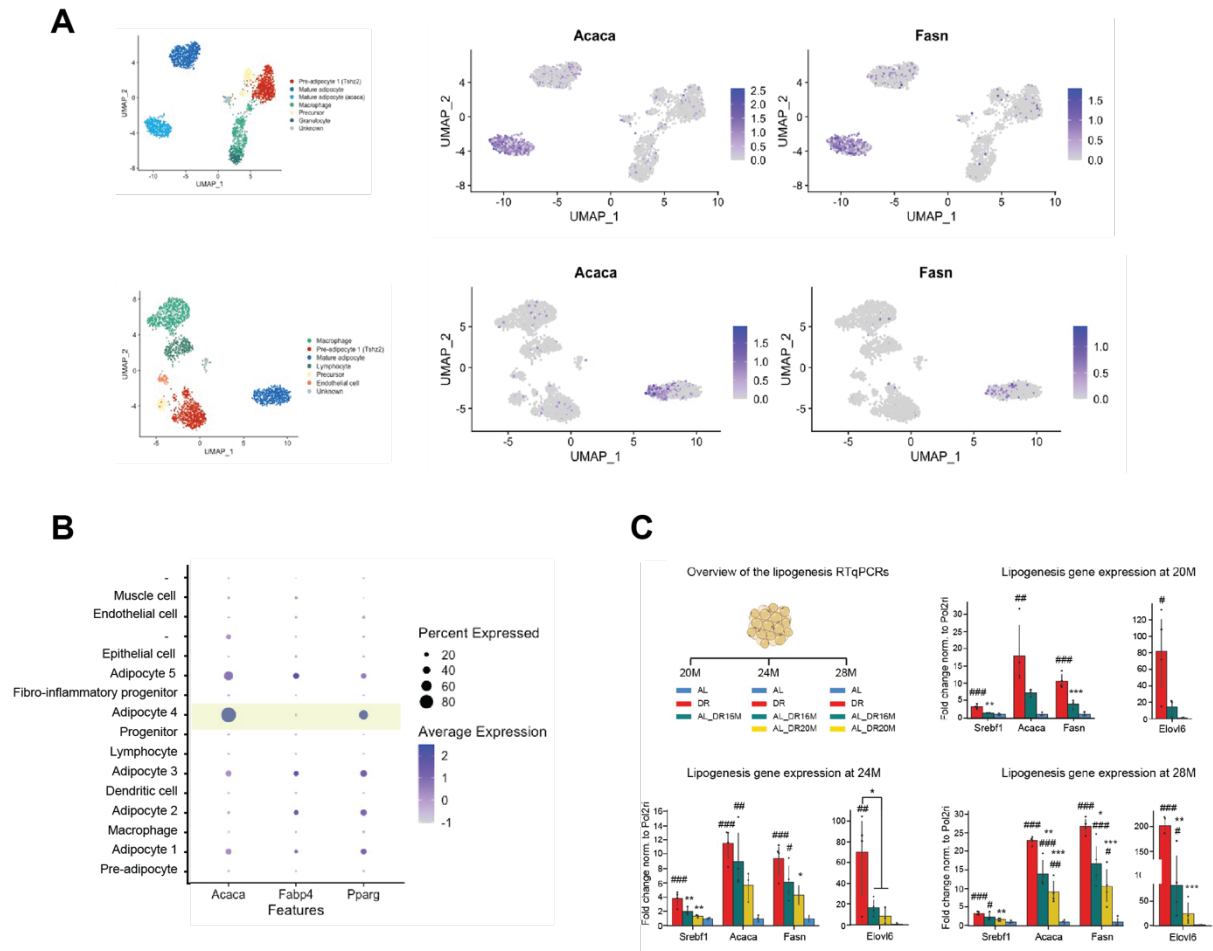
**Sup.Figure 10 Venn diagram of differentially expressed genes between AL old/DR old, AL young/DR old, DR young/DR old**

*Venn diagram of differential expressed genes between mature adipocytes of AL\_24, AL\_5, DR\_5 compared to DR\_24.*

*Fisher test to test statistical significance of overlap between AL\_24/DR\_24 and DR\_5/DR\_24, p.value <2.2e-16.*

*Fisher test of overlap between AL\_24/DR\_24 and AL\_5/DR\_24, p.value <2.2e-16.*

*Fisher test of overlap between AL\_5/DR\_24 and DR\_5/DR\_24, p.value <2.2e-16.*

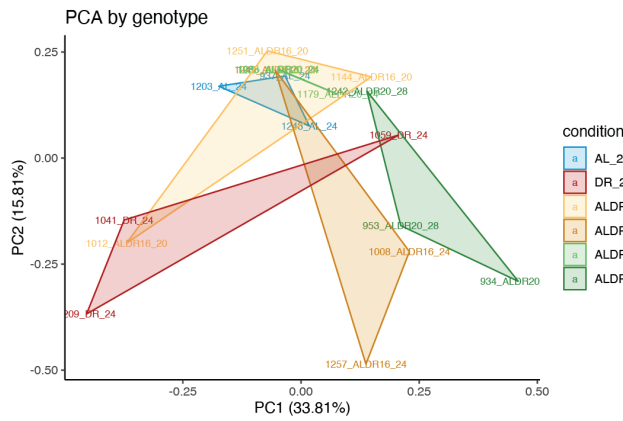
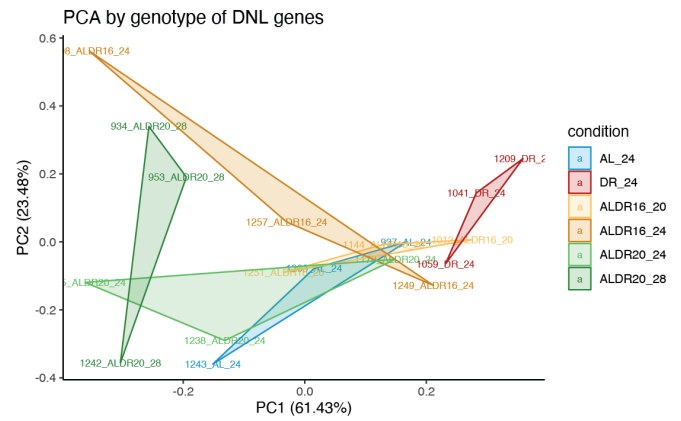
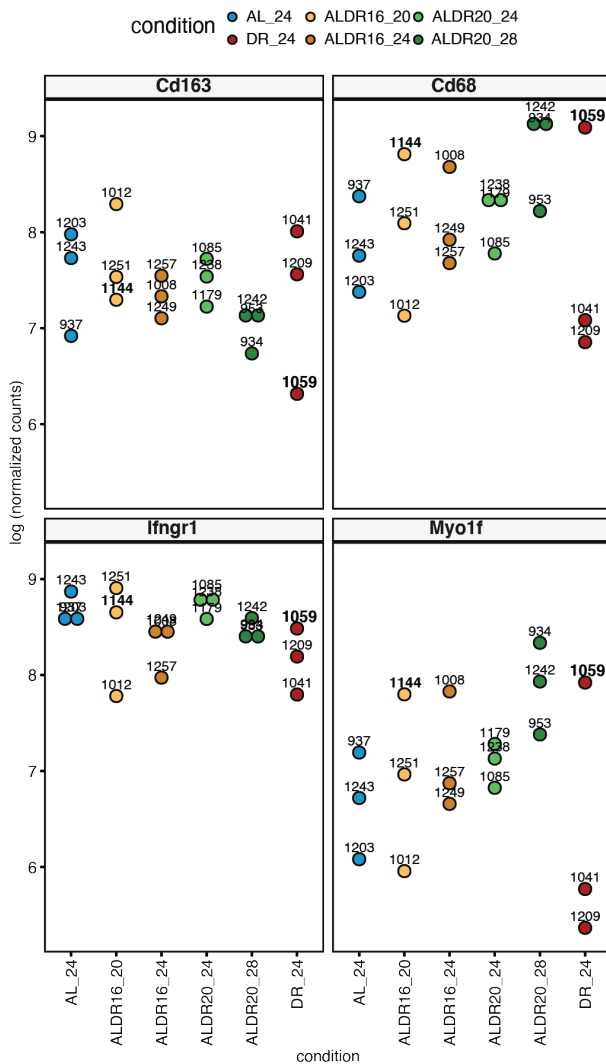
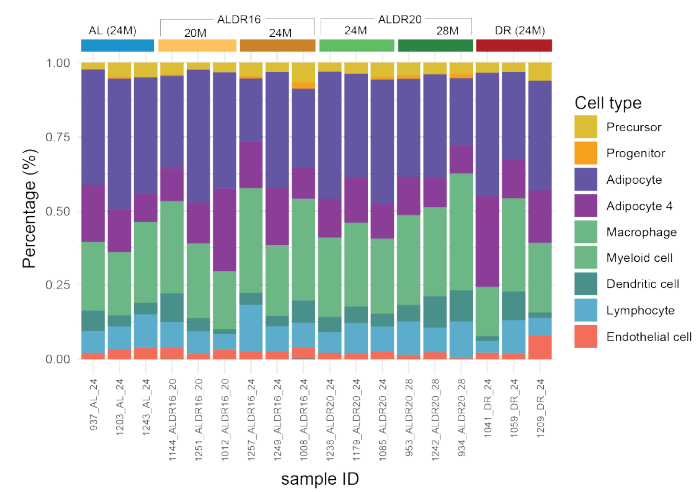


### Sup.Figure 11 De-novo-lipogenesis pathway is enriched in ALDR16 adipocytes

A, UMAP of ALDR16 and ALDR20 sNuc-seq data, with feature plots showing expression of *Acaca* and *Fasn*.

B, Dot plot showing the average expression of selected markers of different stage of maturation in adipocytes.

C, Expression of lipogenesis genes by RTqPCRs in WAT at 20, 24 and 28M for AL, DR, ALDR16 and ALDR20.

**A****B****C****D**

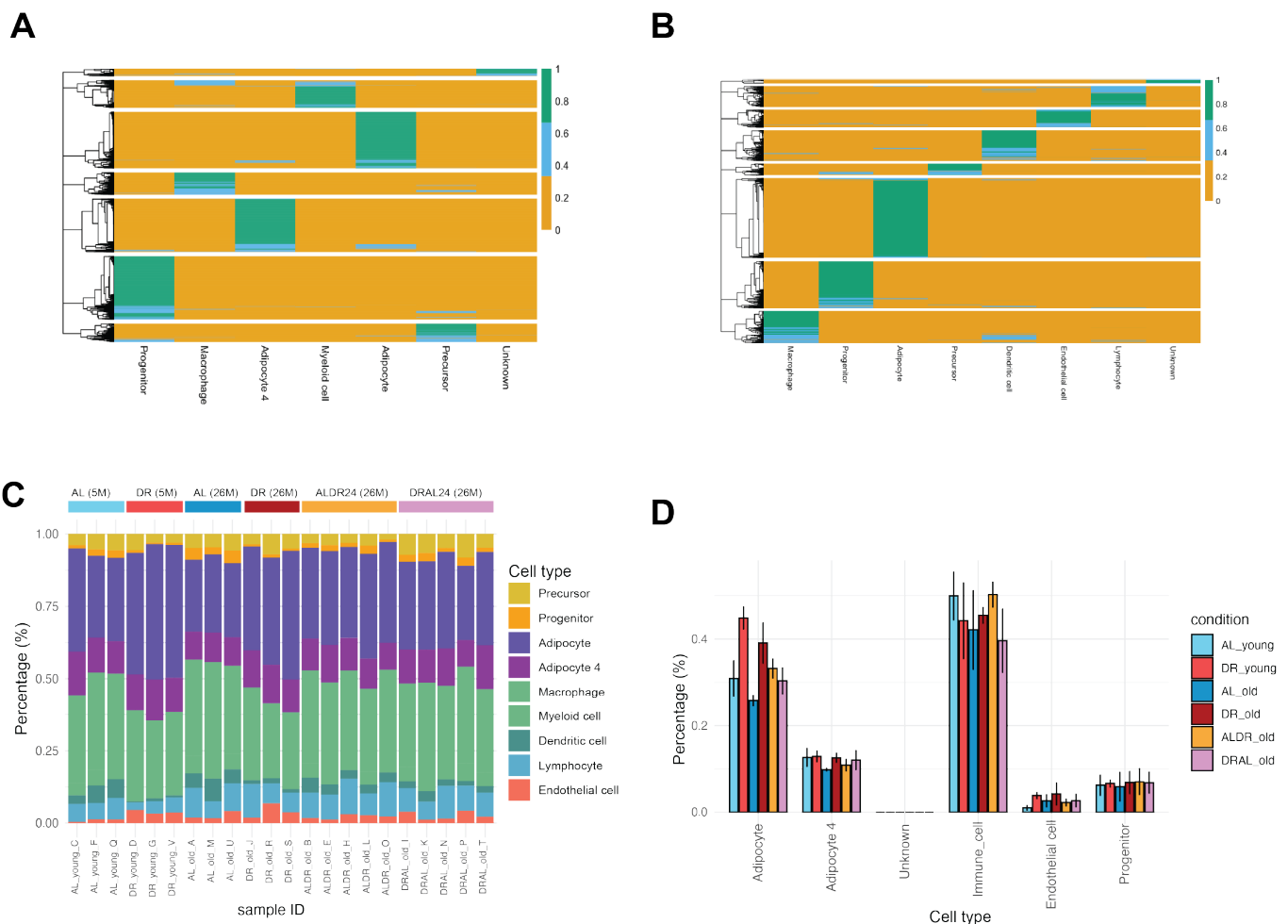
### Sup.Figure 12 Bulk RNA-seq analysis and deconvolution analysis enable to validate cell type proportion variation

A, Principal component analysis of bulk RNA-seq dataset using all genes expressed, by conditions (AL at 24M, DR at 24M, ALDR16 at 20M and 24M, ALDR20 at 24M and 28M).

B, Principal component analysis of bulk RNA-seq dataset using only DNL genes, by conditions (AL at 24M, DR at 24M, ALDR16 at 20M and 24M, ALDR20 at 24M and 28M).

C, Gene level expression (log of normalised counts based on median of ratios methods) of inflammation markers in all samples.

D, Barplot of predicted percentages of cell types for each sample in all conditions, using SCDC deconvolution method.



### Sup.Figure 13 Deconvolution analysis of Hahn et al. dataset using ALDR16 and AL\_24 as reference

A, Heatmap of cells from SNuc-seq AL\_24dataset, clustered by cell-types. Cells having a similar profile to the other cells in the clusters are scored from 0.7 and above (green) and are used to construct the reference dataset.

B, Heatmap of cells from SNuc-seq ALDR16 dataset, clustered by cell-types. Cells having a similar profile to the other cells in the clusters are scored from 0.7 and above (green) and are used to construct the reference dataset.

C, stacked bar plot of predicted percentages of cell types for each sample in all conditions of the dataset from (Hahn et al., 2019), using SCDC deconvolution method.

D, Barplot of percentage of cell-type categories per samples based on deconvolution analysis with SCDC

**Table 5-1 Differentially expressed genes upregulated between adipocyte 5 (DR\_24) and adipocyte 4 (ALDR\_16)**

Gene symbol	p.val	Avg.log2FC	pct.1	pct.2	p.val.adj
Gm42418	1.402047e-17	19.0063168	0.993	0.973	1.370221e-13
Neat1	8.987489e-23	17.0655531	0.986	0.911	8.783473e-19
Nnat	2.697974e-12	9.5936460	0.313	0.143	2.636730e-08
Atp1a2	2.022433e-28	8.4297933	0.829	0.605	1.976523e-24
Slc1a3	5.925544e-37	7.0906552	0.857	0.624	5.791034e-33
Adrb3	3.052118e-70	6.6261589	0.724	0.193	2.982835e-66
Fam13a	6.772255e-46	6.4653280	0.577	0.154	6.618525e-42
Thrsp	1.983053e-08	5.9877019	0.306	0.476	1.938037e-04
St3gal4	4.175506e-10	5.5571973	0.196	0.064	4.080722e-06
Tns1	2.808227e-27	4.7767820	0.673	0.345	2.744480e-23
Acs1	6.173910e-42	4.6976636	0.731	0.324	6.033762e-38
Cd1d1	2.366644e-63	4.5445913	0.680	0.177	2.312921e-59
Sorbs1	9.669433e-09	4.2287912	0.748	0.603	9.449936e-05
Snhg11	1.772823e-26	3.2105777	0.528	0.218	1.732580e-22
Fam214a	2.476413e-23	3.1145578	0.439	0.162	2.420198e-19
Art3	6.385419e-31	2.9912312	0.570	0.225	6.240470e-27
Lipe	3.536888e-34	2.9533133	0.701	0.337	3.456600e-30
Ctcflos	1.109457e-07	2.7064247	0.315	0.175	1.084272e-03
Acacb	1.918809e-22	2.5400379	0.458	0.175	1.875252e-18
Acss3	3.205830e-26	2.4474534	0.425	0.127	3.133058e-22
Fabp4	1.320568e-39	2.1275031	0.509	0.125	1.290591e-35
Slc1a5	1.206955e-20	2.0371172	0.591	0.308	1.179557e-16
Fry	2.710553e-28	1.9996748	0.551	0.216	2.649023e-24
Zbtb16	3.851658e-15	1.9652274	0.402	0.185	3.764226e-11
Ivns1abp	1.714842e-11	1.9318050	0.227	0.075	1.675915e-07

Differentially expressed genes from Wilcoxon rank test. p.val is the p-value from Wilcoxon test. avg\_logFC is log fold-change of the average expression between the two groups. Positive values indicate that the gene is more highly expressed in the first group. pct.1 is the percentage of cells where the gene is detected in the first group. pct.2 is the percentage of cells where the gene is detected in the second group. p\_val\_adj is the adjusted p-value, based on bonferroni correction using all genes in the dataset.

**Table 5-2 Differentially expressed genes downregulated between adipocyte 5 (DR\_24) and adipocyte 4 (ALDR\_16)**

Gene symbol	p.val	Avg.log2FC	pct.1	pct.2	p.val.adj
Acly	1.999523e-57	-13.1783249	0.367	0.802	1.954134e-53
Acaca	2.336224e-34	-12.8373438	0.699	0.904	2.283191e-30
Ghr	2.044467e-19	-9.8283841	0.883	0.960	1.998058e-15
Pparg	3.570883e-10	-9.0850990	0.449	0.628	3.489824e-06
Me1	1.007326e-43	-8.1633221	0.143	0.566	9.844592e-40
Mlxipl	2.936904e-14	-6.7125103	0.481	0.665	2.870236e-10
Tshr	5.567291e-17	-6.2092817	0.404	0.667	5.440914e-13
Mir99ahg	1.024637e-15	-5.3326920	0.381	0.618	1.001378e-11
Xist	2.880770e-07	-5.2092221	0.874	0.750	2.815377e-03
Zeb2	1.300369e-06	-4.6695305	0.395	0.534	1.270851e-02
Dlc1	4.518092e-15	-4.4862192	0.393	0.601	4.415531e-11
Pik3r1	2.079274e-06	-3.1427234	0.456	0.584	2.032075e-02
Ebf1	1.044041e-12	-3.0709348	0.617	0.763	1.020341e-08
Elovl6	6.226648e-16	-2.9695486	0.119	0.347	6.085303e-12
Pnpla3	2.628229e-07	-2.5668436	0.360	0.501	2.568569e-03
Cidec	7.708825e-54	-2.5418797	0.806	0.378	7.533834e-50
Pakap	2.862977e-06	-2.4227255	0.269	0.389	2.797988e-02
Col15a1	5.500736e-19	-2.1171890	0.171	0.428	5.375870e-15
Adamts5	6.657261e-12	-1.9022073	0.063	0.222	6.506141e-08
Tmem45b	9.486593e-10	-1.4153314	0.068	0.206	9.271248e-06
Sema3c	3.738719e-16	-1.3729896	0.049	0.239	3.653850e-12
Mycbp2	4.770473e-12	-1.2807607	0.173	0.362	4.662183e-08
Fasn	3.583961e-09	-1.2773881	0.624	0.780	3.502605e-05
Nabp1	5.839772e-09	-1.2449557	0.138	0.281	5.707209e-05
Prkd1	2.189719e-08	-1.1550653	0.140	0.285	2.140012e-04

*Differentially expressed genes from Wilcoxon rank test. p.val is the p-value from Wilcoxon test. avg\_logFC is log fold-change of the average expression between the two groups. Positive values indicate that the gene is more highly expressed in the first group. pct.1 is the percentage of cells where the gene is detected in the first group. pct.2 is the percentage of cells where the gene is detected in the second group. p\_val\_adj is the adjusted p-value, based on bonferroni correction using all genes in the dataset.*

## 6 List of figures

<b>Figure 2-1 Experimental design for SNuc-seq and Bulk RNA-seq.....</b>	<b>23</b>
<b>Figure 2-2- Single-nuclei wet lab workflow. ....</b>	<b>24</b>
<b>Figure 2-3 - Read format structure from the Nadia Instrument and 10X Chromium protocols.....</b>	<b>30</b>
<b>Figure 3-1 Deconvolution application to cell composition analysis.....</b>	<b>40</b>
<b>Figure 3-2 Nuclei isolation from DroNc-seq protocol.....</b>	<b>42</b>
<b>Figure 3-3 Nuclei solution after cell lysis and centrifugation.....</b>	<b>43</b>
<b>Figure 3-4 Testing protocol to extract all nuclei from fat layer .....</b>	<b>45</b>
<b>Figure 3-5 SNuc-seq dataset of young AL and DR from 10X Chromium.....</b>	<b>48</b>
<b>Figure 3-6 SNuc-seq dataset of young AL and DR from Nadia Instrument.....</b>	<b>51</b>
<b>Figure 3-7 FACS of nuclei after isolation protocol .....</b>	<b>53</b>
<b>Figure 3-8 SNuc-seq dataset of young AL and DR using FACS and 10X Chromium .....</b>	<b>56</b>
<b>Figure 3-9 Merged SNuc-seq dataset of AL and DR young using FACS and Chromium 10X.....</b>	<b>57</b>
<b>Figure 3-10 Comparison of deconvolution methods using Tabula Muris single cell data from adipose tissue .....</b>	<b>61</b>
<b>Figure 3-11 Comparison of deconvolution methods using single-nuclei as reference.....</b>	<b>62</b>
<b>Figure 3-12 Deconvolution results of Emont pseudobulk using Tabula Muris as reference.....</b>	<b>64</b>
<b>Figure 3-13 Deconvolution results of Emont pseudobulk using ALDR16 sNuc-seq as reference .....</b>	<b>65</b>
<b>Figure 3-14 Deconvolution results of Emont pseudobulk (filtered for nuclei genes) using ALDR16 sNuc-seq as reference .....</b>	<b>66</b>
<b>Figure 3-15 Comparison of prediction results between methods using single-cell or single-nuclei as reference .....</b>	<b>67</b>

<b>Figure 3-16 Deconvolution results of Emont pseudobulk using ALDR16 and AL_24sNuc-seq as reference.....</b>	<b>68</b>
<b>Figure 4-1 Single nuclei transcriptomic analysis of young and old murine adipose tissue, under AL and DR feeding and diet switch.....</b>	<b>77</b>
<b>Figure 4-2 Compositional and transcriptional changes in the murine adipose tissue in function of age and diet.....</b>	<b>78</b>
<b>Figure 4-3 Adipocytes show subtypes depending on diet and age.....</b>	<b>83</b>
<b>Figure 4-4 A specific type of mature adipocyte emerges from the switch of DR at 16M.....</b>	<b>86</b>
<b>Figure 4-5 Age is a key a factor in the metabolic flexibility of the WAT .....</b>	<b>90</b>
<b>Figure 4-6 Memory genes analysis from bulk and single-nuclei data .....</b>	<b>94</b>

## 7 List of supplementary figures

<b>Sup.Figure 1 SNuc-seq data from AL young from 10X Chromium .....</b>	<b>106</b>
<b>Sup.Figure 2 SNuc-seq data from DR young from 10X Chromium.....</b>	<b>107</b>
<b>Sup.Figure 3 SNuc-seq data from DR young from Nadia Instrument.....</b>	<b>108</b>
<b>Sup.Figure 4 SNuc-seq data from AL young from FACS+10X Chromium .....</b>	<b>109</b>
<b>Sup.Figure 5 SNuc-seq data from DR young from FACS+10X Chromium.....</b>	<b>110</b>
<b>Sup.Figure 6 Clustering of cells for Tabula Muris single-cell deconvolution reference dataset .....</b>	<b>111</b>
<b>Sup.Figure 7 Clustering of cells for Emont single-cell deconvolution reference dataset .....</b>	<b>112</b>
<b>Sup.Figure 8 Cell-type landscape of WAT in function of biological and technical parameters .....</b>	<b>113</b>
<b>Sup.Figure 9 All gene markers from merged SNuc-seq data .....</b>	<b>114</b>
<b>Sup.Figure 10 Venn diagram of differentially expressed genes between AL old/DR old, AL young/DR old, DR young/DR old .....</b>	<b>115</b>
<b>Sup.Figure 11 De-novo-lipogenesis pathway is enriched in ALDR16 adipocytes .....</b>	<b>116</b>
<b>Sup.Figure 12 Bulk RNA-seq and deconvolution analysis enable to validate cell type proportion variation .....</b>	<b>117</b>
<b>Sup.Figure 13 Deconvolution analysis of Hahn et al. dataset using ALDR16 and AL_24 as reference .....</b>	<b>118</b>

## 8 List of tables

<b>Table 3-1 cDNA concentration of libraries of AL and DR sample, with or without FACS step</b> .....	53
<b>Table 3-2 Comparison between all data based on metrics after pre-processing with Seurat package.</b> .....	54
<b>Table 3-3 Comparison between 10X data with or without FACS sorting based on Cellranger metrics.</b> .....	54
<b>Table 5-1 Differentially expressed genes upregulated between adipocyte 5 (DR_24) and adipocyte 4 (ALDR_16)</b> .....	119
<b>Table 5-2 Differentially expressed genes downregulated between adipocyte 5 (DR_24) and adipocyte 4 (ALDR_16)</b> .....	120

## 9 Contributions

Prof. Dr. Linda Partridge, Prof. Dr. Andreas Beyer and Dr. Sebastian Grönke supervised my PhD research.

Dr. Sebastian Grönke and Prof. Dr. Linda Partridge designed the multiple DR switch study including the lifespan, phenotyping and tissue collection cohorts.

Dr. Lisa Drews conducted the post-mortem pathologies, the phenotypings and the RNA extraction used for the bulk RNA-seq study. The first DR switch study was analyzed by Dr. Oliver Hahn, which provided the context for designing the study around WAT transcriptional flexibility.

I optimized and designed the protocol to generate sNuc-seq data from WAT.

Drs. Peter Tessarz and Chrysa Nikopoulou provided excellent advice for how to optimize the protocol for sNuc-seq.

Dr. Carolina Monzó helped making the libraries of the Nadia instrument. Dr. Carolina Monzó and Lisonia Gkioni helped with the nuclei isolation experiment to generate the final dataset.

Nuclei sorting was carried out with the help and support of the FACS and Imaging facility staff Lena Schumacher and Kat Folz-Donahue. The generation of libraries for 10X Chromium and sequencing were done by the Cologne Center of Genomics with the help of Marek Franitza and under the supervision of Janine Altmüller.

I did the bioinformatic analysis and interpretation of the data for the sNuc-seq data and Bulk RNA-seq data under the supervision of Prof. Dr. Andreas Beyer.

## 10 References

- Adil, A., Kumar, V., Jan, A. T., & Asger, M. (2021). Single-Cell Transcriptomics: Current Methods and Challenges in Data Acquisition and Analysis. *Front Neurosci*, 15, 591122. <https://doi.org/10.3389/fnins.2021.591122>
- Aiba, Y., Yamazaki, T., Okada, T., Gotoh, K., Sanjo, H., Ogata, M., & Kurosaki, T. (2006). BANK negatively regulates Akt activation and subsequent B cell responses. *Immunity*, 24(3), 259-268. <https://doi.org/10.1016/j.immuni.2006.01.002>
- Alsinet, C., Primo, M. N., Lorenzi, V., Bello, E., Kelava, I., Jones, C. P., Vilarrasa-Blasi, R., Sancho-Serra, C., Knights, A. J., Park, J. E., Wyspianska, B. S., Trynka, G., Tough, D. F., Bassett, A., Gaffney, D. J., Alvarez-Errico, D., & Vento-Tormo, R. (2022). Robust temporal map of human in vitro myelopoiesis using single-cell genomics. *Nat Commun*, 13(1), 2885. <https://doi.org/10.1038/s41467-022-30557-4>
- Andrews, S. (2010). *A quality control tool for high throughput sequence data*. In <https://www.bioinformatics.babraham.ac.uk/projects/fastqc/>
- Aran, D., Hu, Z., & Butte, A. J. (2017). xCell: digitally portraying the tissue cellular heterogeneity landscape. *Genome Biol*, 18(1), 220. <https://doi.org/10.1186/s13059-017-1349-1>
- Aran, D., Looney, A. P., Liu, L., Wu, E., Fong, V., Hsu, A., Chak, S., Naikawadi, R. P., Wolters, P. J., Abate, A. R., Butte, A. J., & Bhattacharya, M. (2019). Reference-based analysis of lung single-cell sequencing reveals a transitional profibrotic macrophage. *Nat Immunol*, 20(2), 163-172. <https://doi.org/10.1038/s41590-018-0276-y>
- Arimochi, H., Sasaki, Y., Kitamura, A., & Yasutomo, K. (2016). Differentiation of preadipocytes and mature adipocytes requires PSMB8. *Sci Rep*, 6, 26791. <https://doi.org/10.1038/srep26791>
- Arriola Apelo, S. I., & Lamming, D. W. (2016). Rapamycin: An InhibiTOR of Aging Emerges From the Soil of Easter Island. *J Gerontol A Biol Sci Med Sci*, 71(7), 841-849. <https://doi.org/10.1093/gerona/glw090>
- Avila Cobos, F., Alquicira-Hernandez, J., Powell, J. E., Mestdagh, P., & De Preter, K. (2020). Benchmarking of cell type deconvolution pipelines for transcriptomics data. *Nat Commun*, 11(1), 5650. <https://doi.org/10.1038/s41467-020-19015-1>
- Avila Cobos, F., Vandesompele, J., Mestdagh, P., & De Preter, K. (2018). Computational deconvolution of transcriptomics data from mixed cell populations. *Bioinformatics*, 34(11), 1969-1979. <https://doi.org/10.1093/bioinformatics/bty019>
- Backdahl, J., Franzen, L., Massier, L., Li, Q., Jalkanen, J., Gao, H., Andersson, A., Bhalla, N., Thorell, A., Ryden, M., Stahl, P. L., & Mejhert, N. (2021). Spatial mapping reveals human adipocyte subpopulations with distinct sensitivities to insulin. *Cell Metab*, 33(11), 2301. <https://doi.org/10.1016/j.cmet.2021.10.012>
- Bakken, T. E., Hodge, R. D., Miller, J. A., Yao, Z., Nguyen, T. N., Aevermann, B., Barkan, E., Bertagnolli, D., Casper, T., Dee, N., Garren, E., Goldy, J., Graybuck, L. T., Kroll, M., Lasken, R. S., Lathia, K., Parry, S., Rimorin, C., Scheuermann, R. H., Schork, N. J., Shehata, S. I., Tieu, M., Phillips, J. W.,

- Bernard, A., Smith, K. A., Zeng, H., Lein, E. S., & Tasic, B. (2018). Single-nucleus and single-cell transcriptomes compared in matched cortical cell types. *PLoS One*, *13*(12), e0209648. <https://doi.org/10.1371/journal.pone.0209648>
- Balasubramanian, P., Howell, P. R., & Anderson, R. M. (2017). Aging and Caloric Restriction Research: A Biological Perspective With Translational Potential. *EBioMedicine*, *21*, 37-44. <https://doi.org/10.1016/j.ebiom.2017.06.015>
- Bast-Habersbrunner, A., Kiefer, C., Weber, P., Fromme, T., Schießl, A., Schwalie, P. C., Deplancke, B., Li, Y., & Klingenspor, M. (2021). LncRNA Ctcfls orchestrates transcription and alternative splicing in thermogenic adipogenesis. *EMBO Rep*, *22*(7), e51289. <https://doi.org/10.15252/embr.202051289>
- Becht, E., McInnes, L., Healy, J., Dutertre, C. A., Kwok, I. W. H., Ng, L. G., Ginhoux, F., & Newell, E. W. (2018). Dimensionality reduction for visualizing single-cell data using UMAP. *Nat Biotechnol*. <https://doi.org/10.1038/nbt.4314>
- Boumelhem, B. B., Assinder, S. J., Bell-Anderson, K. S., & Fraser, S. T. (2017). Flow cytometric single cell analysis reveals heterogeneity between adipose depots. *Adipocyte*, *6*(2), 112-123. <https://doi.org/10.1080/21623945.2017.1319536>
- Buhmann, C. D. S. a. J. M. (2008). Expectation-Maximization for Sparse and Non-Negative PCA. *Proc. 25th International Conference on Machine Learning*. <https://doi.org/10.1145/1390156.1390277>
- Burl, R. B., Ramseyer, V. D., Rondini, E. A., Pique-Regi, R., Lee, Y.-H., & Granneman, J. G. (2018). Deconstructing Adipogenesis Induced by  $\beta$ 3-Adrenergic Receptor Activation with Single-Cell Expression Profiling. *Cell Metabolism*, *28*(2), 300-309.e304. <https://doi.org/https://doi.org/10.1016/j.cmet.2018.05.025>
- Burl, R. B., Ramseyer, V. D., Rondini, E. A., Pique-Regi, R., Lee, Y. H., & Granneman, J. G. (2018). Deconstructing Adipogenesis Induced by beta3-Adrenergic Receptor Activation with Single-Cell Expression Profiling. *Cell Metab*, *28*(2), 300-309 e304. <https://doi.org/10.1016/j.cmet.2018.05.025>
- Byron, S. A., Van Keuren-Jensen, K. R., Engelthaler, D. M., Carpten, J. D., & Craig, D. W. (2016). Translating RNA sequencing into clinical diagnostics: opportunities and challenges. *Nat Rev Genet*, *17*(5), 257-271. <https://doi.org/10.1038/nrg.2016.10>
- Chen, W., Li, Y., Easton, J., Finkelstein, D., Wu, G., & Chen, X. (2018). UMI-count modeling and differential expression analysis for single-cell RNA sequencing. *Genome Biol*, *19*(1), 70. <https://doi.org/10.1186/s13059-018-1438-9>
- Chen, Y., Song, Y., Du, W., Gong, L., Chang, H., & Zou, Z. (2019). Tumor-associated macrophages: an accomplice in solid tumor progression. *J Biomed Sci*, *26*(1), 78. <https://doi.org/10.1186/s12929-019-0568-z>
- Cho, D. S., Lee, B., & Doles, J. D. (2019). Refining the adipose progenitor cell landscape in healthy and obese visceral adipose tissue using single-cell gene expression profiling. *Life Sci Alliance*, *2*(6). <https://doi.org/10.26508/lsa.201900561>
- Chung, C. L., Lawrence, I., Hoffman, M., Elgindi, D., Nadhan, K., Potnis, M., Jin, A., Sershon, C., Binnebose, R., Lorenzini, A., & Sell, C. (2019). Topical rapamycin reduces markers of senescence and aging in human skin: an exploratory, prospective, randomized trial. *Geroscience*, *41*(6), 861-869. <https://doi.org/10.1007/s11357-019-00113-y>
- Collins, J. M., Neville, M. J., Hoppa, M. B., & Frayn, K. N. (2010). De novo lipogenesis and stearoyl-CoA desaturase are coordinately regulated in the human adipocyte and protect against palmitate-induced cell injury. *J Biol Chem*, *285*(9), 6044-6052. <https://doi.org/10.1074/jbc.M109.053280>

- Cypess, A. M., Lehman, S., Williams, G., Tal, I., Rodman, D., Goldfine, A. B., Kuo, F. C., Palmer, E. L., Tseng, Y. H., Doria, A., Kolodny, G. M., & Kahn, C. R. (2009). Identification and importance of brown adipose tissue in adult humans. *N Engl J Med*, 360(15), 1509-1517. <https://doi.org/10.1056/NEJMoa0810780>
- Das, S. K., Balasubramanian, P., & Weerasekara, Y. K. (2017). Nutrition modulation of human aging: The calorie restriction paradigm. *Mol Cell Endocrinol*, 455, 148-157. <https://doi.org/10.1016/j.mce.2017.04.011>
- Dave, R. K., Dinger, M. E., Andrew, M., Askarian-Amiri, M., Hume, D. A., & Kellie, S. (2013). Regulated expression of PTPRJ/CD148 and an antisense long noncoding RNA in macrophages by proinflammatory stimuli. *PLoS One*, 8(6), e68306. <https://doi.org/10.1371/journal.pone.0068306>
- Davie, K., Janssens, J., Koldere, D., De Waegeneer, M., Pech, U., Kreft, L., Aibar, S., Makhzami, S., Christiaens, V., Bravo Gonzalez-Blas, C., Poovathingal, S., Hulselmans, G., Spanier, K. I., Moerman, T., Vanspauwen, B., Geurs, S., Voet, T., Lammertyn, J., Thienpont, B., Liu, S., Konstantinides, N., Fiers, M., Verstreken, P., & Aerts, S. (2018). A Single-Cell Transcriptome Atlas of the Aging *Drosophila* Brain. *Cell*, 174(4), 982-998 e920. <https://doi.org/10.1016/j.cell.2018.05.057>
- DeFuria, J., Belkina, A. C., Jagannathan-Bogdan, M., Snyder-Cappione, J., Carr, J. D., Nersesova, Y. R., Markham, D., Strissel, K. J., Watkins, A. A., Zhu, M., Allen, J., Bouchard, J., Toraldo, G., Jasuja, R., Obin, M. S., McDonnell, M. E., Apovian, C., Denis, G. V., & Nikolajczyk, B. S. (2013). B cells promote inflammation in obesity and type 2 diabetes through regulation of T-cell function and an inflammatory cytokine profile. *Proc Natl Acad Sci U S A*, 110(13), 5133-5138. <https://doi.org/10.1073/pnas.1215840110>
- Dhahbi, J. M., Kim, H. J., Mote, P. L., Beaver, R. J., & Spindler, S. R. (2004). Temporal linkage between the phenotypic and genomic responses to caloric restriction. *Proc Natl Acad Sci U S A*, 101(15), 5524-5529. <https://doi.org/10.1073/pnas.0305300101>
- Ding, C., Li, Y., Guo, F., Jiang, Y., Ying, W., Li, D., Yang, D., Xia, X., Liu, W., Zhao, Y., He, Y., Li, X., Sun, W., Liu, Q., Song, L., Zhen, B., Zhang, P., Qian, X., Qin, J., & He, F. (2016). A Cell-type-resolved Liver Proteome. *Mol Cell Proteomics*, 15(10), 3190-3202. <https://doi.org/10.1074/mcp.M116.060145>
- Dobin, A., Davis, C. A., Schlesinger, F., Drenkow, J., Zaleski, C., Jha, S., Batut, P., Chaisson, M., & Gingeras, T. R. (2013). STAR: ultrafast universal RNA-seq aligner. *Bioinformatics*, 29(1), 15-21. <https://doi.org/10.1093/bioinformatics/bts635>
- Donato, A. J., Henson, G. D., Hart, C. R., Layec, G., Trinity, J. D., Bramwell, R. C., Enz, R. A., Morgan, R. G., Reihl, K. D., Hazra, S., Walker, A. E., Richardson, R. S., & Lesniewski, L. A. (2014). The impact of ageing on adipose structure, function and vasculature in the B6D2F1 mouse: evidence of significant multisystem dysfunction. *J Physiol*, 592(18), 4083-4096. <https://doi.org/10.1113/jphysiol.2014.274175>
- Dong, M., Thennavan, A., Urrutia, E., Li, Y., Perou, C. M., Zou, F., & Jiang, Y. (2021). SCDC: bulk gene expression deconvolution by multiple single-cell RNA sequencing references. *Brief Bioinform*, 22(1), 416-427. <https://doi.org/10.1093/bib/bbz166>
- Duerre, D. J., & Galmozzi, A. (2022). Deconstructing Adipose Tissue Heterogeneity One Cell at a Time. *Front Endocrinol (Lausanne)*, 13, 847291. <https://doi.org/10.3389/fendo.2022.847291>

- Efeyan, A., Comb, W. C., & Sabatini, D. M. (2015). Nutrient-sensing mechanisms and pathways. *Nature*, 517(7534), 302-310. <https://doi.org/10.1038/nature14190>
- Eissing, L., Scherer, T., Todter, K., Knippschild, U., Greve, J. W., Buurman, W. A., Pinnschmidt, H. O., Rensen, S. S., Wolf, A. M., Bartelt, A., Heeren, J., Buettner, C., & Scheja, L. (2013). De novo lipogenesis in human fat and liver is linked to ChREBP-beta and metabolic health. *Nat Commun*, 4, 1528. <https://doi.org/10.1038/ncomms2537>
- Emont, M. P., Jacobs, C., Essene, A. L., Pant, D., Tenen, D., Colletuori, G., Di Vincenzo, A., Jorgensen, A. M., Dashti, H., Stefek, A., McGonagle, E., Strobel, S., Laber, S., Agrawal, S., Westcott, G. P., Kar, A., Veregge, M. L., Gulko, A., Srinivasan, H., Kramer, Z., De Filippis, E., Merkel, E., Ducie, J., Boyd, C. G., Gourash, W., Courcoulas, A., Lin, S. J., Lee, B. T., Morris, D., Tobias, A., Khera, A. V., Claussnitzer, M., Pers, T. H., Giordano, A., Ashenberg, O., Regev, A., Tsai, L. T., & Rosen, E. D. (2022). A single-cell atlas of human and mouse white adipose tissue. *Nature*, 603(7903), 926-933. <https://doi.org/10.1038/s41586-022-04518-2>
- Fabbiano, S., Suarez-Zamorano, N., Rigo, D., Veyrat-Durebex, C., Stevanovic Dokic, A., Colin, D. J., & Trajkovski, M. (2016). Caloric Restriction Leads to Browning of White Adipose Tissue through Type 2 Immune Signaling. *Cell Metab*, 24(3), 434-446. <https://doi.org/10.1016/j.cmet.2016.07.023>
- Fabbiano, S., Suárez-Zamorano, N., Rigo, D., Veyrat-Durebex, C., Stevanovic Dokic, A., Colin, D. J., & Trajkovski, M. (2016). Caloric Restriction Leads to Browning of White Adipose Tissue through Type 2 Immune Signaling. *Cell Metab*, 24(3), 434-446. <https://doi.org/10.1016/j.cmet.2016.07.023>
- Frankish, A., Diekhans, M., Jungreis, I., Lagarde, J., Loveland, J. E., Mudge, J. M., Sisu, C., Wright, J. C., Armstrong, J., Barnes, I., Berry, A., Bignell, A., Boix, C., Carbonell Sala, S., Cunningham, F., Di Domenico, T., Donaldson, S., Fiddes, I. T., Garcia Giron, C., Gonzalez, J. M., Grego, T., Hardy, M., Hourlier, T., Howe, K. L., Hunt, T., Izuogu, O. G., Johnson, R., Martin, F. J., Martinez, L., Mohanan, S., Muir, P., Navarro, F. C. P., Parker, A., Pei, B., Pozo, F., Riera, F. C., Ruffier, M., Schmitt, B. M., Stapleton, E., Suner, M. M., Sycheva, I., Uszczynska-Ratajczak, B., Wolf, M. Y., Xu, J., Yang, Y. T., Yates, A., Zerbino, D., Zhang, Y., Choudhary, J. S., Gerstein, M., Guigo, R., Hubbard, T. J. P., Kellis, M., Paten, B., Tress, M. L., & Flicek, P. (2021). Gencode 2021. *Nucleic Acids Res*, 49(D1), D916-D923. <https://doi.org/10.1093/nar/gkaa1087>
- Fraser, H. C., Kuan, V., Johnen, R., Zwierzyna, M., Hingorani, A. D., Beyer, A., & Partridge, L. (2022). Biological mechanisms of aging predict age-related disease co-occurrence in patients. *Aging Cell*, 21(4), e13524. <https://doi.org/10.1111/accel.13524>
- Frith, J., Day, C. P., Henderson, E., Burt, A. D., & Newton, J. L. (2009). Non-alcoholic fatty liver disease in older people. *Gerontology*, 55(6), 607-613. <https://doi.org/10.1159/000235677>
- Gaedcke, S., Sinning, J., Dittrich-Breiholz, O., Haller, H., Soerensen-Zender, I., Liao, C. M., Nordlohne, A., Sen, P., von Vietinghoff, S., DeLuca, D. S., & Schmitt, R. (2022). Single cell versus single nucleus: transcriptome differences in the murine kidney after ischemia-reperfusion injury. *Am J Physiol Renal Physiol*, 323(2), F171-F181. <https://doi.org/10.1152/ajprenal.00453.2021>
- Galbas, T., Raymond, M., Sabourin, A., Bourgeois-Daigneault, M.-C., Guimont-Desrochers, F., Yun, T. J., Cailhier, J.-F., Ishido, S., Lesage, S., Cheong, C., & Thibodeau, J. (2017). MARCH1 E3 Ubiquitin Ligase Dampens the Innate

- Inflammatory Response by Modulating Monocyte Functions in Mice. *The Journal of Immunology*, 198(2), 852-861. <https://doi.org/10.4049/jimmunol.1601168>
- Gao, F., Liu, C., Guo, J., Sun, W., Xian, L., Bai, D., Liu, H., Cheng, Y., Li, B., Cui, J., Zhang, C., & Cai, J. (2015). Radiation-driven lipid accumulation and dendritic cell dysfunction in cancer. *Sci Rep*, 5, 9613. <https://doi.org/10.1038/srep09613>
- Ghosh, A. K., Mau, T., O'Brien, M., Garg, S., & Yung, R. (2016). Impaired autophagy activity is linked to elevated ER-stress and inflammation in aging adipose tissue. *Aging (Albany NY)*, 8(10), 2525-2537. <https://doi.org/10.18632/aging.101083>
- Gonzales, A. M., & Orlando, R. A. (2007). Role of adipocyte-derived lipoprotein lipase in adipocyte hypertrophy. *Nutr Metab (Lond)*, 4, 22. <https://doi.org/10.1186/1743-7075-4-22>
- Green, C. L., Lamming, D. W., & Fontana, L. (2022). Molecular mechanisms of dietary restriction promoting health and longevity. *Nat Rev Mol Cell Biol*, 23(1), 56-73. <https://doi.org/10.1038/s41580-021-00411-4>
- Habib, N., Avraham-Davidi, I., Basu, A., Burks, T., Shekhar, K., Hofree, M., Choudhury, S. R., Aguet, F., Gelfand, E., Ardlie, K., Weitz, D. A., Rozenblatt-Rosen, O., Zhang, F., & Regev, A. (2017). Massively parallel single-nucleus RNA-seq with DroNc-seq. *Nat Methods*, 14(10), 955-958. <https://doi.org/10.1038/nmeth.4407>
- Hagberg, C. E., Li, Q., Kutschke, M., Bhowmick, D., Kiss, E., Shabalina, I. G., Harms, M. J., Shilkova, O., Kozina, V., Nedergaard, J., Boucher, J., Thorell, A., & Spalding, K. L. (2018). Flow Cytometry of Mouse and Human Adipocytes for the Analysis of Browning and Cellular Heterogeneity. *Cell Rep*, 24(10), 2746-2756 e2745. <https://doi.org/10.1016/j.celrep.2018.08.006>
- Hahn, O., Drews, L. F., Nguyen, A., Tatsuta, T., Gkioni, L., Hendrich, O., Zhang, Q., Langer, T., Pletcher, S., Wakelam, M. J. O., Beyer, A., Gronke, S., & Partridge, L. (2019). A nutritional memory effect counteracts benefits of dietary restriction in old mice. *Nat Metab*, 1(11), 1059-1073. <https://doi.org/10.1038/s42255-019-0121-0>
- Hahn, O., Gronke, S., Stubbs, T. M., Ficiz, G., Hendrich, O., Krueger, F., Andrews, S., Zhang, Q., Wakelam, M. J., Beyer, A., Reik, W., & Partridge, L. (2017). Dietary restriction protects from age-associated DNA methylation and induces epigenetic reprogramming of lipid metabolism. *Genome Biol*, 18(1), 56. <https://doi.org/10.1186/s13059-017-1187-1>
- Han, S., Sun, H. M., Hwang, K. C., & Kim, S. W. (2015). Adipose-Derived Stromal Vascular Fraction Cells: Update on Clinical Utility and Efficacy. *Crit Rev Eukaryot Gene Expr*, 25(2), 145-152. <https://doi.org/10.1615/critreveukaryotgeneexpr.2015013057>
- Han, X., Zhou, Z., Fei, L., Sun, H., Wang, R., Chen, Y., Chen, H., Wang, J., Tang, H., Ge, W., Zhou, Y., Ye, F., Jiang, M., Wu, J., Xiao, Y., Jia, X., Zhang, T., Ma, X., Zhang, Q., Bai, X., Lai, S., Yu, C., Zhu, L., Lin, R., Gao, Y., Wang, M., Wu, Y., Zhang, J., Zhan, R., Zhu, S., Hu, H., Wang, C., Chen, M., Huang, H., Liang, T., Chen, J., Wang, W., Zhang, D., & Guo, G. (2020). Construction of a human cell landscape at single-cell level. *Nature*, 581(7808), 303-309. <https://doi.org/10.1038/s41586-020-2157-4>
- Hao, Y., Hao, S., Andersen-Nissen, E., Mauck, W. M., 3rd, Zheng, S., Butler, A., Lee, M. J., Wilk, A. J., Darby, C., Zager, M., Hoffman, P., Stoeckius, M., Papalexi, E., Mimitou, E. P., Jain, J., Srivastava, A., Stuart, T., Fleming, L. M., Yeung, B.,

- Rogers, A. J., McElrath, J. M., Blish, C. A., Gottardo, R., Smibert, P., & Satija, R. (2021). Integrated analysis of multimodal single-cell data. *Cell*, 184(13), 3573-3587 e3529. <https://doi.org/10.1016/j.cell.2021.04.048>
- Harrison, D. E., Strong, R., Sharp, Z. D., Nelson, J. F., Astle, C. M., Flurkey, K., Nadon, N. L., Wilkinson, J. E., Frenkel, K., Carter, C. S., Pahor, M., Javors, M. A., Fernandez, E., & Miller, R. A. (2009). Rapamycin fed late in life extends lifespan in genetically heterogeneous mice. *Nature*, 460(7253), 392-395. <https://doi.org/10.1038/nature08221>
- Hepler, C., Shan, B., Zhang, Q., Henry, G. H., Shao, M., Vishvanath, L., Ghaben, A. L., Mobley, A. B., Strand, D., Hon, G. C., & Gupta, R. K. (2018). Identification of functionally distinct fibro-inflammatory and adipogenic stromal subpopulations in visceral adipose tissue of adult mice. *Elife*, 7. <https://doi.org/10.7554/eLife.39636>
- Herman, M. A., Peroni, O. D., Villoria, J., Schön, M. R., Abumrad, N. A., Blüher, M., Klein, S., & Kahn, B. B. (2012). A novel ChREBP isoform in adipose tissue regulates systemic glucose metabolism. *Nature*, 484(7394), 333-338. <https://doi.org/10.1038/nature10986>
- Herold, J., & Kalucka, J. (2020). Angiogenesis in Adipose Tissue: The Interplay Between Adipose and Endothelial Cells. *Front Physiol*, 11, 624903. <https://doi.org/10.3389/fphys.2020.624903>
- Higami, Y., Barger, J. L., Page, G. P., Allison, D. B., Smith, S. R., Prolla, T. A., & Weindruch, R. (2006). Energy restriction lowers the expression of genes linked to inflammation, the cytoskeleton, the extracellular matrix, and angiogenesis in mouse adipose tissue. *J Nutr*, 136(2), 343-352. <https://doi.org/10.1093/jn/136.2.343>
- Hildreth, A. D., Ma, F., Wong, Y. Y., Sun, R., Pellegrini, M., & O'Sullivan, T. E. (2021). Single-cell sequencing of human white adipose tissue identifies new cell states in health and obesity. *Nat Immunol*, 22(5), 639-653. <https://doi.org/10.1038/s41590-021-00922-4>
- Himes, S. R., Cronau, S., Mulford, C., & Hume, D. A. (2005). The Runx1 transcription factor controls CSF-1-dependent and -independent growth and survival of macrophages. *Oncogene*, 24(34), 5278-5286. <https://doi.org/10.1038/sj.onc.1208657>
- Hwang, B., Lee, J. H., & Bang, D. (2018). Single-cell RNA sequencing technologies and bioinformatics pipelines. *Exp Mol Med*, 50(8), 1-14. <https://doi.org/10.1038/s12276-018-0071-8>
- Ibrahim, M. M. (2010). Subcutaneous and visceral adipose tissue: structural and functional differences. *Obes Rev*, 11(1), 11-18. <https://doi.org/10.1111/j.1467-789X.2009.00623.x>
- Iizuka, K., Takao, K., & Yabe, D. (2020). ChREBP-Mediated Regulation of Lipid Metabolism: Involvement of the Gut Microbiota, Liver, and Adipose Tissue. *Front Endocrinol (Lausanne)*, 11, 587189. <https://doi.org/10.3389/fendo.2020.587189>
- Institute, B. (2018). *Picard Tools*. In (Version 2.22) Broad Institute. <http://broadinstitute.github.io/picard/>
- Ishaq, A., Schroder, J., Edwards, N., von Zglinicki, T., & Saretzki, G. (2018). Dietary Restriction Ameliorates Age-Related Increase in DNA Damage, Senescence and Inflammation in Mouse Adipose Tissue. *J Nutr Health Aging*, 22(4), 555-561. <https://doi.org/10.1007/s12603-017-0968-2>

- Izquierdo, A. G., Crujeiras, A. B., Casanueva, F. F., & Carreira, M. C. (2019). Leptin, Obesity, and Leptin Resistance: Where Are We 25 Years Later? *Nutrients*, 11(11). <https://doi.org/10.3390/nu11112704>
- Jin, H., & Liu, Z. (2021). A benchmark for RNA-seq deconvolution analysis under dynamic testing environments. *Genome Biol*, 22(1), 102. <https://doi.org/10.1186/s13059-021-02290-6>
- Jolliffe, I. T., & Cadima, J. (2016). Principal component analysis: a review and recent developments. *Philos Trans A Math Phys Eng Sci*, 374(2065), 20150202. <https://doi.org/10.1098/rsta.2015.0202>
- Juricic, P., Lu, Y.-X., Leech, T., Drews, L. F., Paulitz, J., Lu, J., Nespital, T., Azami, S., Regan, J. C., Funk, E., Fröhlich, J., Grönke, S., & Partridge, L. (2022). Long-lasting geroprotection from brief rapamycin treatment in early adulthood by persistently increased intestinal autophagy. *Nature Aging*, 2(9), 824-836. <https://doi.org/10.1038/s43587-022-00278-w>
- Ka, H. I., Han, S., Jeong, A. L., Lee, S., Yong, H. J., Boldbaatar, A., Joo, H. J., Soh, S. J., Park, J. Y., Lim, J. S., Lee, M. S., & Yang, Y. (2017). Neuronatin Is Associated with an Anti-Inflammatory Role in the White Adipose Tissue. *J Microbiol Biotechnol*, 27(6), 1180-1188. <https://doi.org/10.4014/jmb.1702.02049>
- Khan, S., Chan, Y. T., Revelo, X. S., & Winer, D. A. (2020). The Immune Landscape of Visceral Adipose Tissue During Obesity and Aging [Review]. *Frontiers in Endocrinology*, 11. <https://doi.org/10.3389/fendo.2020.00267>
- Kim, D., Paggi, J. M., Park, C., Bennett, C., & Salzberg, S. L. (2019). Graph-based genome alignment and genotyping with HISAT2 and HISAT-genotype. *Nat Biotechnol*, 37(8), 907-915. <https://doi.org/10.1038/s41587-019-0201-4>
- Kim, E. J., Kim, Y. K., Kim, S., Kim, J. E., Tian, Y. D., Doh, E. J., Lee, D. H., & Chung, J. H. (2018). Adipochemokines induced by ultraviolet irradiation contribute to impaired fat metabolism in subcutaneous fat cells. *Br J Dermatol*, 178(2), 492-501. <https://doi.org/10.1111/bjd.15907>
- Kim, S. J., Chae, S., Kim, H., Mun, D. G., Back, S., Choi, H. Y., Park, K. S., Hwang, D., Choi, S. H., & Lee, S. W. (2014). A protein profile of visceral adipose tissues linked to early pathogenesis of type 2 diabetes mellitus. *Mol Cell Proteomics*, 13(3), 811-822. <https://doi.org/10.1074/mcp.M113.035501>
- Kim, S. M., Lun, M., Wang, M., Senyo, S. E., Guillermier, C., Patwari, P., & Steinhauser, M. L. (2014). Loss of white adipose hyperplastic potential is associated with enhanced susceptibility to insulin resistance. *Cell Metab*, 20(6), 1049-1058. <https://doi.org/10.1016/j.cmet.2014.10.010>
- Kobak, D., & Berens, P. (2019). The art of using t-SNE for single-cell transcriptomics. *Nat Commun*, 10(1), 5416. <https://doi.org/10.1038/s41467-019-13056-x>
- Krueger, F. (2012). *Trim Galore*. In (Version 0.6.5) [https://www.bioinformatics.babraham.ac.uk/projects/trim\\_galore/](https://www.bioinformatics.babraham.ac.uk/projects/trim_galore/)
- Krycer, J. R., Fazakerley, D. J., Cater, R. J., K, C. T., Naghiloo, S., Burchfield, J. G., Humphrey, S. J., Vandenberg, R. J., Ryan, R. M., & James, D. E. (2017). The amino acid transporter, SLC1A3, is plasma membrane-localised in adipocytes and its activity is insensitive to insulin. *FEBS Lett*, 591(2), 322-330. <https://doi.org/10.1002/1873-3468.12549>
- Kursawe, R., Caprio, S., Giannini, C., Narayan, D., Lin, A., D'Adamo, E., Shaw, M., Pierpont, B., Cushman, S. W., & Shulman, G. I. (2013). Decreased transcription of ChREBP-alpha/beta isoforms in abdominal subcutaneous adipose tissue of obese adolescents with prediabetes or early type 2 diabetes: associations with

- insulin resistance and hyperglycemia. *Diabetes*, 62(3), 837-844. <https://doi.org/10.2337/db12-0889>
- La Manno, G., Siletti, K., Furlan, A., Gyllborg, D., Vinsland, E., Mossi Albiach, A., Mattsson Langseth, C., Khven, I., Lederer, A. R., Dratva, L. M., Johnsson, A., Nilsson, M., Lonnerberg, P., & Linnarsson, S. (2021). Molecular architecture of the developing mouse brain. *Nature*, 596(7870), 92-96. <https://doi.org/10.1038/s41586-021-03775-x>
- Lake, B. B., Ai, R., Kaeser, G. E., Salathia, N. S., Yung, Y. C., Liu, R., Wildberg, A., Gao, D., Fung, H. L., Chen, S., Vijayaraghavan, R., Wong, J., Chen, A., Sheng, X., Kaper, F., Shen, R., Ronaghi, M., Fan, J. B., Wang, W., Chun, J., & Zhang, K. (2016). Neuronal subtypes and diversity revealed by single-nucleus RNA sequencing of the human brain. *Science*, 352(6293), 1586-1590. <https://doi.org/10.1126/science.aaf1204>
- Lake, B. B., Codeluppi, S., Yung, Y. C., Gao, D., Chun, J., Kharchenko, P. V., Linnarsson, S., & Zhang, K. (2017). A comparative strategy for single-nucleus and single-cell transcriptomes confirms accuracy in predicted cell-type expression from nuclear RNA. *Sci Rep*, 7(1), 6031. <https://doi.org/10.1038/s41598-017-04426-w>
- Lee, J., Lee, J., Jung, E., Kim, Y. S., Roh, K., Jung, K. H., & Park, D. (2010). Ultraviolet A regulates adipogenic differentiation of human adipose tissue-derived mesenchymal stem cells via up-regulation of Kruppel-like factor 2. *J Biol Chem*, 285(42), 32647-32656. <https://doi.org/10.1074/jbc.M110.135830>
- Lee, J. T. H., Patikas, N., Kiselev, V. Y., & Hemberg, M. (2021). Fast searches of large collections of single-cell data using scfind. *Nat Methods*, 18(3), 262-271. <https://doi.org/10.1038/s41592-021-01076-9>
- Lee, M. J., Wu, Y., & Fried, S. K. (2013). Adipose tissue heterogeneity: implication of depot differences in adipose tissue for obesity complications. *Mol Aspects Med*, 34(1), 1-11. <https://doi.org/10.1016/j.mam.2012.10.001>
- Lei, H., Lyu, B., Gertz, E. M., Schaffer, A. A., Shi, X., Wu, K., Li, G., Xu, L., Hou, Y., Dean, M., & Schwartz, R. (2020). Tumor Copy Number Deconvolution Integrating Bulk and Single-Cell Sequencing Data. *J Comput Biol*, 27(4), 565-598. <https://doi.org/10.1089/cmb.2019.0302>
- Lemaitre, J. F., Ronget, V., Tidiere, M., Allaine, D., Berger, V., Cohas, A., Colchero, F., Conde, D. A., Garratt, M., Liker, A., Marais, G. A. B., Scheuerlein, A., Szekely, T., & Gaillard, J. M. (2020). Sex differences in adult lifespan and aging rates of mortality across wild mammals. *Proc Natl Acad Sci U S A*, 117(15), 8546-8553. <https://doi.org/10.1073/pnas.1911999117>
- Li, H., Janssens, J., De Waegeneer, M., Kolluru, S. S., Davie, K., Gardeux, V., Saelens, W., David, F. P. A., Brbic, M., Spanier, K., Leskovec, J., McLaughlin, C. N., Xie, Q., Jones, R. C., Brueckner, K., Shim, J., Tattikota, S. G., Schnorrer, F., Rust, K., Nystul, T. G., Carvalho-Santos, Z., Ribeiro, C., Pal, S., Mahadevaraju, S., Przytycka, T. M., Allen, A. M., Goodwin, S. F., Berry, C. W., Fuller, M. T., White-Cooper, H., Matunis, E. L., DiNardo, S., Galenza, A., O'Brien, L. E., Dow, J. A. T., sign, F. C. A. C. s., Jasper, H., Oliver, B., Perrimon, N., Deplancke, B., Quake, S. R., Luo, L., Aerts, S., Agarwal, D., Ahmed-Braimah, Y., Arbeitman, M., Ariss, M. M., Augsburg, J., Ayush, K., Baker, C. C., Banisch, T., Birker, K., Bodmer, R., Bolival, B., Brantley, S. E., Brill, J. A., Brown, N. C., Buehner, N. A., Cai, X. T., Cardoso-Figueiredo, R., Casares, F., Chang, A., Clandinin, T. R., Crasta, S., Desplan, C., Detweiler, A. M., Dhakan, D. B., Dona, E., Engert, S., Floc'hlay, S., George, N., Gonzalez-Segarra, A. J.,

- Groves, A. K., Gumbin, S., Guo, Y., Harris, D. E., Heifetz, Y., Holtz, S. L., Horns, F., Hudry, B., Hung, R. J., Jan, Y. N., Jaszczak, J. S., Jefferis, G., Karkanias, J., Karr, T. L., Katheder, N. S., Kezos, J., Kim, A. A., Kim, S. K., Kockel, L., Konstantinides, N., Kornberg, T. B., Krause, H. M., Labott, A. T., Laturney, M., Lehmann, R., Leinwand, S., Li, J., Li, J. S. S., Li, K., Li, K., Li, L., Li, T., Litovchenko, M., Liu, H. H., Liu, Y., Lu, T. C., Manning, J., Mase, A., Matera-Vatnick, M., Matias, N. R., McDonough-Goldstein, C. E., McGeever, A., McLachlan, A. D., Moreno-Roman, P., Neff, N., Neville, M., Ngo, S., Nielsen, T., O'Brien, C. E., Osumi-Sutherland, D., Ozel, M. N., Papatheodorou, I., Petkovic, M., Pilgrim, C., Pisco, A. O., Reisenman, C., Sanders, E. N., Dos Santos, G., Scott, K., Sherlekar, A., Shiu, P., Sims, D., Sit, R. V., Slaidina, M., Smith, H. E., Sterne, G., Su, Y. H., Sutton, D., Tamayo, M., Tan, M., Tastekin, I., Treiber, C., Vacek, D., Vogler, G., Waddell, S., Wang, W., Wilson, R. I., Wolfner, M. F., Wong, Y. E., Xie, A., Xu, J., Yamamoto, S., Yan, J., Yao, Z., Yoda, K., Zhu, R., & Zinzen, R. P. (2022). Fly Cell Atlas: A single-nucleus transcriptomic atlas of the adult fruit fly. *Science*, 375(6584), eabk2432. <https://doi.org/10.1126/science.abk2432>
- Li, W. V., & Li, J. J. (2018). An accurate and robust imputation method scImpute for single-cell RNA-seq data. *Nat Commun*, 9(1), 997. <https://doi.org/10.1038/s41467-018-03405-7>
- Liao, Y., Smyth, G. K., & Shi, W. (2014). featureCounts: an efficient general purpose program for assigning sequence reads to genomic features. *Bioinformatics*, 30(7), 923-930. <https://doi.org/10.1093/bioinformatics/btt656>
- Liberzon, A., Birger, C., Thorvaldsdottir, H., Ghandi, M., Mesirov, J. P., & Tamayo, P. (2015). The Molecular Signatures Database (MSigDB) hallmark gene set collection. *Cell Syst*, 1(6), 417-425. <https://doi.org/10.1016/j.cels.2015.12.004>
- Lisa F. Drews, C. M., Andrea Mesaros, Martin Purrio, Ramona Jansen, Oliver Hendrich, Sandra Buschbaum, André Pahl, Emilie Funk, Ramona Hoppe, Sebastian Grönke and Linda Partridge. (2021). *Late-life effects of earlier dietary restriction on lifespan, health span and tissue-specific phenotypes* Universität zu Köln]. [https://kups.ub.uni-koeln.de/61092/1/PhD thesis LisaFranziska Drews final.pdf](https://kups.ub.uni-koeln.de/61092/1/PhD%20thesis%20LisaFranziska%20Drews%20final.pdf)
- Liu, M., Lei, H., Dong, P., Fu, X., Yang, Z., Yang, Y., Ma, J., Liu, X., Cao, Y., & Xiao, R. (2017). Adipose-Derived Mesenchymal Stem Cells from the Elderly Exhibit Decreased Migration and Differentiation Abilities with Senescent Properties. *Cell Transplant*, 26(9), 1505-1519. <https://doi.org/10.1177/0963689717721221>
- Lizcano, F. (2019). The Beige Adipocyte as a Therapy for Metabolic Diseases. *Int J Mol Sci*, 20(20). <https://doi.org/10.3390/ijms20205058>
- Lopez-Otin, C., Blasco, M. A., Partridge, L., Serrano, M., & Kroemer, G. (2013). The hallmarks of aging. *Cell*, 153(6), 1194-1217. <https://doi.org/10.1016/j.cell.2013.05.039>
- Love, M. I., Huber, W., & Anders, S. (2014). Moderated estimation of fold change and dispersion for RNA-seq data with DESeq2. *Genome Biol*, 15(12), 550. <https://doi.org/10.1186/s13059-014-0550-8>
- Lu, S., Guan, Q., Liu, Y., Wang, H., Xu, W., Li, X., Fu, Y., Gao, L., Zhao, J., & Wang, X. (2012). Role of extrathyroidal TSHR expression in adipocyte differentiation and its association with obesity. *Lipids Health Dis*, 11, 17. <https://doi.org/10.1186/1476-511x-11-17>
- Ma, Q., & Xu, D. (2022). Deep learning shapes single-cell data analysis. *Nat Rev Mol Cell Biol*, 23(5), 303-304. <https://doi.org/10.1038/s41580-022-00466-x>

- Mandl, M., Wagner, S. A., Hatzmann, F. M., Ejaz, A., Ritthammer, H., Baumgarten, S., Viertler, H. P., Springer, J., Zwierzina, M. E., Mattesich, M., Brucker, C., Waldegger, P., Pierer, G., & Zwerschke, W. (2020). Sprouty1 Prevents Cellular Senescence Maintaining Proliferation and Differentiation Capacity of Human Adipose Stem/Progenitor Cells. *J Gerontol A Biol Sci Med Sci*, 75(12), 2308-2319. <https://doi.org/10.1093/gerona/glaa098>
- Mannick, J. B., Del Giudice, G., Lattanzi, M., Valiante, N. M., Praestgaard, J., Huang, B., Lonetto, M. A., Maecker, H. T., Kovarik, J., Carson, S., Glass, D. J., & Klickstein, L. B. (2014). mTOR inhibition improves immune function in the elderly. *Sci Transl Med*, 6(268), 268ra179. <https://doi.org/10.1126/scitranslmed.3009892>
- Martinez-Sanchez, N. (2020). There and Back Again: Leptin Actions in White Adipose Tissue. *Int J Mol Sci*, 21(17). <https://doi.org/10.3390/ijms21176039>
- Mattison, J. A., Roth, G. S., Beasley, T. M., Tilmont, E. M., Handy, A. M., Herbert, R. L., Longo, D. L., Allison, D. B., Young, J. E., Bryant, M., Barnard, D., Ward, W. F., Qi, W., Ingram, D. K., & de Cabo, R. (2012). Impact of caloric restriction on health and survival in rhesus monkeys from the NIA study. *Nature*, 489(7415), 318-321. <https://doi.org/10.1038/nature11432>
- McCay, C. M., Crowell, M. F., & Maynard, L. A. (1935). The Effect of Retarded Growth Upon the Length of Life Span and Upon the Ultimate Body Size: One Figure. *The Journal of Nutrition*, 10(1), 63-79. <https://doi.org/10.1093/jn/10.1.63>
- McLaughlin, T., Lamendola, C., Liu, A., & Abbasi, F. (2011). Preferential fat deposition in subcutaneous versus visceral depots is associated with insulin sensitivity. *J Clin Endocrinol Metab*, 96(11), E1756-1760. <https://doi.org/10.1210/jc.2011-0615>
- Melms, J. C., Biermann, J., Huang, H., Wang, Y., Nair, A., Tagore, S., Katsyv, I., Rendeiro, A. F., Amin, A. D., Schapiro, D., Frangieh, C. J., Luoma, A. M., Filliol, A., Fang, Y., Ravichandran, H., Clausi, M. G., Alba, G. A., Rogava, M., Chen, S. W., Ho, P., Montoro, D. T., Kornberg, A. E., Han, A. S., Bakhoun, M. F., Anandasabapathy, N., Suarez-Farinas, M., Bakhoun, S. F., Bram, Y., Borczuk, A., Guo, X. V., Lefkowitz, J. H., Marboe, C., Lagana, S. M., Del Portillo, A., Tsai, E. J., Zorn, E., Markowitz, G. S., Schwabe, R. F., Schwartz, R. E., Elemento, O., Saqi, A., Hibshoosh, H., Que, J., & Izar, B. (2021). A molecular single-cell lung atlas of lethal COVID-19. *Nature*, 595(7865), 114-119. <https://doi.org/10.1038/s41586-021-03569-1>
- Miao, Z., Deng, K., Wang, X., & Zhang, X. (2018). DEsingle for detecting three types of differential expression in single-cell RNA-seq data. *Bioinformatics*, 34(18), 3223-3224. <https://doi.org/10.1093/bioinformatics/bty332>
- Min, H., Kim, J., Kim, Y. J., Yoon, M. S., Pratley, R. E., & Lee, Y. H. (2017). Measurement of altered APP isoform expression in adipose tissue of diet-induced obese mice by absolute quantitative real-time PCR. *Anim Cells Syst (Seoul)*, 21(2), 100-107. <https://doi.org/10.1080/19768354.2017.1290679>
- Mitchell, S. J., Madrigal-Matute, J., Scheibye-Knudsen, M., Fang, E., Aon, M., Gonzalez-Reyes, J. A., Cortassa, S., Kaushik, S., Gonzalez-Freire, M., Patel, B., Wahl, D., Ali, A., Calvo-Rubio, M., Buron, M. I., Guterrez, V., Ward, T. M., Palacios, H. H., Cai, H., Frederick, D. W., Hine, C., Broeskamp, F., Habering, L., Dawson, J., Beasley, T. M., Wan, J., Ikeno, Y., Hubbard, G., Becker, K. G., Zhang, Y., Bohr, V. A., Longo, D. L., Navas, P., Ferrucci, L., Sinclair, D. A., Cohen, P., Egan, J. M., Mitchell, J. R., Baur, J. A., Allison, D. B., Anson, R. M., Villalba, J. M., Madeo, F., Cuervo, A. M., Pearson, K. J., Ingram, D. K., Bernier,

- M., & de Cabo, R. (2016). Effects of Sex, Strain, and Energy Intake on Hallmarks of Aging in Mice. *Cell Metab*, 23(6), 1093-1112. <https://doi.org/10.1016/j.cmet.2016.05.027>
- Morigny, P., Houssier, M., Mairal, A., Ghilain, C., Mouisel, E., Benhamed, F., Masri, B., Recazens, E., Denechaud, P. D., Tavernier, G., Caspar-Bauguil, S., Virtue, S., Sramkova, V., Monbrun, L., Mazars, A., Zanoun, M., Guilmeau, S., Barquissau, V., Beuzelin, D., Bonnel, S., Marques, M., Monge-Roffarello, B., Lefort, C., Fielding, B., Sulpice, T., Astrup, A., Payrastre, B., Bertrand-Michel, J., Meugnier, E., Ligat, L., Lopez, F., Guillou, H., Ling, C., Holm, C., Rabasa-Lhoret, R., Saris, W. H. M., Stich, V., Arner, P., Ryden, M., Moro, C., Viguerie, N., Harms, M., Hallen, S., Vidal-Puig, A., Vidal, H., Postic, C., & Langin, D. (2019). Interaction between hormone-sensitive lipase and ChREBP in fat cells controls insulin sensitivity. *Nat Metab*, 1(1), 133-146. <https://doi.org/10.1038/s42255-018-0007-6>
- Most, J., Tosti, V., Redman, L. M., & Fontana, L. (2017). Calorie restriction in humans: An update. *Ageing Res Rev*, 39, 36-45. <https://doi.org/10.1016/j.arr.2016.08.005>
- Mu, Q., Chen, Y., & Wang, J. (2019). Deciphering Brain Complexity Using Single-cell Sequencing. *Genomics Proteomics Bioinformatics*, 17(4), 344-366. <https://doi.org/10.1016/j.gpb.2018.07.007>
- Muzumdar, R., Allison, D. B., Huffman, D. M., Ma, X., Atzmon, G., Einstein, F. H., Fishman, S., Poduval, A. D., McVei, T., Keith, S. W., & Barzilai, N. (2008). Visceral adipose tissue modulates mammalian longevity. *Aging Cell*, 7(3), 438-440. <https://doi.org/10.1111/j.1474-9726.2008.00391.x>
- Nemesh, J. (2015). *Drop-seq Core Computational Protocol*. [https://mccarrolllab.org/wp-content/uploads/2015/05/Drop-seqAlignmentCookbook\\_v1.1Aug2015.pdf](https://mccarrolllab.org/wp-content/uploads/2015/05/Drop-seqAlignmentCookbook_v1.1Aug2015.pdf)
- Niccoli, T., & Partridge, L. (2012). Ageing as a risk factor for disease. *Curr Biol*, 22(17), R741-752. <https://doi.org/10.1016/j.cub.2012.07.024>
- North, T. E., Stacy, T., Matheny, C. J., Speck, N. A., & de Bruijn, M. F. (2004). Runx1 is expressed in adult mouse hematopoietic stem cells and differentiating myeloid and lymphoid cells, but not in maturing erythroid cells. *Stem Cells*, 22(2), 158-168. <https://doi.org/10.1634/stemcells.22-2-158>
- O'Neill, S., & O'Driscoll, L. (2015). Metabolic syndrome: a closer look at the growing epidemic and its associated pathologies. *Obes Rev*, 16(1), 1-12. <https://doi.org/10.1111/obr.12229>
- Oger, F., Gheeraert, C., Mogilenko, D., Benomar, Y., Molendi-Coste, O., Bouchaert, E., Caron, S., Dombrowicz, D., Pattou, F., Duez, H., Eeckhoute, J., Staels, B., & Lefebvre, P. (2014). Cell-specific dysregulation of microRNA expression in obese white adipose tissue. *J Clin Endocrinol Metab*, 99(8), 2821-2833. <https://doi.org/10.1210/jc.2013-4259>
- Oh, M. S., Hong, J. Y., Kim, M. N., Kwak, E. J., Kim, S. Y., Kim, E. G., Lee, K. E., Kim, Y. S., Jee, H. M., Kim, S. H., Sol, I. S., Park, C. O., Kim, K. W., & Sohn, M. H. (2019). Activated Leukocyte Cell Adhesion Molecule Modulates Th2 Immune Response in Atopic Dermatitis. *Allergy Asthma Immunol Res*, 11(5), 677-690. <https://doi.org/10.4168/aair.2019.11.5.677>
- Ong, P. S., Wang, L. Z., Dai, X., Tseng, S. H., Loo, S. J., & Sethi, G. (2016). Judicious Toggling of mTOR Activity to Combat Insulin Resistance and Cancer: Current Evidence and Perspectives. *Front Pharmacol*, 7, 395. <https://doi.org/10.3389/fphar.2016.00395>

- Ou, M. Y., Zhang, H., Tan, P. C., Zhou, S. B., & Li, Q. F. (2022). Adipose tissue aging: mechanisms and therapeutic implications. *Cell Death Dis*, 13(4), 300. <https://doi.org/10.1038/s41419-022-04752-6>
- Oulhen, N., Foster, S., Wray, G., & Wessel, G. (2019). Identifying gene expression from single cells to single genes. *Methods Cell Biol*, 151, 127-158. <https://doi.org/10.1016/bs.mcb.2018.11.018>
- Parekh, S., Ziegenhain, C., Vieth, B., Enard, W., & Hellmann, I. (2018). zUMIs - A fast and flexible pipeline to process RNA sequencing data with UMIs. *Gigascience*, 7(6). <https://doi.org/10.1093/gigascience/giy059>
- Petrus, P., Mejhert, N., Corrales, P., Lecoutre, S., Li, Q., Maldonado, E., Kulyté, A., Lopez, Y., Campbell, M., Acosta, J. R., Laurencikienė, J., Douagi, I., Gao, H., Martínez-Álvarez, C., Hedén, P., Spalding, K. L., Vidal-Puig, A., Medina-Gomez, G., Arner, P., & Rydén, M. (2018). Transforming Growth Factor- $\beta$ 3 Regulates Adipocyte Number in Subcutaneous White Adipose Tissue. *Cell Rep*, 25(3), 551-560.e555. <https://doi.org/10.1016/j.celrep.2018.09.069>
- Piedra-Quintero, Z. L., Serrano, C., Villegas-Sepúlveda, N., Maravillas-Montero, J. L., Romero-Ramírez, S., Shibayama, M., Medina-Contreras, O., Nava, P., & Santos-Argumedo, L. (2019). Myosin 1F Regulates M1-Polarization by Stimulating Intercellular Adhesion in Macrophages. *Frontiers in immunology*, 9, 3118-3118. <https://doi.org/10.3389/fimmu.2018.03118>
- Quarles, E., Basisty, N., Chiao, Y. A., Merrihew, G., Gu, H., Sweetwyne, M. T., Fredrickson, J., Nguyen, N. H., Razumova, M., Kooiker, K., Moussavi-Harami, F., Regnier, M., Quarles, C., MacCoss, M., & Rabinovitch, P. S. (2020). Rapamycin persistently improves cardiac function in aged, male and female mice, even following cessation of treatment. *Aging Cell*, 19(2), e13086. <https://doi.org/10.1111/acel.13086>
- Ran, L., Wang, X., Mi, A., Liu, Y., Wu, J., Wang, H., Guo, M., Sun, J., Liu, B., Li, Y., Wang, D., Jiang, R., Wang, N., Gao, W., Zeng, L., Huang, L., Chen, X., LeRoith, D., Liang, B., Li, X., & Wu, Y. (2019). Loss of Adipose Growth Hormone Receptor in Mice Enhances Local Fatty Acid Trapping and Impairs Brown Adipose Tissue Thermogenesis. *iScience*, 16, 106-121. <https://doi.org/10.1016/j.isci.2019.05.020>
- Redman, L. M., & Ravussin, E. (2011). Caloric restriction in humans: impact on physiological, psychological, and behavioral outcomes. *Antioxid Redox Signal*, 14(2), 275-287. <https://doi.org/10.1089/ars.2010.3253>
- Reyes-Farias, M., Fos-Domenech, J., Serra, D., Herrero, L., & Sanchez-Infantes, D. (2021). White adipose tissue dysfunction in obesity and aging. *Biochem Pharmacol*, 192, 114723. <https://doi.org/10.1016/j.bcp.2021.114723>
- Richard, A. J., White, U., Elks, C. M., & Stephens, J. M. (2000). Adipose Tissue: Physiology to Metabolic Dysfunction. In K. R. Feingold, B. Anawalt, A. Boyce, G. Chrousos, W. W. de Herder, K. Dhatariya, K. Dungan, J. M. Hershman, J. Hofland, S. Kalra, G. Kaltsas, C. Koch, P. Kopp, M. Korbonits, C. S. Kovacs, W. Kuohung, B. Laferrere, M. Levy, E. A. McGee, R. McLachlan, J. E. Morley, M. New, J. Purnell, R. Sahay, F. Singer, M. A. Sperling, C. A. Stratakis, D. L. Trencce, & D. P. Wilson (Eds.), *Endotext*. <https://www.ncbi.nlm.nih.gov/pubmed/32255578>
- Rondini, E. A., & Granneman, J. G. (2020). Single cell approaches to address adipose tissue stromal cell heterogeneity. *Biochem J*, 477(3), 583-600. <https://doi.org/10.1042/BCJ20190467>

- Rosen, M. J. a. D. D. a. T. A. a. Y. (2022). VISION: Functional interpretation of single cell RNA-seq latent manifolds. <https://yoseflab.github.io/VISION>
- Russo, L., & Lumeng, C. N. (2018). Properties and functions of adipose tissue macrophages in obesity. *Immunology*, 155(4), 407-417. <https://doi.org/10.1111/imm.13002>
- Sárvári, A. K., Van Hauwaert, E. L., Markussen, L. K., Gammelmark, E., Marcher, A. B., Ebbesen, M. F., Nielsen, R., Brewer, J. R., Madsen, J. G. S., & Mandrup, S. (2021). Plasticity of Epididymal Adipose Tissue in Response to Diet-Induced Obesity at Single-Nucleus Resolution. *Cell Metab*, 33(2), 437-453.e435. <https://doi.org/10.1016/j.cmet.2020.12.004>
- Schwalie, P. C., Dong, H., Zachara, M., Russeil, J., Alpern, D., Akchiche, N., Caprara, C., Sun, W., Schlaudraff, K. U., Soldati, G., Wolfrum, C., & Deplancke, B. (2018). A stromal cell population that inhibits adipogenesis in mammalian fat depots. *Nature*, 559(7712), 103-108. <https://doi.org/10.1038/s41586-018-0226-8>
- Scott, C. L., T'Jonck, W., Martens, L., Todorov, H., Sichien, D., Soen, B., Bonnardel, J., De Prijck, S., Vandamme, N., Cannoodt, R., Saelens, W., Vanneste, B., Toussaint, W., De Bleser, P., Takahashi, N., Vandenameele, P., Henri, S., Pridans, C., Hume, D. A., Lambrecht, B. N., De Baetselier, P., Milling, S. W. F., Van Ginderachter, J. A., Malissen, B., Berx, G., Beschin, A., Saeys, Y., & Guillems, M. (2018). The Transcription Factor ZEB2 Is Required to Maintain the Tissue-Specific Identities of Macrophages. *Immunity*, 49(2), 312-325.e315. <https://doi.org/10.1016/j.immuni.2018.07.004>
- Selman, C., Partridge, L., & Withers, D. J. (2011). Replication of extended lifespan phenotype in mice with deletion of insulin receptor substrate 1. *PLoS One*, 6(1), e16144. <https://doi.org/10.1371/journal.pone.0016144>
- Selvarani, R., Mohammed, S., & Richardson, A. (2021). Effect of rapamycin on aging and age-related diseases-past and future. *Geroscience*, 43(3), 1135-1158. <https://doi.org/10.1007/s11357-020-00274-1>
- Sheng, Y., Xia, F., Chen, L., Lv, Y., Lv, S., Yu, J., Liu, J., & Ding, G. (2021). Differential Responses of White Adipose Tissue and Brown Adipose Tissue to Calorie Restriction During Aging. *J Gerontol A Biol Sci Med Sci*, 76(3), 393-399. <https://doi.org/10.1093/gerona/glaa070>
- Shi, R., Jin, Y., Zhao, S., Yuan, H., Shi, J., & Zhao, H. (2022). Hypoxic ADSC-derived exosomes enhance wound healing in diabetic mice via delivery of circ-Snhg11 and induction of M2-like macrophage polarization. *Biomed Pharmacother*, 153, 113463. <https://doi.org/10.1016/j.biopha.2022.113463>
- Sim, C. K., Kim, S. Y., Brunmeir, R., Zhang, Q., Li, H., Dharmasegaran, D., Leong, C., Lim, Y. Y., Han, W., & Xu, F. (2017). Regulation of white and brown adipocyte differentiation by RhoGAP DLC1. *PLoS One*, 12(3), e0174761. <https://doi.org/10.1371/journal.pone.0174761>
- Soefje, S. A., Karnad, A., & Brenner, A. J. (2011). Common toxicities of mammalian target of rapamycin inhibitors. *Target Oncol*, 6(2), 125-129. <https://doi.org/10.1007/s11523-011-0174-9>
- Solinas, G., Boren, J., & Dulloo, A. G. (2015). De novo lipogenesis in metabolic homeostasis: More friend than foe? *Mol Metab*, 4(5), 367-377. <https://doi.org/10.1016/j.molmet.2015.03.004>
- Song, Z., Xiaoli, A. M., & Yang, F. (2018). Regulation and Metabolic Significance of De Novo Lipogenesis in Adipose Tissues. *Nutrients*, 10(10). <https://doi.org/10.3390/nu10101383>

- Souza, C. O., Teixeira, A. A. S., Biondo, L. A., Silveira, L. S., de Souza Breda, C. N., Braga, T. T., Camara, N. O. S., Belchior, T., Festuccia, W. T., Diniz, T. A., Ferreira, G. M., Hirata, M. H., Chaves-Filho, A. B., Yoshinaga, M. Y., Miyamoto, S., Calder, P. C., Sethi, J. K., & Rosa Neto, J. C. (2020). Palmitoleic acid reduces high fat diet-induced liver inflammation by promoting PPAR-gamma-independent M2a polarization of myeloid cells. *Biochim Biophys Acta Mol Cell Biol Lipids*, 1865(10), 158776. <https://doi.org/10.1016/j.bbalip.2020.158776>
- Speakman, J. R. (2005). Body size, energy metabolism and lifespan. *J Exp Biol*, 208(Pt 9), 1717-1730. <https://doi.org/10.1242/jeb.01556>
- Srivastava, N., Sudan, R., & Kerr, W. G. (2013). Role of inositol poly-phosphatases and their targets in T cell biology. *Front Immunol*, 4, 288. <https://doi.org/10.3389/fimmu.2013.00288>
- Starr, M. E., Evers, B. M., & Saito, H. (2009). Age-associated increase in cytokine production during systemic inflammation: adipose tissue as a major source of IL-6. *J Gerontol A Biol Sci Med Sci*, 64(7), 723-730. <https://doi.org/10.1093/gerona/glp046>
- Steen, C. B., Liu, C. L., Alizadeh, A. A., & Newman, A. M. (2020). Profiling Cell Type Abundance and Expression in Bulk Tissues with CIBERSORTx. *Methods Mol Biol*, 2117, 135-157. [https://doi.org/10.1007/978-1-0716-0301-7\\_7](https://doi.org/10.1007/978-1-0716-0301-7_7)
- Subramanian, A., Tamayo, P., Mootha, V. K., Mukherjee, S., Ebert, B. L., Gillette, M. A., Paulovich, A., Pomeroy, S. L., Golub, T. R., Lander, E. S., & Mesirov, J. P. (2005). Gene set enrichment analysis: a knowledge-based approach for interpreting genome-wide expression profiles. *Proc Natl Acad Sci U S A*, 102(43), 15545-15550. <https://doi.org/10.1073/pnas.0506580102>
- Subramanian, I., Verma, S., Kumar, S., Jere, A., & Anamika, K. (2020). Multi-omics Data Integration, Interpretation, and Its Application. *Bioinform Biol Insights*, 14, 1177932219899051. <https://doi.org/10.1177/1177932219899051>
- Sun, J., Shen, X., Liu, H., Lu, S., Peng, J., & Kuang, H. (2021). Caloric restriction in female reproduction: is it beneficial or detrimental? *Reprod Biol Endocrinol*, 19(1), 1. <https://doi.org/10.1186/s12958-020-00681-1>
- Surmi, B. K., & Hasty, A. H. (2008). Macrophage infiltration into adipose tissue: initiation, propagation and remodeling. *Future Lipidol*, 3(5), 545-556. <https://doi.org/10.2217/17460875.3.5.545>
- Sutton, G. J., Poppe, D., Simmons, R. K., Walsh, K., Nawaz, U., Lister, R., Gagnon-Bartsch, J. A., & Voineagu, I. (2022). Comprehensive evaluation of deconvolution methods for human brain gene expression. *Nat Commun*, 13(1), 1358. <https://doi.org/10.1038/s41467-022-28655-4>
- Tabula Muris, C. (2020). A single-cell transcriptomic atlas characterizes ageing tissues in the mouse. *Nature*, 583(7817), 590-595. <https://doi.org/10.1038/s41586-020-2496-1>
- Tabula Muris, C., Overall, c., Logistical, c., Organ, c., processing, Library, p., sequencing, Computational data, a., Cell type, a., Writing, g., Supplemental text writing, g., & Principal, i. (2018). Single-cell transcriptomics of 20 mouse organs creates a Tabula Muris. *Nature*, 562(7727), 367-372. <https://doi.org/10.1038/s41586-018-0590-4>
- Tang, F., Barbacioru, C., Wang, Y., Nordman, E., Lee, C., Xu, N., Wang, X., Bodeau, J., Tuch, B. B., Siddiqui, A., Lao, K., & Surani, M. A. (2009). mRNA-Seq whole-transcriptome analysis of a single cell. *Nat Methods*, 6(5), 377-382. <https://doi.org/10.1038/nmeth.1315>

- Tang, X., Huang, Y., Lei, J., Luo, H., & Zhu, X. (2019). The single-cell sequencing: new developments and medical applications. *Cell Biosci*, 9, 53. <https://doi.org/10.1186/s13578-019-0314-y>
- Tchkonia, T., Morbeck, D. E., Von Zglinicki, T., Van Deursen, J., Lustgarten, J., Scrable, H., Khosla, S., Jensen, M. D., & Kirkland, J. L. (2010). Fat tissue, aging, and cellular senescence. *Aging Cell*, 9(5), 667-684. <https://doi.org/https://doi.org/10.1111/j.1474-9726.2010.00608.x>
- team, R. c. (2013). *R: A Language and Environment for Statistical Computing*. In R Foundation for Statistical Computing. <http://www.R-project.org/>
- Templeman, N. M., Flibotte, S., Chik, J. H. L., Sinha, S., Lim, G. E., Foster, L. J., Nislow, C., & Johnson, J. D. (2017). Reduced Circulating Insulin Enhances Insulin Sensitivity in Old Mice and Extends Lifespan. *Cell Rep*, 20(2), 451-463. <https://doi.org/10.1016/j.celrep.2017.06.048>
- Tomczyk, S., Fischer, K., Austad, S., & Galliot, B. (2015). Hydra, a powerful model for aging studies. *Invertebr Reprod Dev*, 59(sup1), 11-16. <https://doi.org/10.1080/07924259.2014.927805>
- Trapnell, C., Cacchiarelli, D., Grimsby, J., Pokharel, P., Li, S., Morse, M., Lennon, N. J., Livak, K. J., Mikkelsen, T. S., & Rinn, J. L. (2014). The dynamics and regulators of cell fate decisions are revealed by pseudotemporal ordering of single cells. *Nat Biotechnol*, 32(4), 381-386. <https://doi.org/10.1038/nbt.2859>
- Travaglini, K. J., Nabhan, A. N., Penland, L., Sinha, R., Gillich, A., Sit, R. V., Chang, S., Conley, S. D., Mori, Y., Seita, J., Berry, G. J., Shrager, J. B., Metzger, R. J., Kuo, C. S., Neff, N., Weissman, I. L., Quake, S. R., & Krasnow, M. A. (2020). A molecular cell atlas of the human lung from single-cell RNA sequencing. *Nature*, 587(7835), 619-625. <https://doi.org/10.1038/s41586-020-2922-4>
- Trayhurn, P. (2013). Hypoxia and adipose tissue function and dysfunction in obesity. *Physiol Rev*, 93(1), 1-21. <https://doi.org/10.1152/physrev.00017.2012>
- Tsochatzis, E., Papatheodoridis, G. V., & Archimandritis, A. J. (2006). The evolving role of leptin and adiponectin in chronic liver diseases. *Am J Gastroenterol*, 101(11), 2629-2640. <https://doi.org/10.1111/j.1572-0241.2006.00848.x>
- van Dijk, D., Sharma, R., Nainys, J., Yim, K., Kathail, P., Carr, A. J., Burdziak, C., Moon, K. R., Chaffer, C. L., Pattabiraman, D., Bieri, B., Mazutis, L., Wolf, G., Krishnaswamy, S., & Pe'er, D. (2018). Recovering Gene Interactions from Single-Cell Data Using Data Diffusion. *Cell*, 174(3), 716-729 e727. <https://doi.org/10.1016/j.cell.2018.05.061>
- van Heemst, D. (2010). Insulin, IGF-1 and longevity. *Aging Dis*, 1(2), 147-157. <https://www.ncbi.nlm.nih.gov/pubmed/22396862>
- Vargas-Castillo, A., Fuentes-Romero, R., Rodriguez-Lopez, L. A., Torres, N., & Tovar, A. R. (2017). Understanding the Biology of Thermogenic Fat: Is Browning A New Approach to the Treatment of Obesity? *Arch Med Res*, 48(5), 401-413. <https://doi.org/10.1016/j.arcmed.2017.10.002>
- Vatner, D. E., Zhang, J., Oydanich, M., Guers, J., Katsyuba, E., Yan, L., Sinclair, D., Auwerx, J., & Vatner, S. F. (2018). Enhanced longevity and metabolism by brown adipose tissue with disruption of the regulator of G protein signaling 14. *Aging Cell*, 17(4), e12751. <https://doi.org/10.1111/accel.12751>
- Vijay, J., Gauthier, M. F., Biswell, R. L., Louiselle, D. A., Johnston, J. J., Cheung, W. A., Belden, B., Pramatarova, A., Biertho, L., Gibson, M., Simon, M. M., Djambazian, H., Staffa, A., Bourque, G., Laitinen, A., Nystedt, J., Vohl, M. C., Fraser, J. D., Pastinen, T., Tchernof, A., & Grundberg, E. (2020). Single-cell

- analysis of human adipose tissue identifies depot and disease specific cell types. *Nat Metab*, 2(1), 97-109. <https://doi.org/10.1038/s42255-019-0152-6>
- Wang, F., Flanagan, J., Su, N., Wang, L. C., Bui, S., Nielson, A., Wu, X., Vo, H. T., Ma, X. J., & Luo, Y. (2012). RNAscope: a novel in situ RNA analysis platform for formalin-fixed, paraffin-embedded tissues. *J Mol Diagn*, 14(1), 22-29. <https://doi.org/10.1016/j.jmoldx.2011.08.002>
- Wang, L., Sebra, R. P., Sfakianos, J. P., Allette, K., Wang, W., Yoo, S., Bhardwaj, N., Schadt, E. E., Yao, X., Galsky, M. D., & Zhu, J. (2020). A reference profile-free deconvolution method to infer cancer cell-intrinsic subtypes and tumor-type-specific stromal profiles. *Genome Med*, 12(1), 24. <https://doi.org/10.1186/s13073-020-0720-0>
- Wang, T., Hill, R. C., Dzieciatkowska, M., Zhu, L., Infante, A. M., Hu, G., Hansen, K. C., & Pei, M. (2020). Site-Dependent Lineage Preference of Adipose Stem Cells. *Front Cell Dev Biol*, 8, 237. <https://doi.org/10.3389/fcell.2020.00237>
- Wang, X., Park, J., Susztak, K., Zhang, N. R., & Li, M. (2019). Bulk tissue cell type deconvolution with multi-subject single-cell expression reference. *Nat Commun*, 10(1), 380. <https://doi.org/10.1038/s41467-018-08023-x>
- Wardhana, D. A., Ikeda, K., Barinda, A. J., Nugroho, D. B., Qurania, K. R., Yagi, K., Miyata, K., Oike, Y., Hirata, K.-i., & Emoto, N. (2018). Family with sequence similarity 13, member A modulates adipocyte insulin signaling and preserves systemic metabolic homeostasis. *Proceedings of the National Academy of Sciences*, 115(7), 1529-1534. <https://doi.org/doi:10.1073/pnas.1720475115>
- Weinreich, J., Lob, S., Loffler, M., Konigsrainer, I., Zieker, D., Konigsrainer, A., Coerper, S., & Beckert, S. (2011). Rapamycin-induced impaired wound healing is associated with compromised tissue lactate accumulation and extracellular matrix remodeling. *Eur Surg Res*, 47(1), 39-44. <https://doi.org/10.1159/000327972>
- Weiss, E. P., & Holloszy, J. O. (2007). Improvements in body composition, glucose tolerance, and insulin action induced by increasing energy expenditure or decreasing energy intake. *J Nutr*, 137(4), 1087-1090. <https://doi.org/10.1093/jn/137.4.1087>
- Wickham, H. (2016). *ggplot2: Elegant Graphics for Data Analysis*. Springer-Verlag New York. <https://ggplot2.tidyverse.org>
- Willcox, B. J., Donlon, T. A., He, Q., Chen, R., Grove, J. S., Yano, K., Masaki, K. H., Willcox, D. C., Rodriguez, B., & Curb, J. D. (2008). FOXO3A genotype is strongly associated with human longevity. *Proc Natl Acad Sci U S A*, 105(37), 13987-13992. <https://doi.org/10.1073/pnas.0801030105>
- Wilson, K. A., Chamoli, M., Hilsabeck, T. A., Pandey, M., Bansal, S., Chawla, G., & Kapahi, P. (2021). Evaluating the beneficial effects of dietary restrictions: A framework for precision nutrigenetics. *Cell Metabolism*, 33(11), 2142-2173. <https://doi.org/https://doi.org/10.1016/j.cmet.2021.08.018>
- Witte, N., Muenzner, M., Rietscher, J., Knauer, M., Heidenreich, S., Nuotio-Antar, A. M., Graef, F. A., Fedders, R., Tolkachov, A., Goehring, I., & Schupp, M. (2015). The Glucose Sensor ChREBP Links De Novo Lipogenesis to PPARgamma Activity and Adipocyte Differentiation. *Endocrinology*, 156(11), 4008-4019. <https://doi.org/10.1210/EN.2015-1209>
- Wu, T., Hu, E., Xu, S., Chen, M., Guo, P., Dai, Z., Feng, T., Zhou, L., Tang, W., Zhan, L., Fu, X., Liu, S., Bo, X., & Yu, G. (2021). clusterProfiler 4.0: A universal enrichment tool for interpreting omics data. *Innovation (Camb)*, 2(3), 100141. <https://doi.org/10.1016/j.xinn.2021.100141>

- Ximerakis, M., Lipnick, S. L., Innes, B. T., Simmons, S. K., Adiconis, X., Dionne, D., Mayweather, B. A., Nguyen, L., Niziolek, Z., Ozek, C., Butty, V. L., Isserlin, R., Buchanan, S. M., Levine, S. S., Regev, A., Bader, G. D., Levin, J. Z., & Rubin, L. L. (2019). Single-cell transcriptomic profiling of the aging mouse brain. *Nat Neurosci*, 22(10), 1696-1708. <https://doi.org/10.1038/s41593-019-0491-3>
- Xu, M., Palmer, A. K., Ding, H., Weivoda, M. M., Pirtskhalava, T., White, T. A., Sepe, A., Johnson, K. O., Stout, M. B., Giorgadze, N., Jensen, M. D., LeBrasseur, N. K., Tchkonja, T., & Kirkland, J. L. (2015). Targeting senescent cells enhances adipogenesis and metabolic function in old age. *Elife*, 4, e12997. <https://doi.org/10.7554/eLife.12997>
- Yaghootkar, H., Witcher, B., Bell, J. D., & Thomas, E. L. (2020). Ethnic differences in adiposity and diabetes risk - insights from genetic studies. *J Intern Med*, 288(3), 271-283. <https://doi.org/10.1111/joim.13082>
- Yang, W. S., Lee, W. J., Huang, K. C., Lee, K. C., Chao, C. L., Chen, C. L., Tai, T. Y., & Chuang, L. M. (2003). mRNA levels of the insulin-signaling molecule SORBS1 in the adipose depots of nondiabetic women. *Obes Res*, 11(4), 586-590. <https://doi.org/10.1038/oby.2003.82>
- Yip, S. H., Sham, P. C., & Wang, J. (2019). Evaluation of tools for highly variable gene discovery from single-cell RNA-seq data. *Brief Bioinform*, 20(4), 1583-1589. <https://doi.org/10.1093/bib/bby011>
- Zhang, X., Li, T., Liu, F., Chen, Y., Yao, J., Li, Z., Huang, Y., & Wang, J. (2019). Comparative Analysis of Droplet-Based Ultra-High-Throughput Single-Cell RNA-Seq Systems. *Mol Cell*, 73(1), 130-142 e135. <https://doi.org/10.1016/j.molcel.2018.10.020>
- Zheng, G. X., Terry, J. M., Belgrader, P., Ryvkin, P., Bent, Z. W., Wilson, R., Ziraldo, S. B., Wheeler, T. D., McDermott, G. P., Zhu, J., Gregory, M. T., Shuga, J., Montesclaros, L., Underwood, J. G., Masquelier, D. A., Nishimura, S. Y., Schnall-Levin, M., Wyatt, P. W., Hindson, C. M., Bharadwaj, R., Wong, A., Ness, K. D., Beppu, L. W., Deeg, H. J., McFarland, C., Loeb, K. R., Valente, W. J., Ericson, N. G., Stevens, E. A., Radich, J. P., Mikkelsen, T. S., Hindson, B. J., & Bielas, J. H. (2017). Massively parallel digital transcriptional profiling of single cells. *Nat Commun*, 8, 14049. <https://doi.org/10.1038/ncomms14049>
- Zhu, Y., Zhang, X., Gu, R., Liu, X., Wang, S., Xia, D., Li, Z., Lian, X., Zhang, P., Liu, Y., & Zhou, Y. (2020). LAMA2 regulates the fate commitment of mesenchymal stem cells via hedgehog signaling. *Stem Cell Res Ther*, 11(1), 135. <https://doi.org/10.1186/s13287-020-01631-9>

# 11 Eidesstattliche Erklärung

## **Erklärung zur Dissertation** gemäß der Promotionsordnung vom 12. März 2020

***Diese Erklärung muss in der Dissertation enthalten sein.***  
***(This version must be included in the doctoral thesis)***

„Hiermit versichere ich an Eides statt, dass ich die vorliegende Dissertation selbstständig und ohne die Benutzung anderer als der angegebenen Hilfsmittel und Literatur angefertigt habe. Alle Stellen, die wörtlich oder sinngemäß aus veröffentlichten und nicht veröffentlichten Werken dem Wortlaut oder dem Sinn nach entnommen wurden, sind als solche kenntlich gemacht. Ich versichere an Eides statt, dass diese Dissertation noch keiner anderen Fakultät oder Universität zur Prüfung vorgelegen hat; dass sie - abgesehen von unten angegebenen Teilpublikationen und eingebundenen Artikeln und Manuskripten - noch nicht veröffentlicht worden ist sowie, dass ich eine Veröffentlichung der Dissertation vor Abschluss der Promotion nicht ohne Genehmigung des Promotionsausschusses vornehmen werde. Die Bestimmungen dieser Ordnung sind mir bekannt. Darüber hinaus erkläre ich hiermit, dass ich die Ordnung zur Sicherung guter wissenschaftlicher Praxis und zum Umgang mit wissenschaftlichem Fehlverhalten der Universität zu Köln gelesen und sie bei der Durchführung der Dissertation zugrundeliegenden Arbeiten und der schriftlich verfassten Dissertation beachtet habe und verpflichte mich hiermit, die dort genannten Vorgaben bei allen wissenschaftlichen Tätigkeiten zu beachten und umzusetzen. Ich versichere, dass die eingereichte elektronische Fassung der eingereichten Druckfassung vollständig entspricht.“

Teilpublikationen:

Datum, Name und Unterschrift

4.9.22, Nathalie Jauré



# 12 Curriculum vitae

## Nathalie Jauré

### Bioinformatics / Data analysis

Nationality French – 50672, Cologne, GERMANY

☎ +49 176 21 25 48 57 • ✉ nathaliejaure@hotmail.fr • [in](#) nathalie-jaure

---

**PhD level bioinformatician proficient at designing and optimising pipelines to generate Omics dataset and analysing them with bioinformatics methods.** Extensive expertise in Data Analysis, Genomics, with special emphasis on Metabolism and Ageing. Efficient, adaptable and autonomous worker who takes initiative and responsibility. Natural planner with strong presentation and writing skills. Used to work in collaborative teams on multiple interdisciplinary research projects. Looking for a position offering collaborative and challenging projects using data analysis to find new solutions in healthcare, and beyond.

---

### Education

---

#### University education

- **Ph.D in Bioinformatics** **Cologne-Germany**  
*Max Planck Institute for Biology of Ageing - CECAD (Cluster of Excellence for Ageing Research)* 2017–  
Supervised by Prof. Linda Partridge and Prof. Andreas Beyer.
  - Studying the effects of dietary restriction on the transcriptomal flexibility of the white adipose tissue.
  - Designing and optimizing of a novel experimental workflow for generating Single-cell data.
  - Analysing of Multi-Omics datasets and biological interpretation.
- **Master of Bioinformatics and Modelling** **Lyon-France**  
*Institut National des Sciences Appliquées (INSA) - Engineering school* 2014–2017
- **Master of Bioinformatics and System Biology (Erasmus)** **Lyngby- Denmark**  
*Technical University of Denmark* 2016–2017
- **Bachelor in Molecular biology and Biochemistry** **Nantes-France**  
*Nantes University* 2012–2014

#### Bioinformatic internships

- **L'Oréal** **Paris - France**  
*Master 2 Industry Internship (duration : 6 months)* 2017  
Benchmarking and implementation of new pipelines for correlation network analysis. Determination of model parameters for biological interpretation of transcriptomics human skin dataset.
- **National French Institute of Forensic science (INPS)** **Ecully - France**  
*Master 1 Internship (duration : 5 months)* 2016  
Creation of a web-application with the Shiny platform (Rstudio) to analyze NGS profiles of individuals with statistical models and data mining tools.
- **Research laboratory : Protein Engineering and Functionality Unit (UFIP)** **Nantes - France**  
*Bachelor Internship (duration : 200h)* 2014  
Development and validation of a molecular docking protocol for drug design pipelines.

## Standard and specialized skills

---

- **IT skills :**
  - *Programming* : R, Shiny (Rstudio), Shell Unix, Python, C++, L<sup>A</sup>T<sub>E</sub>X, MySQL, HTML.
  - *Software* : Matlab, SAS, Pymol, Autodock Vina, Knime, SQL developer.
- **Data analysis :**
  - Machine learning. RNA-seq, Single-cell, Proteomics pipelines. Differential expression analysis, Functional enrichment, Deconvolution methods, Correlation networks, Biostatistics.
- **Biology knowledge :**
  - Molecular biology, Biochemistry (enzymology and metabolism), Immunology, Cellular biology, System biology, Pharmacology, Microbiology, Population genetics.
- **Wet lab :**
  - Single nuclei isolation, single nuclei/cell droplet-based protocol and library preparation, RNA-seq library preparation, Microscopy, Experimental design.

## Academic soft skills

---

- **Conferences :**
  - Single Cell Analysis : from Development to Disease, Online, 2020.
  - Poster presentation at SAB Symposium (Scientific Advisory Board), Cologne, Germany, 2019.
  - Healthy Ageing From Molecules to Organisms, Wellcome Genome Campus, UK, 2018.
- **Oral presentation :**
  - Chair and presentation at scientific retreats.
  - Animation of break-out session at scientific retreat.
  - Presentation at Institute seminar and regular presentations in front of biological researchers and bioinformaticians.
- **Writing :** Grant reviewing support, project reports.
- **Workshops :** Good scientific practice, Scientific writing, Collaborative efficient communication.

## Language

---

- **French :** Native proficiency.
- **English :** Full professional proficiency. Test of English for International Communication (TOEIC) : score of 990/990. CEFR level : C1.
- **German :** CEFR level : A2.

## Extracurricular activities

---

- Drawing and painting, classic and digital (Member of the INSA Art section), art exhibition. Photography. Collaborative boardgames.
- Dance. Jogging. Surfing. Hiking. Yoga.